MASTER IN BIOCHEMISTRY AND MOLECULAR AND CELL BIOLOGY RESEARCH FOCUS

X-ray irradiation for immune-modulation in head and neck cancer

SCHIFFLERS, Christoph

Award date:
2019

Awarding institution:
University of Namur

Faculté des Sciences

X-ray irradiation for immune-modulation in head and neck cancer

Thesis presented to obtain

the academic grade of master 120 in biochemistry, molecular and cellular biology

Christoph SCHIFFLERS

January 2019

University of Namur
Faculty of Science

X-ray Irradiation for Immune Modulation in Head and Neck Cancer

Christoph Schifflers

Thesis presented to obtain the academic grade of master 120 in biochemistry, cellular and molecular biology

Jury members :

Professor C. Michiels (Director)
Cell biology research unit (URBC)
NARILIS, UNamur

Professors M. Raes
Cell biology research unit (URBC)
NARILIS, UNamur

Professor J.P. Gillet
Laboratory of molecular cancer research (URPhyM)
NARILIS, UNamur

Doctor A.C. Wéra
Cell biology research unit (URBC)
NARILIS, UNamur

C. Warnon
Cell biology research unit (URBC)
NARILIS, UNamur

January 2019

Université de Namur
FACULTE DES SCIENCES
Secrétariat du Département de Biologie
Rue de Bruxelles 61 - 5000 NAMUR
Téléphone: + 32(0)81.72.44.18 - Téléfax: + 32(0)81.72.44.20
E-mail: joelle.jonet@unamur.be - http://www.unamur.be

X-ray irradiation for immune-modulation in head and neck cancer

SCHIFFLERS Christoph

Summary

Programmed death ligand-1 (PD-L1) expression in various cancers including head and neck cancer favors cancer cell survival and proliferation as it allows them to escape the immune system. PD-L1 binds to its receptor at the surface of cytotoxic tumor infiltrating T cells (CD8+ TILs). and induces an inhibitory signaling pathway that interferes with T cell activation after specific antigen recognition through the T cell receptor. Blocking this negative pathway by preventing ligand-receptor interactions with an antibody is a Nobel Prize-winning powerful emerging tool in immunotherapy and frequently associated to conventional treatment strategies. Beyond PD-L1 expression, cancer cells are also capable of polarizing tumor-associated macrophages (TAMs) towards a M2-like phenotype, which adds several immunosuppressive properties to the tumor microenvironment and induces inactivation or even apoptosis of tumor infiltrating lymphocytes. It has been shown that radiotherapy can be used to repolarize macrophages from a M2 towards a M1-like immuno-stimulating phenotype. Furthermore, X-ray irradiation induces an increased PD-L1 expression in cancer cells through the activation of DNA-damage response pathways. Therefore, a treatment combining irradiation and an anti-PD-1 immune checkpoint blockage (ICB) effectively provoke cancer cell eradication by alleviating multiple immunosuppressive mechanisms present in numerous types of cancer, for instance in head and neck squamous cell carcinoma (HNSCC). In this study, we investigated the expression of PD-L1 after X-ray and proton irradiation at several doses and timings after irradiation, in order to determine in which condition an anti-PD-1 ICB in combination with X-ray irradiation would lead to an optimal treatment response. Based on these *in vitro* results, a syngenic *in vivo* mouse model of HNSCC was set up to assess TAM repolarization and its impact on CD8+ TIL activation and exhaustion. We discovered that unlike proton irradiation, X-ray irradiation induced a dose- and time dependent increase in PD-L1 expression, both at mRNA and protein levels. Additionally, although the combination of an anti-PD-1 ICB with X-ray irradiation increased tumor infiltration by immune cells and favors CD8+ TILs response to cancer cells, this process seemed not to be mediated by radiation-induced macrophage repolarization.

Thesis of master 120 in biochemistry, cellular and molecular biology
January 2019
Director: C. Michiels

Université de Namur
FACULTE DES SCIENCES
Secrétariat du Département de Biologie
Rue de Bruxelles 61 - 5000 NAMUR
Téléphone: + 32(0)81.72.44.18 - Téléfax: + 32(0)81.72.44.20
E-mail: joelle.jonet@unamur.be - http://www.unamur.be

X-ray irradiation for immune-modulation in head and neck cancer

SCHIFFLERS Christoph

Résumé

Dans de nombreux types de cancer y compris les cancers tête et cou, l'expression de Programmed death ligand-1 (PD-L1) par les cellules cancéreuses leur permet de survivre et proliférer étant donné que cette protéine leur permet d'échapper au système immunitaire. PD-L1 se lie à son récepteur à la surface des lymphocytes T cytotoxiques infiltrant la tumeur (CD8+ TILs) et induit une voie de signalisation inhibitrice interférant avec l'activation des lymphocytes T suite à la reconnaissance d'un antigène spécifique via le T cell receptor. Le blocage des voies inhibitrices en empêchant l'interaction entre le ligand et son récepteur, une stratégie qui a mené au prix Nobel de médecine et physiologie en 2018, est un nouvel outil puissant en immunothérapie et est fréquemment associé aux traitements conventionnels. Outre l'expression de PD-L1, les cellules cancéreuses sont capables de polariser les macrophages associés aux tumeurs (TAMs) vers un phénotype M2-like favorisant plusieurs mécanismes immunosuppresseurs au niveau du microenvironnement tumoral et induisant l'inactivation ou même l'apoptose des lymphocytes infiltrant la tumeur. Il a été démontré qu'une irradiation peut repolariser les macrophages d'un phénotype M2 vers un phénotype immunostimulant M1-like. En plus, une irradiation par rayons X induit la surexpression de PD-L1 dans les cellules cancéreuses en activant les voies de réponse aux dommages à l'ADN. Un traitement combiné d'irradiation par rayons X et un blocage du checkpoint immunitaire (ICB) anti-PD-1 peut donc provoquer l'éradication efficiente des cellules cancéreuses en diminuant les propriétés immunosuppressives de nombreuses cellules cancéreuses, par exemple dans le cancer épidermoïde de la tête et du cou (HNSCC). Dans la présente étude, nous avons investigué l'expression de PD-L1 suite à l'irradiation par rayons X ou par protons à différentes doses et timings afin de déterminer dans quelle condition un ICB anti-PD-1 en combinaison avec l'irradiation par rayons X pourrait induire une réponse au traitement optimale. Sur base des résultats *in vitro*, *in vivo* un modèle murin syngénique d'HNSCC a été mis au point pour évaluer la repolarisation des TAMs et son impact sur l'activation et l'exhaustion des TILs CD8+. Nous avons découvert que contrairement à une irradiation par protons, les rayons X induisent une surexpression de PD-L1 dépendante de la dose et du timing au niveau ARN ainsi qu'un niveau protéique. En plus, malgré que la combinaison d'un ICB anti-PD-1 et d'une irradiation par rayons X augmente l'infiltration tumorale par les cellules immunitaire et la réponse des TILS CD8+ envers les cellules cancéreuses, ce processus semble être indépendant d'une repolarisation des TAMs par irradiation.

Mémoire de master 120 en biochimie, biologie moléculaire et cellulaire
Janvier 2019
Promoteur : C. Michiels

First of all, I want to thank my tutor Eléonore for giving me the great opportunity to work on a project which combined my most favorite topics, oncology, immunology and radiotherapy. During these 11 months, you thought me very patiently many aspects of translational research in the biomedical field. In addition to the experiments, you encouraged me to attend several lectures and presentation, such as the EDT cancéro, the immuno-oncology course from Bordet, the presentation on mouse models in immuno-oncology from Crown Bioscience, etc., which I greatly appreciated. During the course of this project, you allowed me to adapt it and go beyond the original ideas. You gave me a great deal of responsibility, which I tried to fulfill to the best of my abilities, not to forget with you helping and advising me when needed. You also gave me a good lecture about independence and autonomy. This allowed me to work more efficiently, organize myself better and focus on my task without hesitating too much, as I did when I started this project. And finally, I want to thank you for all the fun we had and the great deal of patience you often had with me. I'm sure, it was not always easy ;-) It was a great pleasure working with you and I was very happy and very lucky that you became my tutor.

I thank my promotor Carine, who was the main reason for me to stay in Namur pursue my interest in radiotherapy. Eventually, thanks to you, I had the chance to realize my master thesis in this field, an experience that I enjoyed very much! Despite your numerous duties and responsibilities, you always kept a close look at this project and remained at all time available, when more of your help and precious advice was needed. I appreciated working for you very much, even if it was for a short period only. Considering all of this in retrospective, I'm very glad I chose to stay in Namur.

To all current (and some former) members of the TumHyp team, especially Géraldine, Sophie and AnK, thank you! Each one of you, at some point (or more often) could help me, whether with theoretical knowledge, advice for the experiments, by reviewing my work or preparing my thesis, but also for all the personal and professional advices that went beyond this master thesis. Every time there was a problem, every one of you always was willing to help or to encourage me when I experienced some difficulties.

I also thank all the technicians that during this long period constantly helped all of us, directly when asked or indirectly by all the things you do every day to make the lab work, the things we unfortunately often take for granted… I specially thank Guy, Kévin (URBM), Benoit (LabCeTi), Olivia (Physio générale), Maude, Antoine etc. You all contributed to the successful outcome of my project and the good experience I made in the URBC.

All the other members of the URBC, I also thank enormously. Most of them also, at some point, helped with advice. But most importantly, every single member contributed to a great atmosphere at university or the after work. Despite all the hard times I had, whether it was the long nights, the weekends at work, the X-ray or the FACS playing very bad jokes on us, there always was someone there to make me smile again or change my mind. Thanks to all them, coming every day to work was an enormous pleasure and made me enjoy this master thesis that much, that now that it ends I regret that it is already over. Thanks to all of you!!!

My project relied on many new techniques and ideas that were totally new and required a huge deal of set ups and failures. Eventually, they all worked out very well but only thank a special group of people. First of all, Florian Juszczak. He initially brought me to the idea of using the gentleMACS technology for tumor dissociation and established the connections with the necessary people. In addition, I thank him for the many hours, we discussed about research in general or specific topics. It often helped to proceed, get new ideas and motivation as it helped not to stay stuck on setbacks. Thanks to Soryah Megari and Guerric Epron from Miltenyi Biotech, with whom I spent many hours to familiarize with rare cell magnetic isolations, tissue dissociation using the gentleMACS, optimal sample preparation for flow cytometry analysis and the most challenging part, creating reference settings for multistained flow cytometry analysis. To end our good collaboration as well as it started, I enjoyed helping with the organization of the flow cytometry seminary as much as I enjoyed the seminary itself. I thank Pierre-Florent Petit from the Deduve Institute, who showed me how to practically dissociate tumors using the gentleMACS technology. I thank Prof. A.E. Declèves and Florian Juszczak from University of Mons for providing us with the gentleMACS dissociator. Thanks to Prof. N. Caron and her team, including Olivia, Ines, Florian and Pauline, we were able to execute our *in vivo* protocol, since they provided us with all the necessary equipment and advice. For this *in vivo* part, I also greatly thank Roxane Dewree, veterinary of the animal facility. Without her help during the setup and execution of our first *in vivo* project, both projects would probably not have been performed, certainly not during the duration of my master thesis. I thank Caroline Canon for helping me to see much clearer the sometimes very obscure microscopic structures for histologic analyses.

Finally, I thank Prof. S. Lucas and Prof. A.C. Heuskin for allowing me to work in the LARN to perform the irradiations. In this context, some special thanks go to Tijani, for supervising my initial work in the LARN, for the training for the particle accelerator and for offering his help at several occasions.

3D-CRT	Three-Dimensional Conformal Radiation Therapy
5-FU	5-Fluoro-Uracyl
AKT	RAC-alpha Serine/Threonine-Protein Kinase
ATM	Ataxia Telangiectasia Mutated
BPM	Bip Profile Monitor
BMDM	Bone Marrow-Derived Macropahges
BSA	Bovine Serum Albumin
CCD	Charged-Coupled Device
CCL2	Chemokine Ligand 2
CD8	Cluster of Differentiation 8
CREB	Cyclic AMP-Responsive Element-Binding Protein
CSF1	Macrophage Colony-Stimulating Factor
CTLA-4	Cytotoxic T Lymphocyte-Associated Protein 4
CXCL12	Stromal Cell-Derived Factor 1
DC	Dendritic Cell
DDR	DNA-damage response
DMEM	Dulbecco's Modified Eagle's Medium
DMSO	Dimethyl Sulfoxide
DNA-PKcs	DNA-Dependant Protein Kinase Catalytic Subunit
DSB	Double Strand Break
EDTA	Ethylene Diamine Tetracetic Acid
EGFR	Epidermal Growth Factor Receptor
FBS	Foetal Bovine Serum
FDA	Food and Drug Administration
FdUMP	Fluorodeoxyuridine Monophosphate
FdUTP	Fluorodeoxyuridine Triphosphate
FUTP	Fluorouridine Triphosphate
γH2AX	Phosphorylated Histone H2AX at Serine 139
Grb2	Growth Factor Receptor-bound Protein 2
HEJ	Homologous Endjoing
HES	Hemalum-Erythrosin-Safran
HIS	Heat-inactivated Serum
HNC	Head and Neck Cancer
HNSCC	Head and Neck Squamous Cell Carcinoma
HPV	Human Papilloma Virus
ICB	Immune Checkpoint Blockage
IFN-γ	Interferon- γ
IL-2	Interleukine-2
IMRT	Intensity-Modulated Radiation Therapy
I.P.	Intra-Peritoneal
IR	Ionizing Radiation

LAT	Linker for Activation of T-cells Family Member 1
LCK	Lymphocyte-specific protein Tyrosine Kinase
LCP2	Lymphocyte Cytosolic Protein 2
LET	Linea Energy Transfer
MAPK	Mitogen Activated Protein Kinase
MAC	Membrane Attack Complex
MEM	Minimal Essential Medium
MHC	Major Histocompatibility Complex
MKK	MAPK Kinase7
MRE11	Double Strand Break Repair Nuclease MRE11
MRN	MRE11-RAD50-NBS1 complex
mTOR	Mechanistic Target of Rapamycin
NBS1	Nibrin
NHEJ	Non-Homologous Endjoining
NFAT	Nuclear Factor for Activated T-cells
NFkB	Nuclear Factor Kappa B
NK	Natural Killer
PBS	Phosphate-Buffered Saline
PD-1	Programmes Cell Death Protein 1
PD-L1	Programmed Death Ligand 1
P.I.	Post-Irradiation
PI	Propidium Iodide
PIPS	Passivated Implanted Planar Silicon
PI3K	Phosphoinositide 3-Kinase
PKCθ	Protein Kinase C Theta
PLCγ1	1-Phosphatidylinositol 4,5-Bisphosphate Phosphodiesterase Gamma-1
PMA	Phorbol 12-Myristate 13-Acetat
PP2-A	Protein Phosphatase 2
RAD50	Double Strand Break Repair Protein 50
RBE	Relative Biological Effectiveness
ROS	Reactive Oxygen Species
RPMI	Roswell Park Memoral Institute 1640 Medium
SHP-1	Src Homology Region 2 Domain-containing Phosphatase-1
SHP-2	Src Homology Region 2 Domain-containing Phosphatase-2
SSB	Single Strand Break
TAM	Tumor-Associated Macrophage
TCR	T Cell Receptor
TIL	Tumor-Infiltrating Lymphocyte
TME	Tumor Microenvironment
TNF- α	Tumor Necrosis Factor α

Foreword

With an estimated number of 9.6 million deaths in 2018, cancer is a significant global health threat and the second cause of death worldwide, following cardio-vascular diseases. Since its first description by Hippocrates, the so-called Father of Medicine, tremendous efforts have been made, trying to understand the nature of cancer and how to cure it. Nowadays, cancer is commonly considered as an adaptive genetic disease, which originates from the malignant transformation of one of our own cells consecutive to the accumulation of genomic alterations, including mutations and epigenetic modifications.

Cancer cells can be characterized by ten hallmarks, as descripted by D. Hanahan and R. Weinberg. According to this definition, cancer cells present sustained proliferative signaling, growth suppressor evasion, enabled replicative immortality, active invasion and formation of metastasis, genome instability and mutations, resistance to cell death, dysregulated cellular metabolism, induction of angiogenesis, evasion of immune destruction and stimulation of tumor-promoting inflammation (Hanahan and Weinberg, 2000 and Hanahan and Weinberg, 2011).

During the lifespan of a person, random or stress-induced mutations arise in cells and cumulate over the years. Since life expectancy is constantly increasing, the number of accumulated mutations also increases. This partially explains the increasing incidence of cancer. Additionally, during the last decades and centuries, the average lifestyle changed. Nowadays, many people are smokers, consume high quantities of alcohol on a regular basis, do not pay attention to an equilibrated nutrition and are more and more sedentary. All of these factors are well known risk factors for the development of cancer. While some of them are directly mutagenic, others favor cell proliferation. This explains why combining the exposure to risk factors like alcoholism and smoking promotes, in combination, synergistically cancer development, especially cancers of the head and neck region and the gastro-intestinal tract. People's lifestyle as well as their socio-economic status but also ethnics therefore significantly impact the individual risk to develop cancer.

We currently possess a large arsenal of cancer therapies, including surgery, chemotherapy, radiotherapy, targeted therapies and immunotherapies. While the number of anti-cancer treatments continuously increases, the number of cancer-associated deaths also increases. This is partly due to the resistance of several cancers to therapy. Therefore, in addition to inventing new cancer therapies, existing cancer therapies are further investigated, so that better understanding of the underlying mechanisms can lead to improve these therapies and allow to treat patients more efficiently and to treat those that were non-responsive or developed resistance to the treatment previously.

In this context, this project aimed to investigate the combination of radiotherapy, one of the oldest anti-cancer therapies, and immune-checkpoint blockage (ICB), a new addition to conventional treatment strategies. One of the advantages is that this combination can be applicable to a large number of cancer types and that it became, thanks to recent advances in the field of radiotherapy and diagnostic techniques, highly precise and induces unlike chemotherapy, very little collateral damage to healthy tissues. Since radiation is capable of

altering the immune response to cancer cells, a closer investigation of the combined treatment of radiotherapy and ICB could allow to improve the way this treatment is used and to make it applicable to previously resistant patients.

I. Introduction

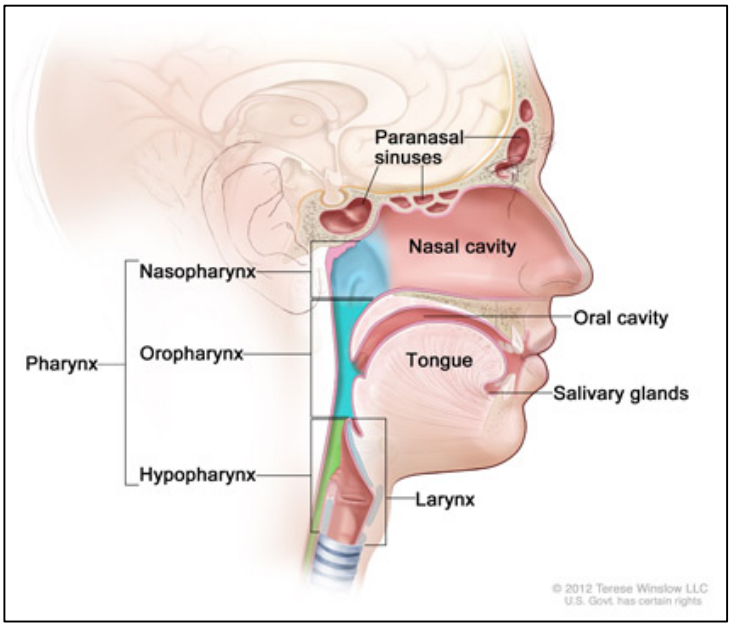

Figure 1. Regions of origin of head and neck cancer. (adapted from: National Cancer Institute, 2016)

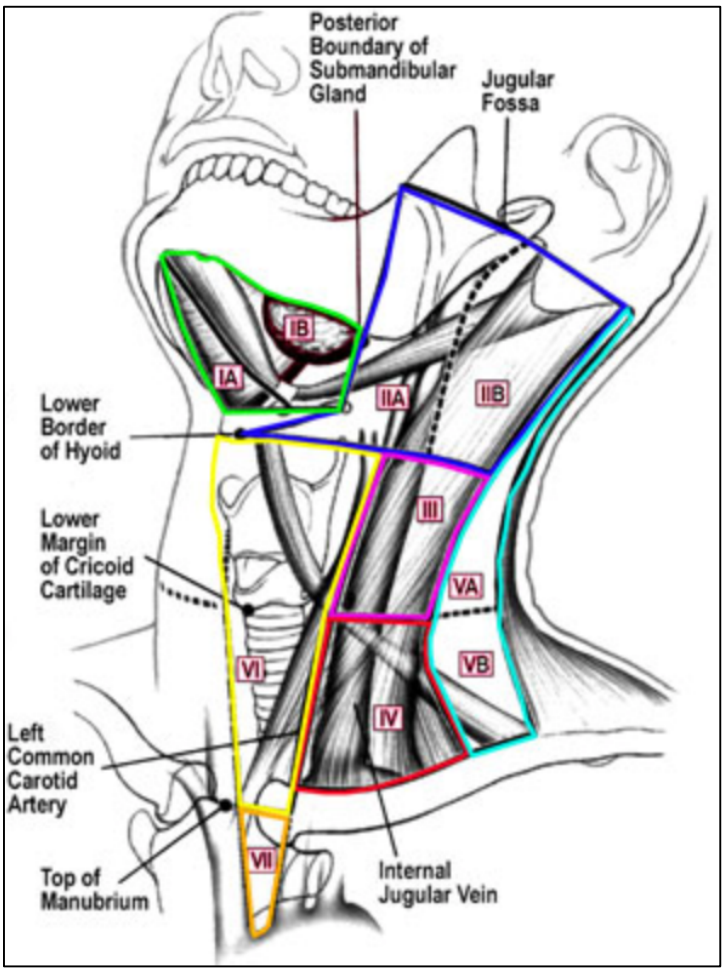

Figure 2. Lymph node (LN) compartments of the head and neck region. Submental (Ia) and submandibular LNs (Ib) forming the level I LNs. The level 2 upper jugulary LNs are subdevinded anterio-media (IIa)l and posterior-lateral (IIb) LNs. Level 3 and 4 LNs are middle jugular (III) and lower jugular (IV) LNs respectively. Level V LNs consist of the accessory nodes (Va) and transverse cervical and supraclavicular nodes (Vb). Pretrachial, paratracheal, precricoid and perithyroid LNs form level VI LNs, while suprasternal LN form level VII nodes. (adapted from: http://www.endocrinesurgery.net.au/lymph-node-management)

1 Head and neck cancer

1.1 Characteristics

Head and neck cancer (HNC) is the sixth leading cancer worldwide, with an incidence of approximately 600 000 new cases each year. It is characterized by a 5-year survival of 40-50% (Jemal et al., 2011; Leemans et al., 2011; Siegel et al., 2017). It may arise in different segments of the upper aero-digestive tract, including the larynx, pharynx, tongue, oral and nasal cavity as well as the paranasal sinuses (Figure 1). These parts of the body are particularly sensitive to the induction of carcinogenesis, since they are the first line barriers between the body and ingested or inhaled substances.

The lymphatic drainage of all of these regions occurs through several lymph nodes (LN) of the neck and upper mediastinum. These LNs are located in seven compartments (Figure 2). Precise determination of the individual lymphatic drainage of each HNC patient has shown to be crucial, not only for surgical resection but also to set up the optimal irradiation protocols of head and neck tumors (Grégoire et al., 2014). According to their possible locations, the side effects of tumor growth and treatment protocols can lead to sever discomfort and impairment or even loss of several functions including swallowing, speaking, breathing and production of saliva. The determination of the precise lymph drainage of head and neck tumors not only allows a decreased probability of relapse but it also significantly reduces the irradiation of healthy tissues and thereby significantly lowers the side effects HNC treatment (Daisne et al., 2015).

Considering the anatomic and histologic differences of the potential tissues of origin, there is a broad range of head and neck squamous cell carcinomas (HNSCC), adenocarcinomas and sarcomas. In this project, we exclusively focused on the most frequent type of HNC, the HNSCC.

Following precancerous lesions including leuko- and erythroplakia, smoking and alcohol consumption represent the two leading risk factors, which act in combination synergistically. While smoking directly induces mutagenesis, alcohol consumption irritates the aero-digestive tract killing epithelial cells of the mucosae and thereby stimulation stem cell proliferation. Combined smoking and alcohol consumption therefore favors clonal expansion of potentially mutated cells, which greatly increases the risk to develop a HNSCC. Epidemiologic studies indicate a decreased incidence in western countries, an increased incidence in males with African descendants but also in countries with lower socio-economic status, which can be explained by a higher exposure to risk factors (Kim et al., 2010). In addition, oropharynx infections by some strains of human papilloma virus (HPV) have in recent years been associated to a significantly increased prevalence of HNSCC but also to a better prognosis (Gregoire et al., 2010). The mechanisms of pathogenesis in HPV^+ and HPV^- HNC are different. Therefore, studies analyzing fundamental processes of HNC should clearly distinguish these two types of cancer. In the present study, we exclusively focus on HPV^- HNSCC.

Primary tumor (T)	
T1	Tumor ≤2 cm in greatest dimension
T2	Tumor >2 cm and ≤4 cm in greatest dimension
T3	Tumor >4 cm in greatest dimension
T4a	Moderately advanced local disease. Tumor invades adjacent structures only (through cortical bone [mandible or maxilla], into deep [extrinsic] muscle of tongue, maxillary sinus, skin of face)
T4b	Very advanced local disease. Tumor invades masticator space, pterygoid plates, or skull base and/or encases internal carotid artery
Regional Lymph Nodes (N)	
N1	Metastasis in a single ipsilateral lymph-node, ≤3 cm in greatest dimension
N2a	Metastasis in a single ipsilateral lymph-node, >3 cm and ≤6 cm in greatest dimension
N2b	Metastasis in multiple ipsilateral lymph-nodes, none >6 cm in greatest dimension
N2c	Metastasis in bilateral or controlateral lymph-nodes, none >6 cm in greatest dimension
N3	Metastasis in lymph-nodes >6 cm in greatest dimension
Distant metastasis (M)	
M1	Distant metastasis

Figure 3. TNM classification for oral cancer. (adapted from: De Filece et al., 2014)

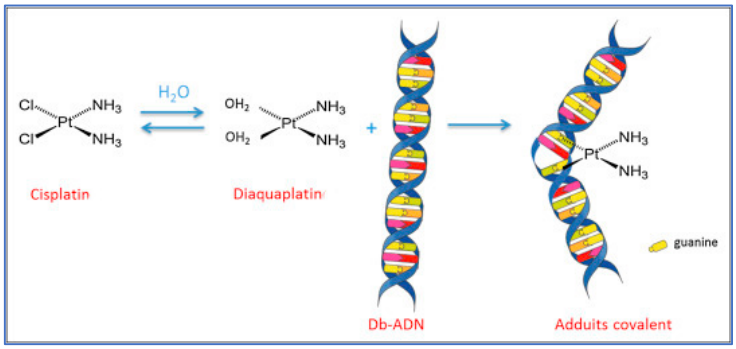

Figure 4.Cisplatin-induced DNA adducts after covalent binding to purine bases. (adapted from: Rancoule et al., 2017)

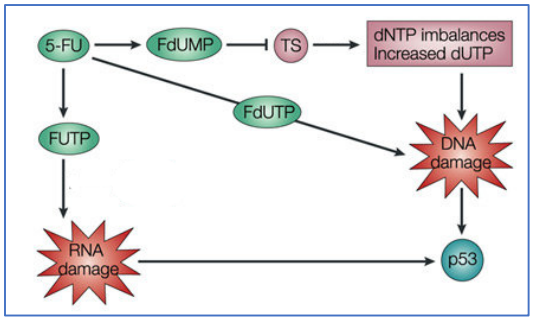

Figure 5. 5-Fluorouracil (5-FU) is converted to three main active metabolites: fluorodeoxyuridine monophosphate (FdUMP), fluorodeoxyuridine triphosphate (FdUTP) and fluorouridine triphosphate (FUTP). 5- Fluorouracil (5-FU) can activate p53 by more than one mechanism: incorporation of fluorouridine triphosphate (FUTP) into RNA, incorporation of fluorodeoxyuridine triphosphate (FdUTP) into DNA and inhibition of thymidylate synthase (TS) by fluorodeoxyuridine monophosphate (FdUMP) with resulting DNA damage. (adapted from: Longly et al., 2003)

1.2 Classification

The TNM classification allows to categorize the extent of a patient's cancer based on three criteria: "T" the primary tumor size; "N" the regional lymph node involvement; "M" the presence of distant metastasis (Figure 3). It is specific to each type of cancer, depending on the tissue of origin. This classification of an otherwise infinitely complex and diverse disease allows to guide the choice of treatment and to provide indications regarding the prognosis and treatment responsiveness.

1.3 Treatment strategy

It is important to note that no official guidelines clearly exist ruling on which therapy to use in each case. However, depending on the TNM stage, current treatment for patients with HNSCC generally consists in surgical excision and/or radiotherapy, possibly combined with chemotherapy in cases of locally advanced tumors, formation of metastasis and tumor recurrence. However, chemo- and radio-resistances remain widely unpredictable and are the primary cause of poor patient outcomes (Vermorken and Specenier, 2010).

1.3.1 Chemotherapy

Chemotherapy is used as cytotoxic and radio-sensitizing agent in cases of locally advanced or metastatic cases of HNSCC if the patient's condition allows chemotherapy treatment. It is most often platinum-based, when combined with radiotherapy or 5-fluoro-uracyl (5-FU) and anti-EGFR inhibitors such as Cetuximab, in case of advanced HNSCC (Vermorken et al., 2008).

1.3.1.1 Cisplatin

Platinum-based chemotherapy such as carboplatin or cisplatine, which is one of the oldest anti-cancer drugs, binds covalently via alkyl groups to purine bases of DNA forming cross-links or DNA-adducts (Figure 4). These cross-links inhibit cell cycle progression in the G1 or S phase and induce cell cycle arrest, which can either be resolved by DNA repair or by the induction of apoptosis via the intrinsic pathway. Additionally, cisplatin induces or increases oxidative stress which damages intracellular molecules. This process further leads to cell damage and may result in apoptosis of cancer cells (Dasari and Tchounwou, 2014).

1.3.1.2 5-fluorouracyl

5-FU is an anti-metabolite, whose active forms fluorodeoxyuridine monophosphate (FdUMP), fluorodeoxyuridine triphosphate (FdUTP) and fluorouridine triphosphate (FUTP) block thymidine synthesis by inhibiting thymidylate synthase and inducing DNA and RNA

damage after entering the cell. These processes lead to cell cycle arrest through p53 activation and can lead to the induction of apoptosis (Figure 5) (Longley et al., 2003).

1.3.1.3 Paclitaxel

In some cases, paclitaxel is used in addition to platin-based chemotherapy. Paclitaxel stabilizes the polymerized form of microtubules assembled during the M phase of the cell cycle and prevents microtubule depolymerization. After microtubules attached the kinetochores at the centromere region of chromosomes, microtubule depolarization is required not only to separate sister chromatids but also to create tension in both chromatids, which inactivates the tension sensor Aurora B Kinase and stabilizes the bipolar binding of sister chromatids. If no tension is generated at the kinetochore, Mad2 inhibits the Cdc20-APC complex that is responsible for M-Cdk and securin degradation necessary for cell cycle progression at the APC/C checkpoint. Thereby, Paclitaxel blocks mitosis and prolongs APC/C checkpoint activation, which leads to cell cycle arrest and apoptosis (Alberts et al., 2008).

1.3.2 Radiotherapy

Radiotherapy is one of the most frequently used strategies for treating HNC at different stages. Due to the high precision of modern radiotherapy coupled with functional and topological medical imaging, in case of early stage HNC, radiotherapy can even replace surgery and serve as primary treatment for unresected tumors. Considering the high risk of occult nodal metastasis, preventive nodal irradiation is often mandatory for locally restricted tumors. In cases of LN infiltration, imaging is used to determine specific lymph drainage of the tumor and to define subsequently the area that will undergo radiotherapy alone or post-surgically. In these cases, post-operative chemo-radiation is recommended. In clinics, fractioned irradiation is used for patient treatment. The total radiation dose is generally 70 Gy, delivered in daily 2 Gy fractions. Nevertheless, depending on the indication, the total dose can be adapted.

1.3.3 Surgery

Similarly to radiotherapy, in early stages, surgery often allows complete resection of local tumors. In case of LN infiltration or some cases of in situ carcinoma, additional post-operative radiation can be needed to obtain clear resection margins.

1.3.4 Cetuximab

Epidermal growth factor receptor blockage is nowadays a commonly used targeted therapy for HNSCC. This can be achieved using Cetuximab, a humanized anti-EGFR antibody. It is used in combination with radiotherapy in cases of locally advanced stages, when patients can not sustain chemotherapy. Patients with metastatic HNSCC are treated with the combination of Cisplatin, 5-FU and Cetuximab. This treatment option also accounts for patients in case of relapse.

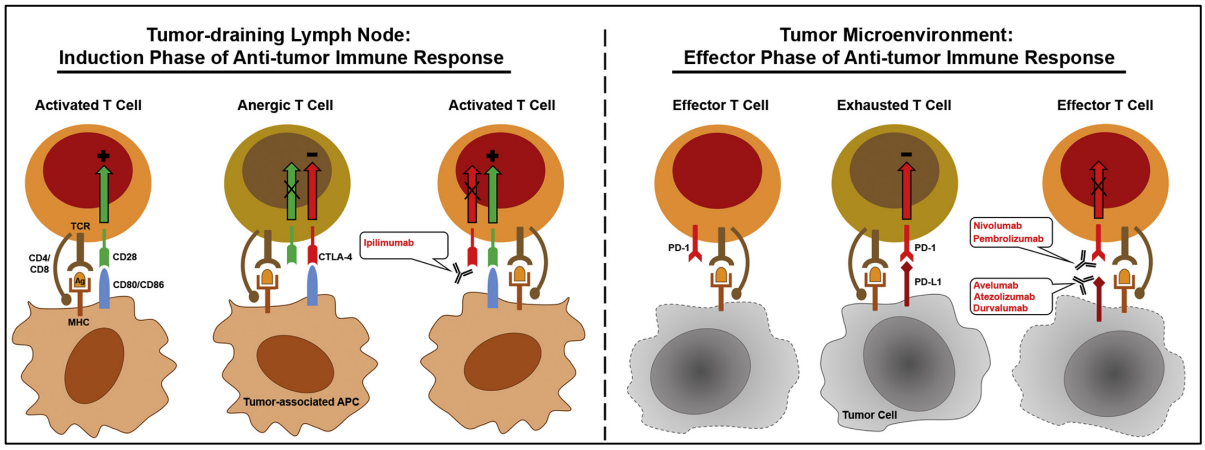

Figure 6. Summary of the CTLA-4 and PD-1 immune checkpoints and the role of FDA-approved immune checkpoint inhibitors in the treatment of cancer. CD80/CD86 co-stimulation through CD28 provides important activating signals that promote T cell expansion and effector differentiation during the induction phase of an immune response. The CTLA-4 co-inhibitory receptor is expressed on recently activated T cells and binds to the same ligands as CD28 but with higher affinity. Engagement of CTLA-4 on T cells during the induction phase of an anti-tumor immune response therefore impedes T cell activation by 1) sequestering CD80/CD86 ligands that would otherwise signal through CD28 and 2) transmitting inhibitory signals that directly suppress T cell activation, both of which lead to the induction of anergy. Anti-tumor T cells that do acquire cytokine-secreting and cytolytic effector functions can undergo additional negative regulation during encounter with tumor cells or tumor-associated APC that express PD-L1 in the tumor microenvironment. Engagement of PD-1 on these T cells transmits signals that promote T cell exhaustion. Immune checkpoint inhibitors (highlighted in red text) targeting CTLA-4, PD-1, or PD-L1 block these mediators of negative regulation in T cells, thereby promoting anti-tumor T cell activation and maintenance of anti-tumor T cell effector function. (adapted from Hargadon et al., 2018)

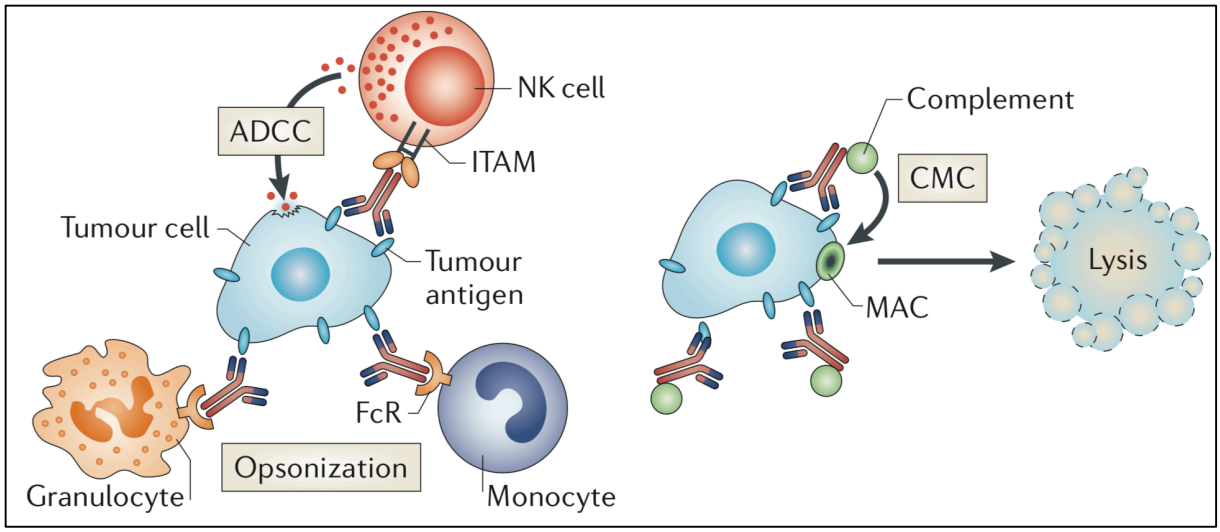

Figure 7. Additional cytotoxic mechanisms induced by IgG1 anti-PD-L1 antibodies. Anti-PD-L1 IgG1 antibodies bind to PD-L1 at the surface of cancer cells and induce, in addition to block receptor-ligand interaction, cancer cell death by NK cell mediated antibody-dependent cellular cytotoxicity, opsonisation followed by phagocytosis as well as complement-mediated cytotoxicity and cell lysis by membrane attack complex (MAC) formation. (adapted from: Weiner, 2015)

1.3.5 Immune-checkpoint blockade

In recent year, advances in immunotherapy provided an additional strategy for HNC treatment. For instance, inhibiting negative immune-checkpoints between cancer cells and immune cells, which will be detailed more extensively in the third part of the introduction, became one of the most famous and efficient additions in cancer therapy. This strategy is particularly interesting since it is applicable to a large proportion of cancer patients and presents only very faint adverse effects compared to conventional treatments, when used to treat locally advanced or metastatic cancer. This new strategy was rewarded in 2018 the Nobel Prize in Physiology and Medicine. Indeed, J. Allison and T. Honjo discovered the two negative immune checkpoints, that are nowadays targeted in cancer therapy, cytotoxic T-lymphocyte-associated protein 4 (CTLA-4) and PD-1.

1.3.5.1 CTLA4 / CD80/86 checkpoint inhibition

Upon T cell activation by antigens and co-stimulation through the interaction of CD28 and CD80 or CD86, T cells express the inhibitory signaling receptor CTLA-4, which also binds CD80 and CD86 but which higher affinity and avidity than CD28, allowing to induce T cell anergy following activation (Figure 6). Blocking this negative pathway was the first FDA approved ICB in 2011. That for, the monoclonal antibody Ipilimumab binds to CTLA-4 and prevents its interaction with CD80 and CD86, favoring prolonged T cell activation (Hargadon et al., 2018).

1.3.5.2 PD-1 checkpoint inhibition

The PD-1/PD-L1 axis is a negative regulator of T cells contributing to immune-homeostasis and allowing T cell inactivation after their stimulation by an antigen (Figure 6). This negative regulator allows to avoid excessive immune activation or auto-immune reactions. Cancer cells can exploit this pathway to escape T cells. Blockage of the PD-1 receptor prevents receptor ligand interaction and allows to maintain the effector phase of anti-tumor T cell response. In 2014, the Food and Drug Administration (FDA) approved two anti-PD-1 IgG4 antibodies, Nivolumab and Pembrolizumab.

1.3.5.3 PD-L1 checkpoint inhibition

Similarly to PD-1 checkpoint inhibition, anti-PD-L1 antibodies prevent receptor ligand interaction and allow to maintain the effector phase of anti-tumor T cell response. However, the target of these antibodies is not located on immune cells but cancer cells. During the development of anti-PD-L1 monoclonal antibodies, IgG1 antibodies were selected. The Fc fraction of G1 immunoglobulins, generates two additional secondary cytotoxic mechanisms, which favor cancer cell destruction by the immune system (Figure 7). First, the Fc fraction of IgG1 antibodies can bind to $Fc_{\gamma}R$ receptors I, II-A, II-B1, II-B2 and RIII, present at the surface of different immune cells, for instance macrophages, natural killer (NK) cells and granulocytes. While on macrophages $Fc_{\gamma}R$ activation induces polarization toward a pro-inflammatory

phenotype, $Fc_{\gamma}RIII$ activation on NK cell induces antibody dependent cytotoxicity, which will induce cancer cell lysis similarly to cytotoxic T cells (Bournazos et al., 2016). This mechanism will be described in section 3.1.2.1. The second additional mechanism of cytotoxicity is mediated by the activation of the complement, which is part of the innate immune system. The C1 complex binds to the Fc fraction of the IgG1 antibodies via the C1q subunit inducing a conformational change of the C1 complex. This leads to the activation of the auto-catalytic activity of the C1r subunit inducing the cleavage of the activated C1s subunit, which is a serine protease. This protease cleaves C2 into C2a and C2b but it also cleaves C4 into C4b, which binds covalently to the surface of the cancer cell. C2a associates to C4b, forming the active convertase C3, which cleaves C3 into C3a and C3b. C3b remains bound to the surface of cancer cells, while C3a is released and acts as a mediator of inflammation. Since C3b opsonizes cancer cells and thereby favors their phagocytosis of the target cells. C3b also binds to the C3 complex, which then, in its active form, can cleave C5 into C5a and C5b. Similarly to C3a, C5a favors inflammation. It also binds to the C5a receptor at the surface of macrophages, which than can bind C3a by the CR1 receptor and phagocyte opsonized target cells. C5b binds to C6, C7, C8 and C9 forming the membrane attack complex, which disrupts target cell membranes and causes cancer cell lysis (Murphy and Weaver, 2017).

In 2016, the first PD-L1 blocking antibody was approved, Atezolizumab, followed in 2017 by two other PD-L1 blocking antibodies, Avelumab and Durvalumab (Hargadon et al., 2018).

Current investigations aim to determine how the unique features of each of the available treatments can be exploited, to enhance the efficacy of their combination, in order to improve patient outcome.

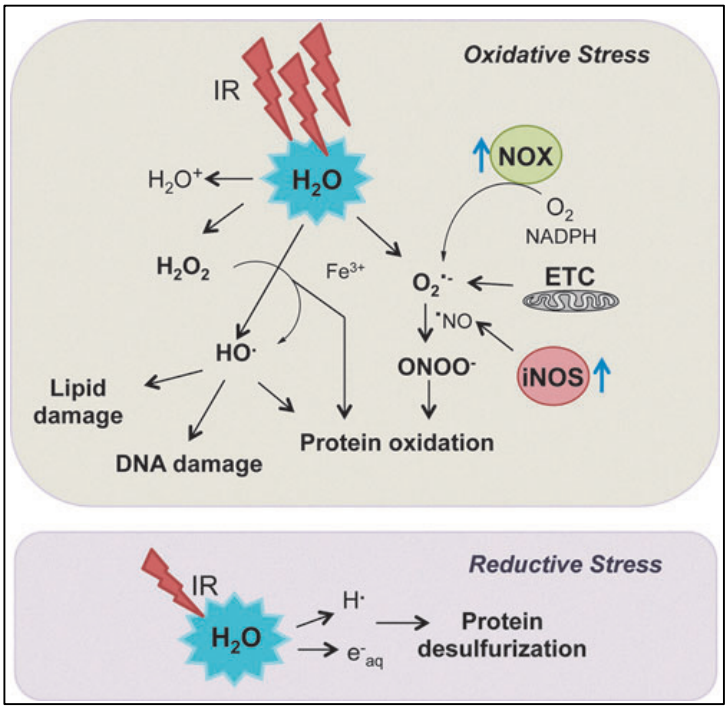

Figure 8. Oxidative and reductive stress induced by ionizing radiation. (adapted from: Reisz et al., 2014)

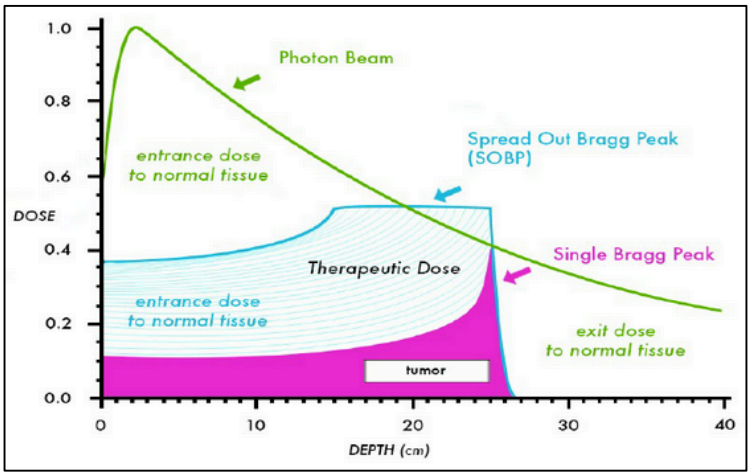

Figure 9. Depth dose profile of charged particles and photons. (adapted from: Ladra and Yock., 2014)

2 Radiotherapy

Since the discovery of X-rays by Wilhelm Röntgen in 1895 and their first applications in cancer treatment at the end of the 19th century, considerable advances have been made in the use of ionizing radiation (IR) for cancer patient treatment (Bernier et al., 2004). These advances allowed to maximize the efficiency of radiotherapy while lowering its adverse effects. Additionally, charged particle therapy has emerged as an alternative to X-ray or γ-ray irradiation, further improving radiotherapy efficiency. Even nowadays, radiotherapy remains one of the most frequently used treatment strategies because of its high cytotoxic effects on cancer cells as well as its immunogenic properties.

2.1 Physical aspects of radiotherapy

During the interaction between ionizing radiation and the electrons of target molecules, the energy deposition of photons and charged particles leads to the ejection of electrons from their orbitals and induces the ionization of target atoms and molecules. This way, highly reactive chemical compounds are formed, including reactive oxygen species (ROS). ROS cause the ionization of other molecules, including lipids, proteins and DNA leading to a catastrophic disruptions of normal cell functions such as metabolism and DNA replication (Figure 8) (Reisz et al., 2014). Additionally, DNA can be directly damaged by ionizing radiation. These physicochemical reactions induced by the interaction between radiation and matter eventually lead to the primary biological effects of radiotherapy.

2.2 Photon irradiation

Conventional radiotherapy uses energy in form of electromagnetic waves (X-ray or γ-ray) to destroy cancer cells. Unlike charged particles, when photons enter into matter, the energy deposition undergoes an initial increase, consistent with the maximal dose of radiation. From then on, the dose of radiation progressively decreases throughout the passage through the matter (Figure 9). As a result, when tumors are treated by conventional radiotherapy, the healthy tissue upstream of the tumor, on the radiation trajectory, absorbs relatively high doses of radiation compared to the tissue downstream the tumor on the same trajectory. Even though precise mapping of the lymphatic drainage as well as technical advances like three-dimensional conformal radiation therapy (3D-CRT) and intensity-modulated radiation therapy (IMRT), decrease the radiation dose absorbed by healthy tissue, further improvements remain to be made to reduce the adverse effects associated to radiotherapy (Schiller et al., 2016).

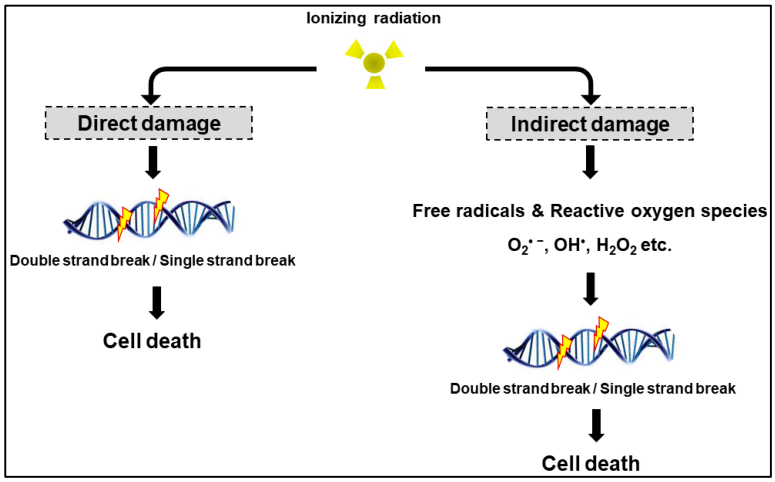

Figure 10. Direct and indirect DNA damage induction by ionizing radiation. (adapted from: W. Hur and S.K. Yoon., 2017)

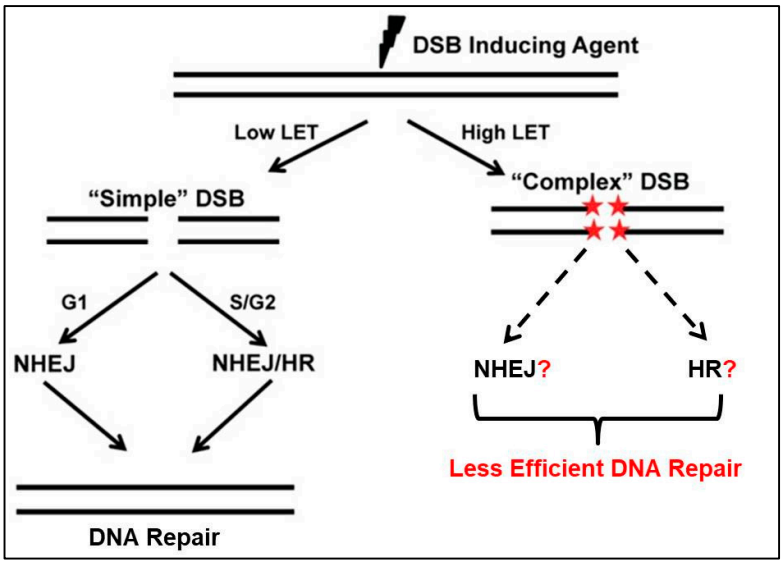

Figure 11. DNA damage induced by low LET and high LET radiation and associated repair mechanisms. (adapted from: Mohammed et al., 2017)

2.3 Charged particle irradiation

In case of charged particle irradiation, such as carbon ion or proton irradiation, the accelerated particles slow down once they entered the target matter, leading to a small energy deposition by the transfer of the particle kinetic energy to the target, called liner energy transfer (LET). At a certain point on their trajectory, depending on the initial energy of the particles, they rapidly slow down, delivering the majority of their energy at that specific point in space. The depth-dose profile distribution of charged particle irradiation, shows, depending on the initial particle energy, the depth at which occurs a maximal dose deposition, called the Bragg peak (Figure 9). This explains how irradiation of tumors by charged particles leads to very low irradiation of healthy tissue upstream the target and almost zero irradiation downstream of the target, compared to conventional radiotherapy. The use of proton and carbon ion irradiation therefore allows to use much higher radiation doses and a reduction of off-target irradiation (Schiller et al., 2016; Chen and Ahmad, 2012). Additionally, it has been shown that the relative biological effectiveness of charged particle irradiation, which compares the biological effectiveness compared to X-ray irradiation, especially that of carbon ions, reaches 2 or 3, further indicating advantages of charged particle irradiation over conventional radiotherapy in cancer treatment (Miller et al., 2013).

2.4 Chemical and biological effects of radiotherapy

2.4.1 DNA damage

Unlike most molecules inside a cell, there are only few copies of DNA and it is not continuously resynthesized, unless a cell undergoes mitosis. In addition, DNA plays a key role in most cell functions. Therefore, DNA damage induced directly or indirectly by IR has more significant long term consequences than for example the ionization of a lipid or mRNA molecule and can eventually lead to cell death (Figure 10). It has been shown that radiation LET determines the nature of DNA damage resulting from target irradiation. Indeed, the majority of DNA damage induced by photons is the result of indirect damage caused by the interaction with ROS, such as hydroxyl radicals and superoxide, produced by water molecule radiolysis (Reisz et al., 2014). These reactions mainly result in single strand breaks (SSB) of the DNA, which can subsequently give rise to simple double strand breaks (DSB), that present a widespread spatial resolution (Khanna, 2015). On the other hand, high LET radiation induces more complex clustered DNA double strand breaks (DSB) and this, primarily through direct DNA damage (Figure 11) (Lomax et al., 2013). While simple DSB usually are repaired by homologous endjoining (HEJ) during the S phase and by non-HEJ (NHEJ) during the G1 and S phase of the cell cycle, complex DSB induced by high LET radiation, protons for instance, cannot be repaired by NHEJ and are less efficiently repaired by HEJ (Wang et al., 2008; Rostek et al., 2008; Grosse et al., 2013), causing thereby more extensive damage to target cells.

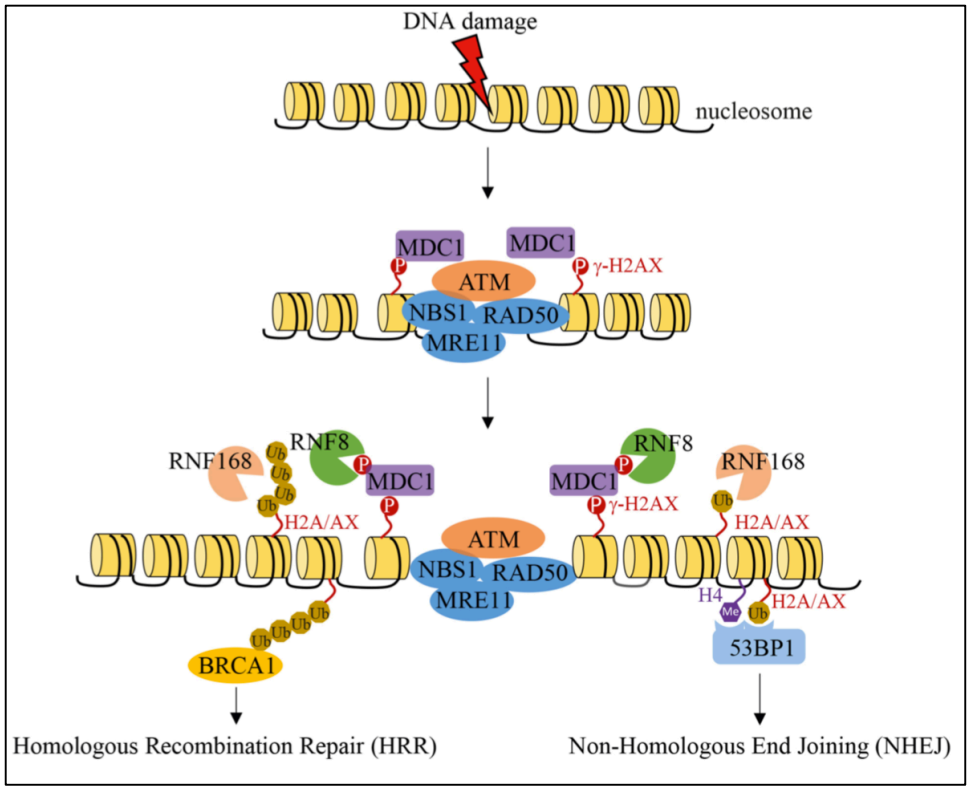

Figure 12. DNA damage response initiation. (adapted from: Lee at al., 2016)

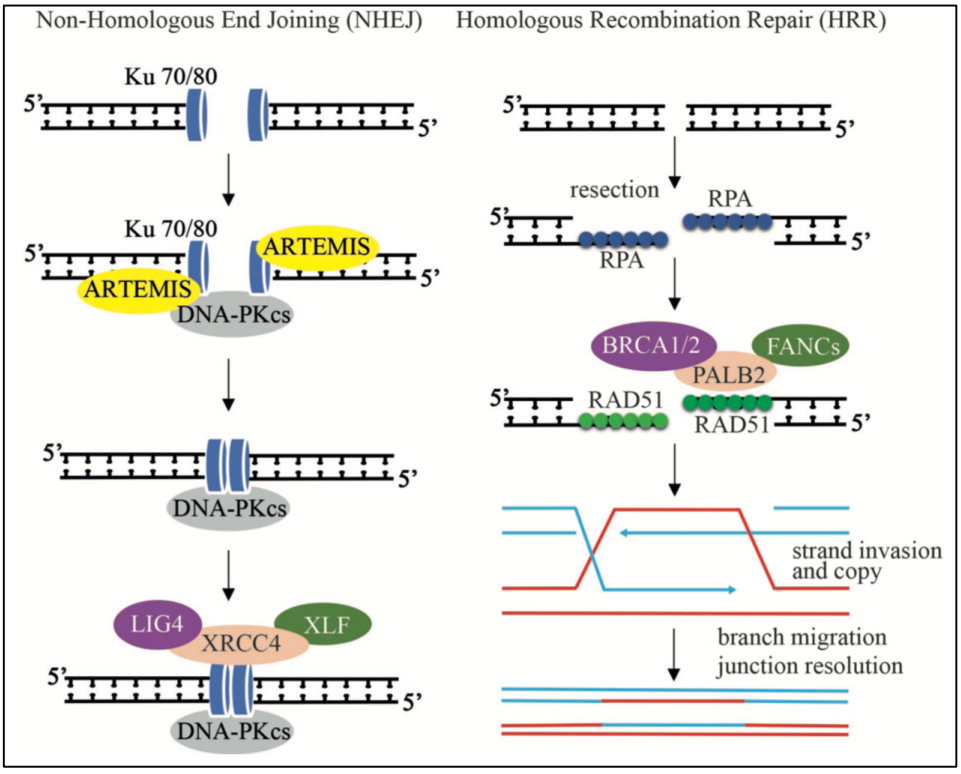

Figure 13. DSB repair mechanisms by HR and NHEJ. (adapted from: Lee at al., 2016)

2.4.2 DNA repair mechanisms

2.4.2.1 Damage response initiation

Once DSB occur, they are recognized by the MRN complex formed of the MRE11, RAD50 and NBS1 heterohexatrimer, which binds to the damaged site and recruits the kinase ataxia telangiectasia mutated (ATM) (William et al., 2010). Upon activation by auto-phosphorylation on serine 1981, the kinase ATM phosphorylates histone H2AX at serine 139 (γH2AX) at the damaged site. γH2AX is then recognized by MDC1, which will extend the H2AX phosphorylation. MDC1 recruits RNF8 and RNF186, which subsequently polyubiquitinylate the histone H2A leading to the recruitment of BRCA1 promoting DNA repair by homologous recombination (Figure 12). Methylated histones H2A and H2AX as well as monoubiquitinylated histones H2A and H2AX by RNF186 are bound by 53BP1, which favors DNA repair by NHEJ. p53 and Chk1 can also be recruited by MDC1 and γH2AX. Upon their activation by phosphorylation through ATM, these proteins induce cell cycle arrest, but if the damage becomes persistent, it can lead to apoptosis (Lee et al., 2016).

2.4.2.2 Non-homologous end joining

In case of NHEJ, the KU70/80 heterodimer binds to DNA at the site of the DSB protecting it from enzymatic degradation by DNA exonucleases and activation of the HE repair mechanism. KU70/80 recruits DNA PKcs, capable of phosphorylating downstream effectors. Depending on the length of the single strand ends at the break point, they can be either trimmed by the DNA exonuclease Artemis or filled by DNA polymerase μ or λ in order to obtain compatible ends at both sites of the break before being ligated by the XRCC4-Lig4-XLF protein complex (Figure 13) (Brandsma and van Gent, 2012; Lee et al., 2016).

2.4.2.3 Homologous end joining

Unlike the error-prone NHEJ, HEJ occurs only during the S and G2 phases of the cell cycle since it uses sister chromatids as template to insure a more reliable DNA DSB repair. The MRN complex bound to the site of the DSB further binds CtIP, which then recruits Exo1 to process the DNA to single strand ends. The RPA complex and hSSB1 bind to the single strand end and protect it from degradation until the recruitment of the BRCA2-RDA51 complex. This complex initiates the formation of the Holiday junction between the two sister chromatids, which are joined together by cohesion proteins, before DNA polymerase δ starts the repair of the damaged chromatid (Figure 13) (Borrego-Soto et al., 2015).

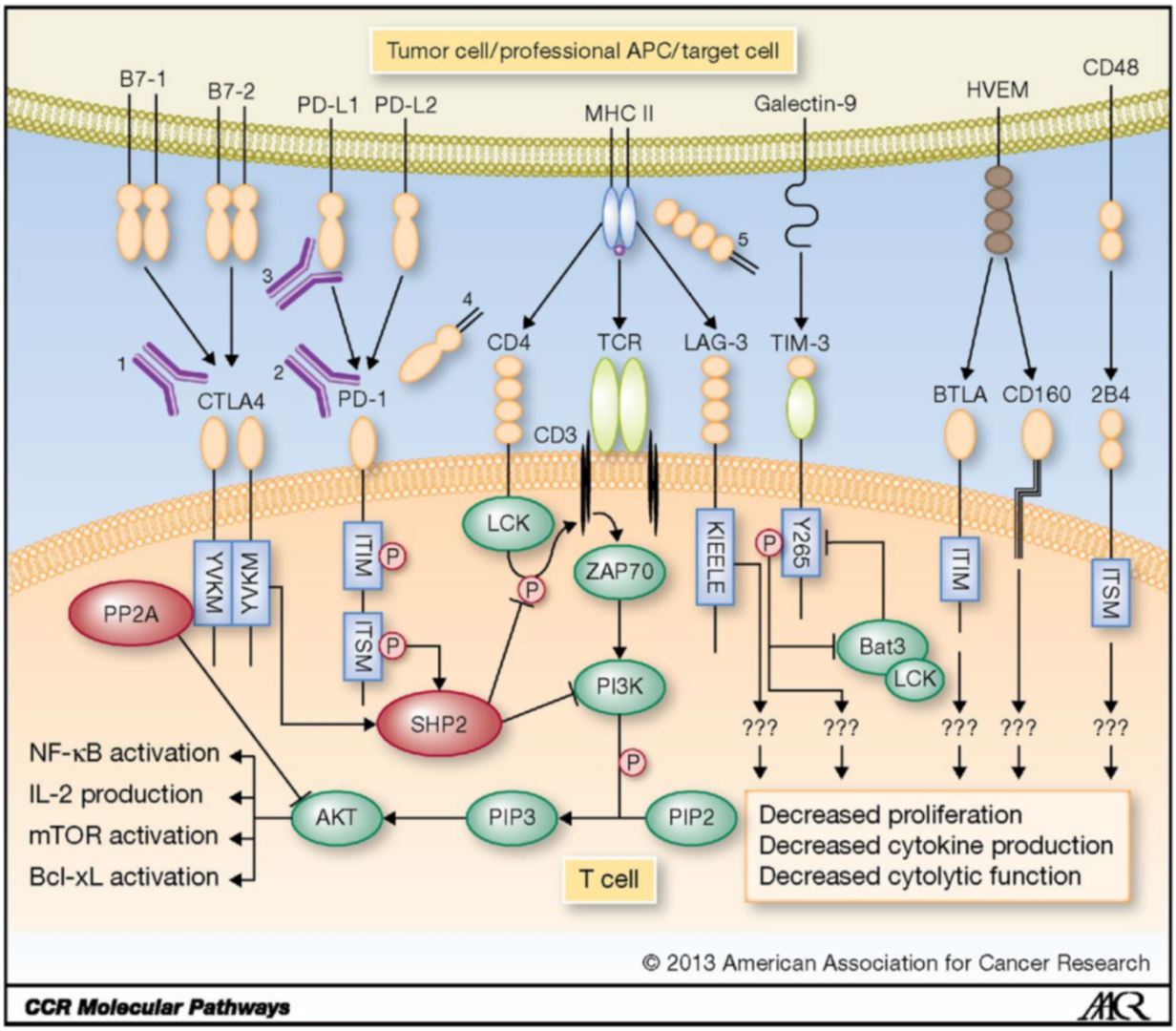

Figure 14. T cell activating and down-regulating pathways and therapeutics targets. Upon binding CD80 or CD86, CTLA-4 recruits the phosphatases SHP2 and PP2A via the YVKM motif on its cytoplasmic domain. SHP2 recruitment results in the attenuation of TCR signaling by dephosphorylating the CD3ζ chain. PP2A recruitment results in downstream dephosphorylation of AKT, further dampening the T-cell activation pathway. PD-1 ligation by PD-L1 or PD-L2 also recruits SHP2 to its ITSM domain, resulting in T cell signaling attenuation. (adapted from: Nirschl and Drank, 2013)

3 Cancer immunology

3.1 Tumor infiltrating lymphocytes

3.1.1 T cell activation

Within the tumor microenvironment (TME), T cells play an important role in detecting and destroying cancer cells by specific tumor antigen recognition. Immunogenic cancer cells lead to the maturation of dendritic cells (DCs), antigen processing and presentation to T cells. Unlike immature DCs, mature DCs additionally express high levels of costimulatory molecules and Major Histocompatibility Complex (MHC) (Kroemer et al., 2013). The presented antigens can be recognized by naive T cells through the T-cell receptor (TCR) and MHC recognition by CD4/CD8. Following the co-stimulation by the interaction between CD28 and CD80/CD86 (also called B7-1 and B7-2), lymphocyte activation pathways are engaged, which result in clonal expansion of effector T cells (Figure 14). This process, called T cell priming by DCs, allows T cells to destroy target cells upon antigen recognition by the TCR and CD4/CD8 binding to MHC II / MHC I, without the need of co-stimulation. This induces the activation of the tyrosine-protein kinases LCK and FYN, which phosphorylate the TCR-bound CD3-ζ chain. In addition, LCK phosphorylates the tyrosine-protein kinase ZAP70, which is subsequently recruited to the phosphorylated CD3-ζ chain. ZAP70 then phosphorylates LAT associated to GRB2, LCP2 and PLCγ1 and thereby activates multiple signaling pathways including MAPK, NFAT and CREB, involved in cell proliferation, differentiation, motility and interleukine-2 (IL-2) transcription. In case of co-stimulation by the interaction of CD80/CD86 and CD28, the activated LCK kinase further phosphorylates the intracellular domain of CD28, inducing the PI3K-AKT-mTOR and PI3K-PKCθ pathways resulting in NFκB and MKK7 activation, enhancing cell survival and proliferation but also favoring IL-2 transcription (Arasanz et al., 2017).

3.1.2 T cell effector functions

3.1.2.1 CD8+ T cells

After antigen recognition, cytotoxic CD8+ T cells are capable of inducing apoptosis of target cells through several mechanisms at the immunologic synapse. Similar to NK cells, activated cytotoxic CD8+ T cells secrete high amounts of perforin and granzymes B upon antigen recognition. These two proteins are then endocytosed by target cells. Endosome acidification induces perforation of the endosome by perforin, releasing granzymes B into the cytosol. This protease cleaves pro-caspase 3 to caspase 3 and Bid to tBid, inducing apoptosis of cancer cells. Activated CD8+ T cells also secrete tumor necrosis factor-α (TNF-α) which induces the extrinsic pathway of apoptosis, while interferon-γ (IFN-γ) secretion enhances macrophage polarization towards and M1-like phenotype and MHC-I as well as MHC-II expression. In parallel, FasL is expressed at the cell membrane of activated CD8+ T cells. This

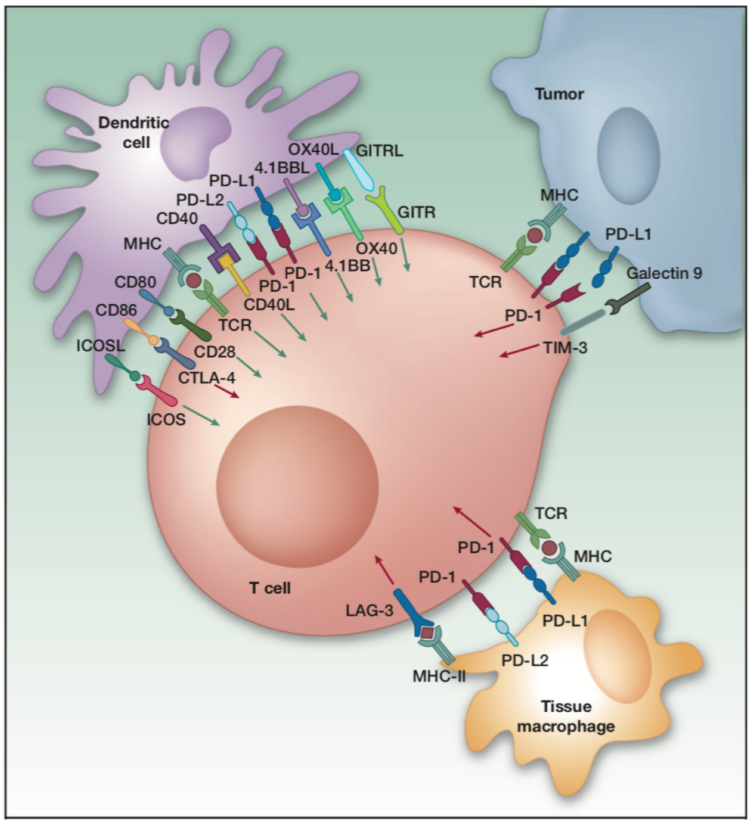

Figure 15. Costimulatory (green arrows) and coinhibitory (red arrows) ligand–receptor interactions between a T cell and a dendritic cell, a tumor cell, and a macrophage, respectively, in the tumor microenvironment. (adapted from: Ott et al., 2013)

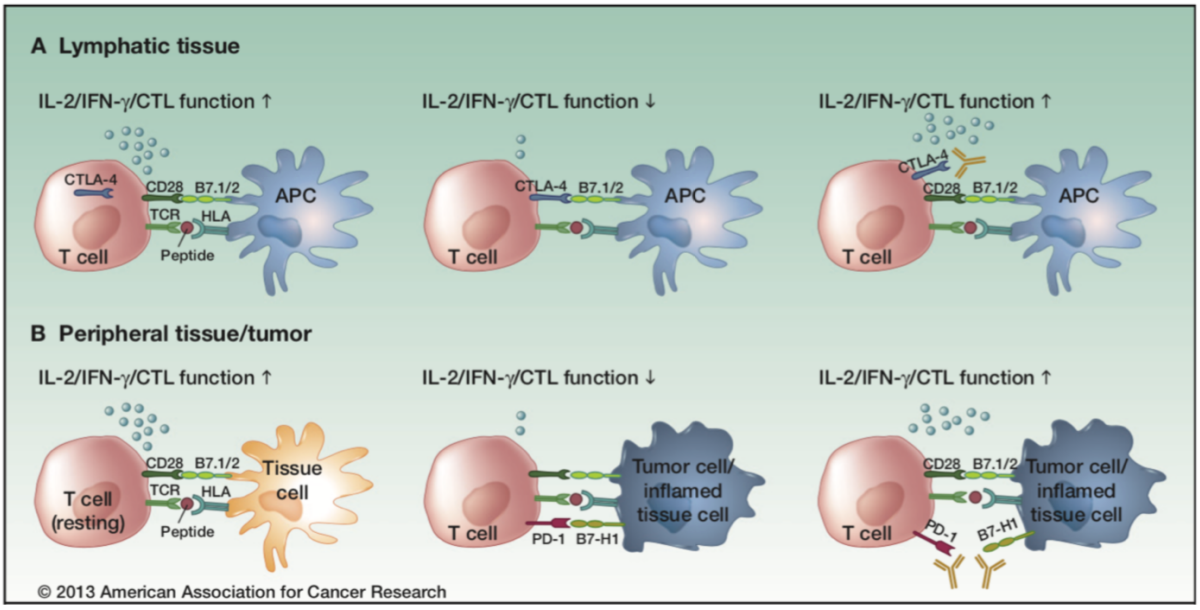

Figure 16. CTLA-4 and PD-1 modulate different aspects of the T-cell response: A, CTLA-4 is upregulated after antigen-specific activation of a T cell in lymphatic tissue, leading to decreased effector function (early activation phase). B, The immune modulation mediated by the PD-1 pathway ensures protection of tissue from collateral damage during an inflammatory response as well as auto-immune reactions. Certain cancer cells express the PD-1 ligands B7-1 (CD80), B7-2 (CD86) or B7-H1 (PD-L1) allowing them to exploit these regulatory mechanisms and evade a tumor-directed T-cell response. (adapted from: Ott et al., 2013)

protein binds to its receptor at the surface of target cells and induces death receptor-mediated apoptosis of cancer cells (Murphy and Weaver, 2016).

3.1.2.2 CD4+ T cells

Activated CD4+ T helper cells produce several immunostimulant cytokines including IFN- γ, TNF-ß as well as interleukins 2 and 10, which further favor macrophage activation and polarization towards a M1-like phenotype and CD8 + T cell activation, survival and clonal expansion. IFN-γ induces increased secretion of IL-12 in macrophages and DCs, which again increases IFN-γ production. This positive feedback loop promotes M1 polarization of macrophages as well as a T_h 1 profile over T_h 2 profile (Murphy and Weaver, 2016).

3.1.2.3 T cell evasion by cancer cells

3.1.2.3.1 Negative immune checkpoints

Cancer cells are capable of evading immune elimination by several mechanisms including the exploitation of negative immune checkpoints such as PD-1/PD-L1 and CTL-A4/CD80 or CTL-A4/CD86, which normally contribute to self-tolerance and avoid auto-immune reactions by interfering with the previously described T cell activation pathways (Figure 14; Figure 15). The interaction between PD-1 and CTLA-4 with their respective ligands leads to the recruitment and activation of SHP-1 and SHP-2, which decrease TCR signaling through the dephosphorylation of the CD3-ζ chain. In addition, these phosphatases inhibit PI3K and thereby the lymphocyte activation pathway downstream the TCR. Furthermore, CTL-A4 induction activates another phosphatase, PP2A, which acts downstream the TCR by inhibiting AKT and contributing to the inhibition of the lymphocyte activation (Nirschl and Drake, 2013). Considering that many cancer cells express PD-L1 and/or CD80/CD86, allowing them to prevent TIL activation and to escape immune elimination, the immunologic synapsis offers an interesting target for immune checkpoint blockage (Figure 16) (Gong et al., 2018).

3.1.2.4 Low immunogenicity

Upon selection by cytotoxic T cells during tumor growth, surviving cancer cells often present low level of immunogenicity and thereby avoid T cell priming by DCs, which results in immune evasion by the cancer cells. Several cancer therapies, such as platin-based chemotherapy, and radiotherapy in case of HNC, induce immunogenic cell death and thereby stimulate the immune reaction against cancer cells, in addition to their intrinsic cytotoxic functions (Kroemer et al., 2013).

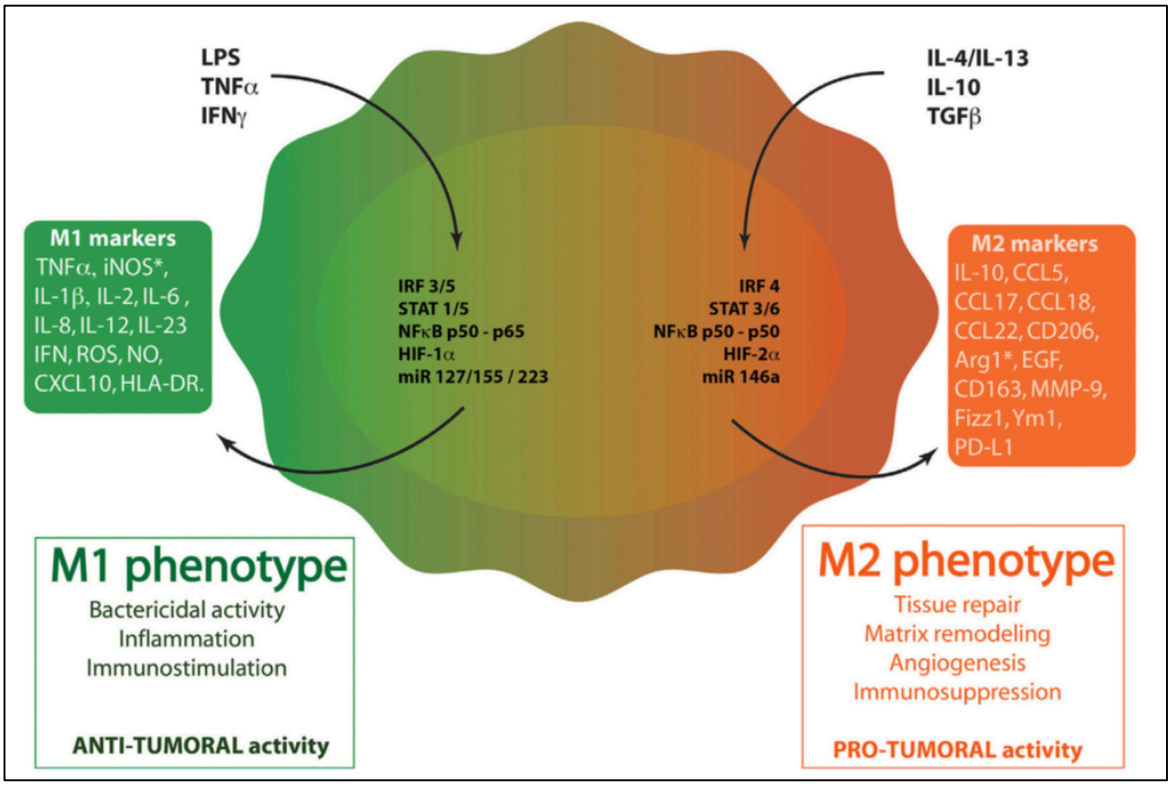

Figure 17. Macrophage polarization. Through the binding to their respective receptors, M1 stimuli LPS, TNFα, and IFNγ trigger the activation of several transcription factors, which include IRF/STAT family members IRF3, IRF5, STAT1, and STAT5, the active NFκ heterodimer p50–p65 and HIF1. miR127, miR 155, and miR223 also regulates M1 polarization. When polarized to M1-like phenotype, macrophages produce specific cytokines (TNFα, IL-1β, IL-2, IL-6, IL-12, IL-23, IFNγ), chemokines (CXCL10) and other molecules (ROS, NO, iNOS and HLA-DR). The M1 phenotype plays key roles in inflammation, immunostimulation and an antibacterial and antitumoral responses. M2 stimuli IL-4, IL-13, IL-10, and TGFβ bind to ILR4α, ILR10, or TGFβR to induce a M2-like phenotype in macrophages. These stimuli activate several transcription factors: IRF/STAT family members IRF4, STAT 3, and STAT6, the inhibitory NFκB homodimer p50–p50 and HIF2. miR14a also influences M2 polarization. When polarized in M2-like phenotype, macrophages produce specific cytokines (IL-10), chemokines (CCL5, CCL17, CCL18, CCL22), and other proteins (CD163, CD206, Arg1, MMP-9, Fizz-1, Ym-1, and PD-L1). M2 macrophages exert diverse functions, such as tissue repair, matrix remodeling, angiogenesis, immunosuppression, and favor tumor growth. (adapted from: Genard et al., 2017)

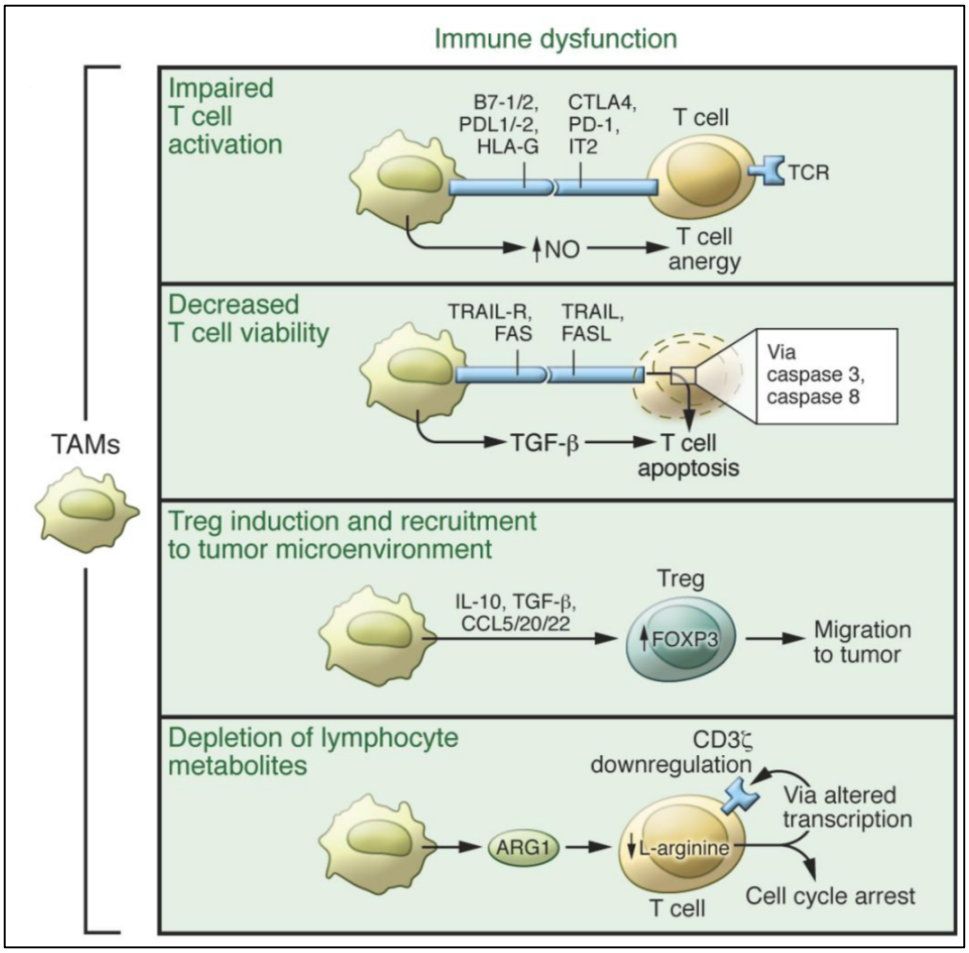

Figure 18. TAM-dependent mechanisms driving tumor progression. TAMs alter immune responses by four main mechanisms: 1) inhibition of T cell activation; 2) inhibition of T cell viability; 3) promotion of Treg induction and recruitment; 4) consumption of metabolites essential for T cell fitness. (adapted from: Ugel et al., 2015)

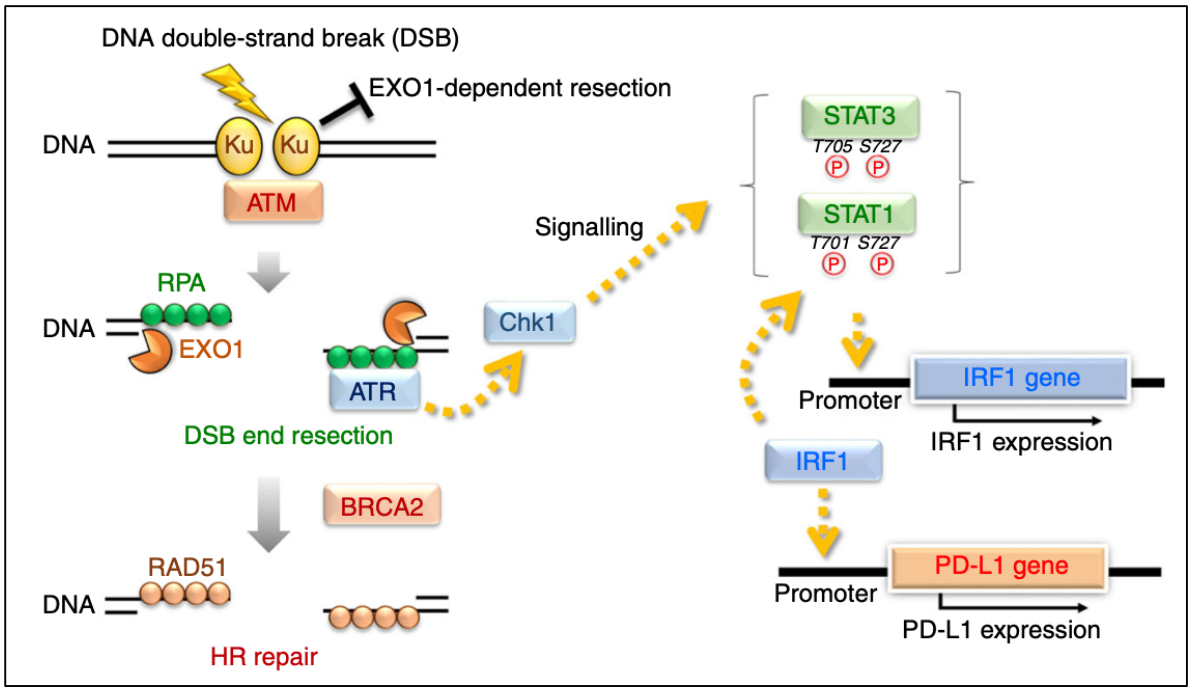

Figure 19. Radiation induced PD-L1 expression. (adapted from: Harris and Kranz, 2016)

3.2 Tumor-associated macrophages

Within the TME, the most predominant immune cells are tumor-associated macrophages (TAMs). The phenotype of TAMs is characterized by a high degree of plasticity following a polarization gradient between a M2 and a M1 phenotype (Figure 17). M1 macrophages are bactericidal, pro-inflammatory and capable of immunostimulation, while M2 macrophages possess anti-inflammatory, angiogenic and immunosuppressive properties (Genin et al., 2015; Genard et al., 2017). Cancer cells are often capable of polarizing TAMs towards and M2-like immunosuppressive phenotype, either through the secretion of specific cytokines such as IL-4, IL-13, TGF-ß, or by creating hypoxic areas within the tumor. TAMs are recruited through the action of chemoattractants such as CCL2, CXCL12, CSF1 and VEGFA (Green et al., 2009). They are able to interact with other cell types within the TME either by direct contact or via secretion products (Hanahan and Coussens, 2012). Cancer cells benefit from several of these interactions since M2-like TAMs are capable of impairing T cell activation (PD-L1/PD-1, CD80/CTLA-4, CD86/CTLA-4), inducing T cell apoptosis (Fas/FasL, TRAIL/TRAIL-R), recruiting and activating T regulatory cells (IL-10, TGF-β, CCL2) or depleting lymphocyte metabolites (L-arginine) and thereby contributing to immunosuppression (Figure 18) (Ugel et al., 2015; Wang et al., 2017).

4 Radiation-induced immune-modulation

4.1 PD-L1 upregulation

It has been shown that, in response to IR exposure, cancer cells present an increased PD-L1 expression, giving an opportunity of increased immune-checkpoint blockage sensitivity (Wu et al., 2016). Recent investigations determined for the first time that this irradiation-induced upregulation is mediated by the formation of double-strand breaks (DSBs) and subsequent ATM-ATR-Chk1 kinase activation (Figure 19) (Sato et al., 2017). Precise targeting of the PD-1/PD-L1 checkpoint in combination with optimally dosed and timed radiotherapy thereby represents a promising strategy in cancer therapy and turned out to be highly successful in some types of cancer (Deng et al., 2014; Bardhan et al., 2016).

4.2 Macrophage polarization

While cancer cells are capable of polarizing TAMs into a M2-like immunosuppressive phenotype, which favors cancer cell survival and the formation of metastasis, repolarizing macrophages from a M2-like (pro-tumoral) towards a pro-inflammatory M1-like (anti-tumoral) phenotype can be used to lower the immunosuppression in tumors and favor cancer cell eradication by the immune system. This repolarization toward a pro-inflammatory M1-like phenotype can be achieved by exposure to IR (Genard et al., 2017). Unlike attempts to

repolarize TAMs by chemicals, which is associated to significant side effects, radiotherapy possesses the advantage to act locally on the parts of the body where the tumor resides, thereby limiting collateral damage. The repolarization of macrophages from a M2-like to a M1-like phenotype has been observed at moderate doses by photon irradiation (Genard et al., 2017). Considering the ballistic advantages of proton irradiation in comparison to X-ray or γ-ray irradiation, recent studies investigated the TAM repolarization by protons. It was confirmed that, in vitro, proton irradiation is capable of polarizing macrophages towards an M1-like phenotype. Furthermore, NFκB signalling was determined as a primary driver during this repolarization process (Genard et al., 2018).

4.3 Immunogenic cell death

Although apoptosis was believed to be immunologically silent and tolerigenic, it has been reported that, as a result of cell stress, injury or dying, apoptosis can come along with the exposure or release of damage-associated molecular patterns (DAMPs). Several chemo-therapeutic agents like cisplatin as well as ionizing photon irradiation have been shown to be able to induce the exposure of DAMPs including calreticulin and heat shock protein 90 at the cell plasma membrane. Other DAMPs can be secreted, ATP and high mobility group protein B1 (HMGB1) for instance. Photon irradiation is therefore capable of triggering the exposure and secretion of DAMPs by cancer cells which can induce a potent anti-cancer immune reaction within the TME (Krysko et al.,2012).

Even though radiotherapy is one of the oldest cancer therapies, it still remains in constant evolution and contributes to the discovery and the improvement of new combined cancer therapies. By lowering immunosuppression through TAM repolarization from a M2-like towards a M1-like phenotype, triggering immunogenic cell death, directly destroying cancer cells in targeted areas and enhancing the efficacy of PD-1/PD-L1 checkpoint blockers, radiotherapy represents an important tool in cancer therapy through radiation-induced immune-modulation.

Objectives

The overall objective of this project was to determine mechanisms underlying the synergic effect of PD-1 ICB and radiotherapy using X-ray irradiation. Since we hypothesized that the synergic effect of anti-PD-1 ICB and X-ray irradiation on HNSCC is mediated by optimal PD-1 ICB administration depending of PD-L1 expression following irradiation and by X-ray-induced TAM repolarization, we focused our attention on the radiation-induced induction of PD-L1 expression and the radiation-induced TAM repolarization.

The first objective of this project was to determine *in vitro* the effects of X-ray irradiation on PD-L1 expression in two human and one murine HNSCC cell lines at different radiation doses and at different timings post-irradiation. The expression of PD-L1 was assessed at mRNA level by RT-qPCR and at protein level by immune-fluorescence labelling. Flow cytometry was then performed to determine the relative PD-L1 induction at cell membrane.

In order to additionally assess PD-L1 expression in THP-1-derived M1 and M2 macrophages, successful macrophages polarization needed to be performed. This was evaluated by measuring the expression of several polarization markers by RT-qPCR. Then *PD-L1* expression was also assessed by RT-qPCR at different doses of X-ray irradiation and at different timings post-irradiation.

Considering the advantages of new radiotherapy techniques such as proton therapy, we also started the study of the immuno-modulatory effects of proton irradiation by assessing PD-L1 expression at mRNA level in one HNSCC cell line at several timings post-irradiation of proton irradiation by different doses.

To investigate the efficiency and the underlying mechanisms of the combined treatment of anti-PD-1 ICB and X-ray irradiation in a model of HNSCC, we had to set up a syngenic mouse model of HNSCC, that allows the assessment of treatment efficiency. **Treatment efficacy was defined by the increase in activation levels and the decrease in exhaustion levels of tumor infiltrating cytotoxic T cells**. Tumor immune-infiltration was thus analyzed by histologic analyses and specific cell isolation techniques needed to be developed. In addition, to verify our hypothesis that X-ray-induced TAM repolarization plays a major role in the synergic effect of the combined treatment, the model also needed to allow TAM isolation and the assessment of TAM polarization, considering technical limitations such as the very limited number of polarization markers that can be assessed by flow cytometry.

Once the syngenic mouse model of HNSCC was set up, the last objective of the project was to assess the role of X-ray irradiation and anti-PD-1 ICB play in the combined treatment. This for, mice were divided into treatment groups of untreated mice, mice treated by X-ray irradiation, mice treated by anti-PD-1 ICB and mice receiving the combined treatment. For each group, tumor infiltrating cytotoxic T cell activation and exhaustion have been assessed in parallel to TAM polarization.

The results of this work should lead to the setup of parameters allowing an optimized combination of radiotherapy and the ICB.

Materials and methods

1 Cell culture

Cal27 (human tongue squamous cell carcinoma, ATCC) and SQD9 (human laryngeal squamous cell carcinoma, a generous gift from Prof. Pierre Sonveaux, UCL) cells were maintained in culture in 75 cm^2 polystyrene flasks (Corning), in 15 mL and 18 mL of Minimum Essential Medium (MEM-GlutaMAX, Gibco) respectively, supplemented with 10% fetal bovine serum (FBS, Thermo Fisher Scientific) at 37°C and 5% CO_2.

SCC-VII (murine oral cavity squamous cell carcinoma, a generous gift from Prof. Olivier Feron, UCL) cells were cultured in 150 cm^2 polystyrene flasks (Corning), in 45 mL of Minimum Essential Medium (MEM-GlutaMAX, Gibco), supplemented with 10% fetal bovine serum (FBS, Thermo Fisher Scientific) at 37°C and 5% CO_2.

THP-1 (transformed human peripheral blood monocytes, ATCC) cells were cultured in 75 cm^2 polystyrene flasks (Corning) at 37°C and 5% CO_2 using Roswell Park Memorial Institute 1640 Medium (RPMI) + L-Glutamine (Gibco) supplemented with 10% heat inactivated serum (HIS), 10 mM 4-(2-hydroxyethyl)-1-piperazineethanesulfonic acid (HEPES), 10 mM pyruvate, 2.5 g/L glucose and 50 nM ß-mercaptoethanol (supplemented RPMI medium).

L-929 murine fibroblasts were cultured in in 150 cm^2 polystyrene flasks (Corning) at 37°C and 5% CO_2 using Dulbecco's Modified Eagle's Medium high glucose (DMEM high Glucose, Gibeco) supplemented with 10 mM pyruvate. To obtain L-929-conditioned medium, 500 000 cells were seeded in 75 cm^2 polystyrene flasks (Corning) containing 20 mL of supplemented medium. After 6 days, the supernatant was collected and frozen at -20°C for two months maximum.

2 Cell counting

Cal27, SQD9 and SCC-VII cells were washed with sterile phosphate-buffered saline (PBS), then trypsinized. Cells were suspended in 10 mL of medium, collected in a 15 mL Falcon tube and centrifuged during 5 min at 1000 rpm. After removing the supernatant, the cell pellet was resuspended in 10 mL of MEM-GlutaMAX medium + 10% FBS. After homogenizing the suspension, 10 µL were mixed with 10 µL of Trypan Blue inside a 1mL tube. 10 µL of this mix were placed in a EVE™ cell counting slide and analyzed by an automated cell counter (Countess™ Invitrogen). This counting was repeated two times and the average count of viable cells was calculated.

THP-1 cells are non-adherent cells and can directly be collected in a 15 mL Falcon tube, then centrifuged during 7 min at 1000 rpm. The following of the procedure was identical to the one described for Cal27 and SQD9 cells.

L-929 murine fibroblasts were washed with sterile phosphate-buffered saline (PBS), then trypsinized. Cells were suspended in 10 mL of DMEM medium, collected in a 15 mL Falcon tube and centrifuged during 5 min at 1000 rpm. After removing the supernatant, the cell pellet was resuspended in 10 mL of DMEM medium + 10% FBS. After homogenizing the suspension, 10 µL were collected and placed on a Neubauer cell for manual cell counting.

3 Macrophage polarization

To differentiate THP-1 cells into M0 macrophages, cells were seeded in 6-well-plates (Corning) at a density of 800 000 cells/well (1 600 000 cells/well for the irradiation) in 3 mL/well supplemented RPMI medium containing 150 nM phorbol 12-myristate 13-acetate (PMA). 24 h later, the wells were washed with sterile PBS. Cells were then incubated in 3 mL/well supplemented RPMI medium (without PMA). After 24 h, the medium was replaced by fresh supplemented serum-free RPMI medium containing 20 ng/mL IL-13 and IL-4 for M2 polarization (during 48 h) or 10 pg/mL LPS and 20 ng/mL IFN-γ for M1 polarization (during 24 h) (Genin et al., 2015).

Murine bone-marrow cells were isolated from femur diaphysis extracted from mice and maintained in culture in 10 cm^2 Petri dishes (Corning) at 37°C and 5% CO_2 in 8 mL of Dulbecco's Modified Eagle's Medium (DMEM, Gibco), supplemented with 10% HIS and 1% penicillin/streptomycin. After 24 h incubation, the medium containing non-adherent cells was collected and transferred into a new 10 cm^2 Petri dish (Corning). The medium was then supplemented by 10% of L-929 murine fibroblast-conditioned medium to induce cell adhesion and differentiation into macrophages. After a 72 h incubation at 37°C and 5% CO_2, the medium was replaced by 8 mL of fresh DMEM medium, supplemented with 10% FBS and 10% L-929-conditioned medium for a 48 h incubation. The medium was then again replaced by fresh DMEM medium, supplemented with 10% FBS and 10% L-929-conditioned medium for a 48h incubation. At this stage, the differentiated bone marrow-derived macrophages (BMDMs) were either frozen at -80 °C in 90% HIS and 10% dimethyl sulfoxide (DMSO) or polarized into M1 macrophages by 24 h incubation in DMEM medium + 10 % HIS + 10 ng/µL lipopolysaccharide (LPS) + 20 ng/µL murine IFN-γ or M2 macrophages by a 24 h incubation in DMEM medium + 10 % HIS + 20 ng/µL murine IL-4 + 20 ng/µL murine IL-13.

4 X-ray irradiation

For downstream RNA extraction, Cal27, SQD9 and SCC-VII cells were seeded in 6-well plates (Costar) at a density of 250 000 cells/well and THP-1 cells at 1 600 000 cells/well. For downstream flow cytometry and western blot analysis, Cal27, SQD9 and SCC-VII cells were seeded in 25 cm^2 polystyrene flasks (Corning) at a density of 520 000 cells/flask. 12 h after Cal27, SQD9 or SCC-VII cell seeding or at the completion of macrophage polarization, cells were irradiated at 0, 2, 5, 10 or 15 Gy doses using the X-RAD 225XL/Xli X-ray generator

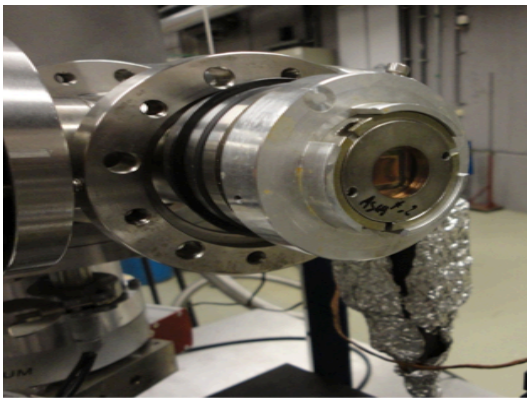

Figure 20. The irradiation chambers are composed of two stainless steel pieces covered by a mylar foil.

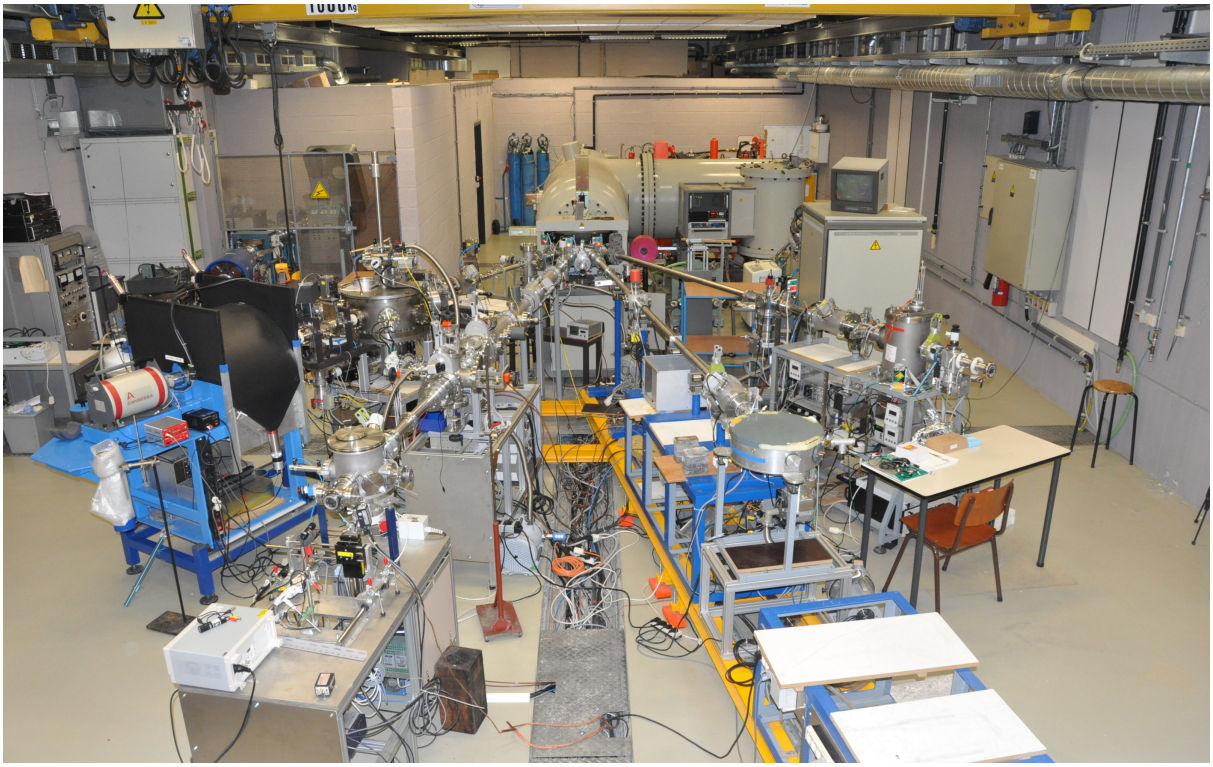

Figure 21. Picture of the accelerator.

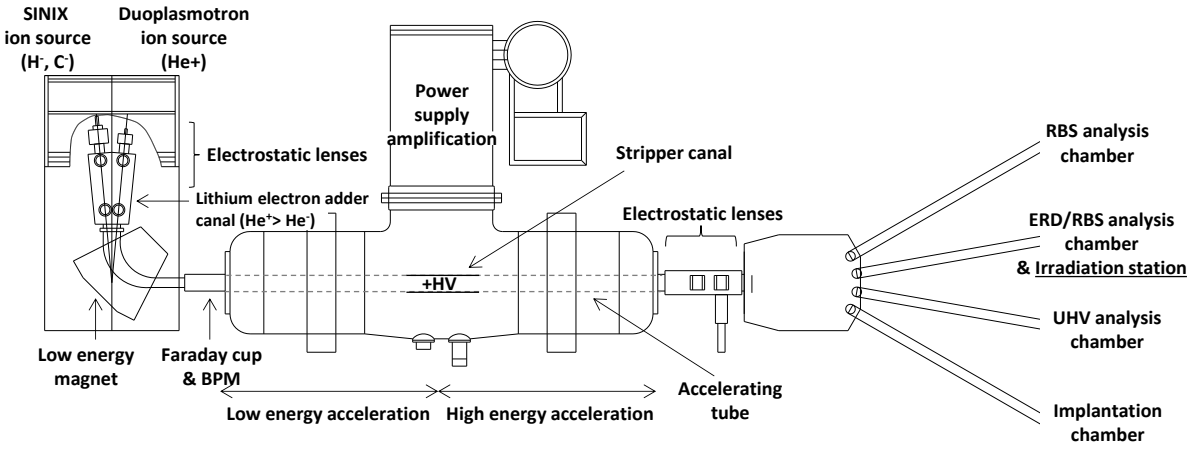

Figure 22. Schematic representation of the ALTAIS accelerator.

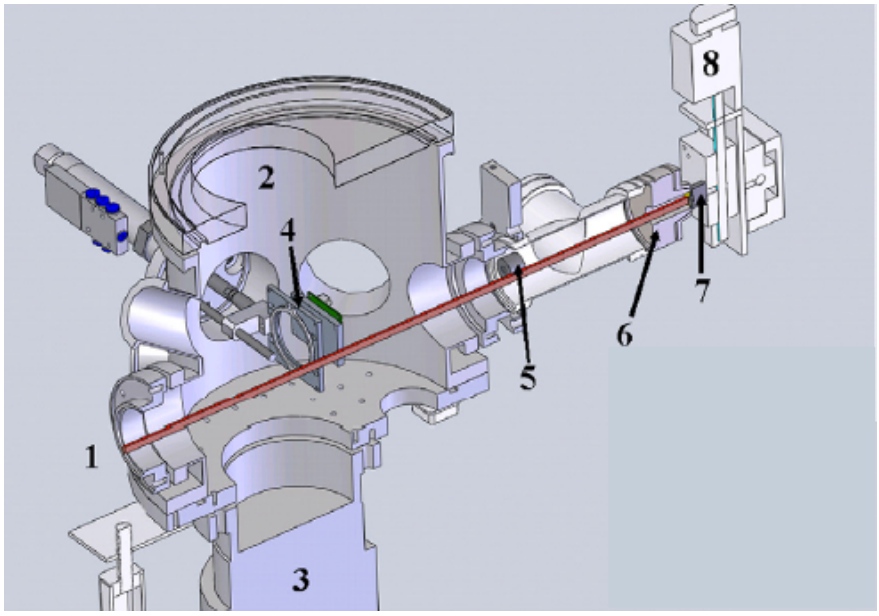

Figure 23. The cell irradiation station is equipped with a charged-couple device (CDD) camera, a passivated implanted planar silicon (PIPS) detector and a plastic scintillator BC-400. The XY motorized table allows the cartography of the beam in order to evaluate its homogeneity. (1) H+, He2+, C4+ broad beam; (2) vacuum chamber; (3) pumping system; (4) BC400 scintillator + CCD camera fixed on a pneumatic jack; (5) PIPS detector placed on the left side of the beam for the dose-rate monitoring; (6) irradiation head; (7) movable PIPS detector; (8) XY motor (Wéra et al., 2011).

(PXI Precision X-ray). To obtain these doses, the generator was programmed at 225 kV and 13.6 mA, a 2 mm aluminum filter was added to the collimator and the table was positioned at a distance of 50 cm beneath the source. These settings allow to obtain a dose rate of 2 Gy/min. Depending on the dose that was to be delivered, the duration of the irradiation was programmed to 0, 60, 150, 300 or 450s. A digital real-time dosimeter (PTW UNIDOS E) was used to monitor the dose rate during the irradiation.

5 Proton irradiation

Irradiation chambers are composed of two stainless steel pieces, covered by a 3 µm thick mylar foil. The bottom and top parts make a sealed irradiation chamber thanks to a sealing joint. The irradiation procedure allows the production of a homogeneous broad beam of 1 cm^2, placed at the center of the irradiation chamber (2 cm diameter) (Figure 20). In order for SCC-VII cells to adhere to the mylar foil, the center of the foil was coated with fibronectin during 40 min at 37 °C. 50 000 cells were seeded in a 35µL drop of MEM medium supplemented with 10% of FBS and 1% penicillin/streptomycin on the fibronectin-coated surface. The irradiation chambers are incubated at 37°C for 5 h. The filling of the irradiation chambers (2 ml of supplemented medium) was made by one of the two holes located on the side, using a syringe. For the irradiation step, it is important to have a homogeneous monolayer of cells because the initial energy (1.3 MeV) of particles is not high enough to go through several layers of cells. In addition, this initial energy was determined to localize the Bragg Peak (LET = 25 keV/µm) and thereby the maximal relative biological effectiveness (RBE) into the nucleus of cells. Therefore, cells outside the field would not be irradiated. In order to irradiate the cells, the irradiation chambers containing the cells were placed on one of the four exit lines of the 2 MV accelerator (High Voltage Engineering Europa, ALTAIS), available at the LARN laboratory (University of Namur) (Figure 21). ALTAIS (for "Accélérateur linéaire Tandétron pour l'Analyse et l'Implantation des Solides") allows the acceleration of ions from light weight (such as hydrogen) to heavy ones (such as uranium). A H+ homogenous broad beam from a TiH_2 860 source was used for the proton irradiation of SCC-VII cells. In more details, positive cesium steams sputter the TiH_2 source and negatively ionize the hydrogen contained into the source. A plasma is thus created and the negative ions are extracted with a negative tension. The ions are then selected with a low energy magnet and accelerated in two times through a Tandetron accelerator (tandem acceleration). Indeed, negative ions are attracted by a high positive tension localized at the middle of the accelerator tube and undergo a first acceleration. In the middle of the accelerator tube, nitrogen, released by a stripper canal, elicits charge changes, making positive ions. H+ ions are then repulsed by the high positive tension and undergo a second acceleration. Finally, the accelerated ions are deflected with a high-energy magnet to the desire beam line. In our experiments, the left 10° beam line was used (Figure 22). Thanks to tools such as Bip Profil Monitor (BPM), the shape and the intensity of the beam were adjusted before and after the acceleration of particles, by playing on parameters such as the position of electrostatic lenses. Once the shape of the beam was adjusted, the homogeneity was tuned with a camera and detectors localized in the cell irradiation station (Figure 23), placed at the end of the beam line. The cell irradiation station consists of a vacuum chamber with a charge-coupled

device (CCD) camera, that was used to shape the beam and to acquire a homogeneous beam. Passivated Implanted Planar Silicon (PIPS) detectors were placed before and after the cell irradiation station. They were used to tune the dose rate and to help ensuring the homogeneity and the stability of the proton beam (Figure 23) (Wéra A.-C., 2011). The H^+ broad beam was thus homogeneous over 1 cm^2 and went through a 1 µm thick Si_3N_4 exit foil. All these adjustments require several hours of settings before cell irradiation. The dose rate was fixed to 2 Gy/min for the irradiation of SCC-VII cells.

6 Total RNA extraction and RT-qPCR

The medium was removed from the 6-well plates and cells were lysed using 350 µL of RLT Lysis Buffer (Qiagen) and subsequent scrapping. Total RNA extraction from the lysates was performed using the RNeasy Mini Kit + DNAse (Qiagen) and the QIAcube device (Qiagen) following the supplier's protocol.

After the extraction, the total RNA was either stored at -80°C or directly processed. RNA concentration was assessed using the ND-1000 Spectrophotometer and the Nanodrop 1000 software (Isogen Life Science). Then, the appropriate volume was collected to contain 2 µg of RNA and reverse transcription was performed using the GoScript™ Reverse Transcription Mix, Oligo(dT) (#A2791, Promega) and the related instructions.

The cDNA was stored at -20°C or immediately diluted for subsequent qPCR analysis. cDNA from Cal27 and SQD9 cells was diluted at a ratio of 1:100 and cDNA from macrophages 1:20 using ultrapure miliQ water. The amplification reaction mix contained 62.5% SYBRGreen PCR Master Mix (#4309155, Applied Biosystem) and 375 nM primers (Table 1). 16 µL of this mix were added in each well of a 96-well plate (Thermo Fisher Scientific) to 4 µL of cDNA. The plate was sealed, centrifuged during 1 min at 1200 rpm and analyzed by a ViiA™ 7 Real-Time PCR System (Thermo Fisher Scientific). Thermal cycling was based on an initial denaturation step at 95°C for 5 min followed by 40 cycles at 95°C for 30 sec and 60°C for 1 min.

Gene	Supplier	Forward Primer	Reverse Primer
h_23kDa	IDT	GCCTACAAGAAAGTTTGCCTATCTG	TGAGCTGTTTCTTCTTCCGGTAGT
h_CCL22	IDT	CACTTCTACTGGACCTCAGAC	AGTAGGCTCTTCATTGGCTCA
h_CD206	IDT	GCTAAACCTACTCATGAATTACTTACAACAA	GAAGACGGTTTAGAAGGGTCCAT
h_IL-10	IDT	CTGGAAACATCTGGAGAGAGGAA	GTAGATGCCTTTCTCTTGGAGCTTA
h_IL-6	IDT	CCTGAACCTTCCAAAGATGGC	CACCAGGCAAGTCTCCTCATT
h_IL-8	IDT	TCTGTGTGAAGGTGCAGTTTT	GGGGTGGAAAGGTTTGGAGTA
h_PD-L1	IDT	GACATGTCAGGCTGAGGG	TCCTCTCTCTTGGAATTGGTGG
h_RPS9	IDT	CTGGATGAGGGCAAGATGAAG	GTCTGCAGGCGTCTCTCTAAGAA
h_TGF- β1	IDT	AGGGCTACCATGCCAACTTCT	CCGGGTTATGCTGGTTGTACA
h_TNF- α	IDT	TTGATCCCTGACATCTGGAATCT	CTGGAAACATCTGGAGAGAGGAA
m_PD-L1	IDT	GCTCCAAAGGACTTGTACGTG	TGATCTGAAGGGCAGCATTTC
m_23kDa	IDT	GAGGTCGGGTGGAAGTACCA	TGCATCTTGGCCTTTTCCTT

Table 1 : Primers used for qPCR

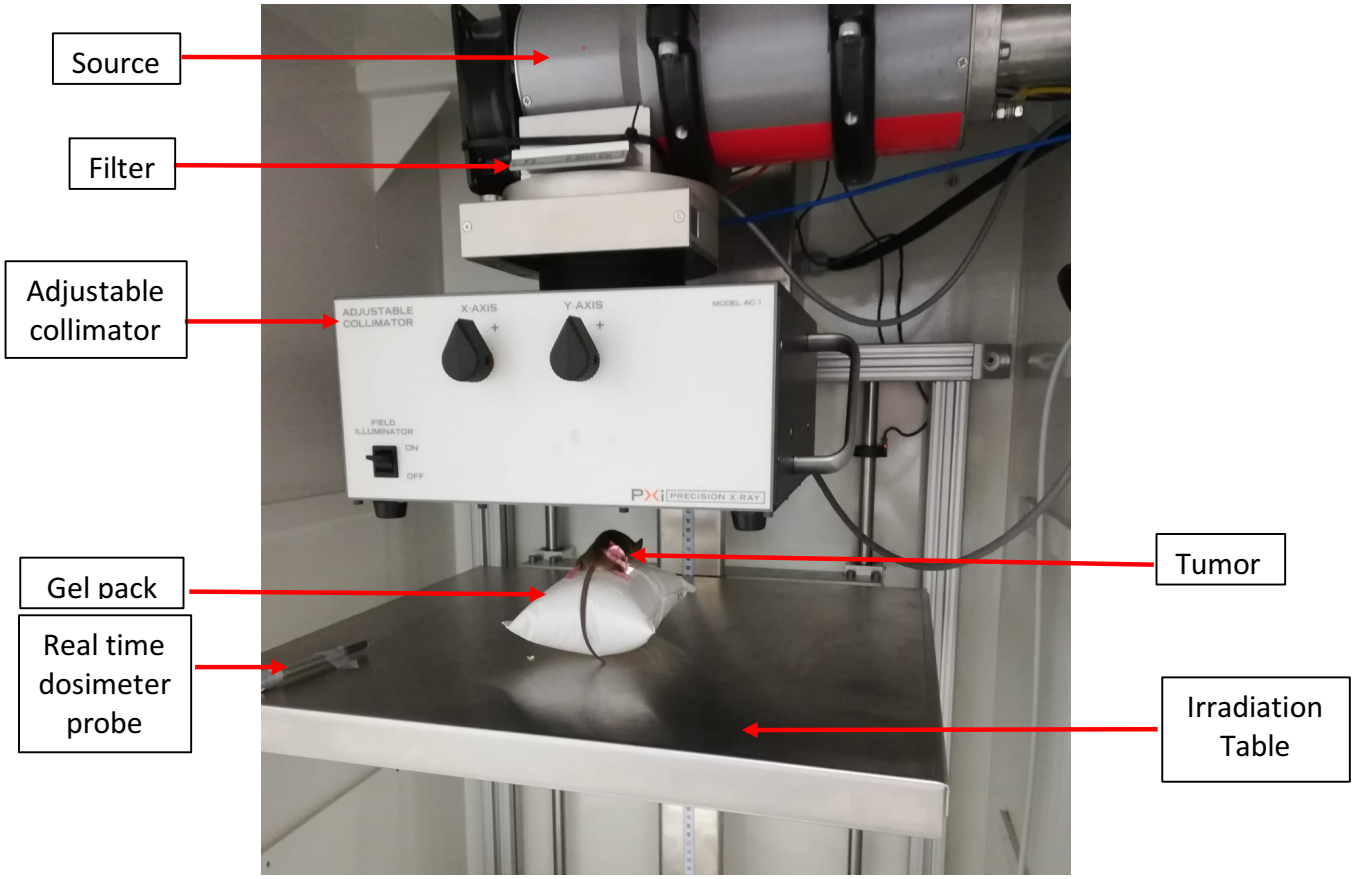

Figure 24. X-ray irradiation of tumor bearing mice. The irradiation table is placed at 40 cm believe the source. The mice were place n prone position on a 5 cm thick gel pack placed on the irradiation table and an adjustable collimator used for X-ray beam focalization.

7 Immunofluorescence labeling and confocal microscopy

Cal27 and SQD9 cells were seeded at 30 000 cells/well in 24-well plates containing a glass coverslip. Cells were fixed during 15 min with paraformaldehyde 4% in PBS at room temperature and then permeabilized with ice cold pure methanol for 10 min at -20°C. Cells were rinsed one time with PBS for 5 min and blocked by a blocking buffer (1X PBS + 5% normal serum + 0.3% Triton™ X-100) during 60 min. Cells were then incubated overnight at 4°C with the primary antibody (Table 2). Primary antibodies were 1:200 (PD-L1) diluted in PBS + 1% BSA + 0.3% Triton X-100. Cells were rinsed three times with PBS for 5 min each and then incubated for 1.5 h with secondary antibody 1:1000 diluted (Anti-Rabbit IgG (H+L), F(ab')2 Fragment (Alexa Fluor® 488 Conjugate) #4412) at room temperature. After washing the cells three times with PBS, nuclei were stained with TOPRO-3 (1:80 diluted in RNAse solution). Cells were then washed three times with PBS. The coverslips were mounted using Mowiol (Sigma) and cells were observed with a confocal microscope (SP5, Leica).

Protein	Primary antibody	Secondary antibody
PD-L1	Anti-PD-L1 (D8T4X) (Rabbit, Cell Signaling Technology #86744, 1/1000)	Anti-rabbit-Alexa 488 nm (Goat, Thermo Fisher Scientific A-11008, 1/1000)

Table 2. Antibodies used for immunofluorescence labeling

8 Mouse model and in vivo experimentation

Sixty-seven 6 weeks old C3H/HeN mice were purchased from Charles River Laboratories (Brussels, Belgium). Housing, maintenance and experimentation were performed according to the regulations approved by the local ethics committee for animal experiments of the University of Namur (AR 18/326, Appendix 1 and 2). After a 1 week resting period, mice were anesthetized by isoflurane inhalation (2.5%, Zoetis), their right flank shaved and disinfected before receiving the injection of SCC-VII cancer cells (number adjusted to the experimental group, as detailed in Appendix 1 and 2) subcutaneously in a total volume of 150 µL of PBS. After reaching a final tumor volume of 250 mm^3 or 350 mm^3 depending on the experimental group (Appendix 1 and 2), mice were anesthetized by intra-peritoneal injection with Ketamine 100 mg/kg (Dechra) and Xylazine 10 mg/kg (VMD Livestock Pharma) and placed in prone position on 5 cm thick heated gel packs located on top of the irradiation table (Figure 24). To irradiate the tumors with a dose of 10 Gy, the generator was programmed at 225 kV and 14.5 mA, a 5 mm copper filter was added to the collimator and the table was positioned at a distance of 40 cm beneath the source. These settings allow to obtain a dose rate of 2 Gy/min. An adjustable collimator was added at the exit of the source, to focalize the radiation beam on the tumor (Figure 24). Mice were irradiated during 300 s to deliver a dose of 10 Gy. After the irradiation, depending on the experimental group, mice were injected with 10 mg/kg of anti-PD-1 antibodies i.p. (#114114, Biolegend). 72 h after the injection, mice were anesthetized by an i.p. injection of 100 mg/kg Ketamine (Dechra) and 10 mg/kg Xylazine (VMD Livestock Pharma) and euthanized by cardiac puncture followed by cervical dislocation. The tumors were then resected as well as the spleen, the abdominal lymph node in proximity

to the tumor, distant lymph nodes in the axillary and mandibular region as well as both femur diaphysis.

9 Tumor dissociation – TIL and TAM isolation

Tumors were dissociated with the tumor dissociation kit (#130-096-730, Miltenyi Biotec) and the gentleMACS octo dissociator with heaters (Miltenyi Biotec) following manufactor's instructions. The single cell suspension was then filtered on a 70 µm smartStainer (#130-098-462, Miltenyi Biotec), collected in a 15 mL Falcon tube and centrifuged at 300g 4 °C for 7 min. Cells were resuspended on ice by cold PBS supplemented by 2 mM EDTA and 0.5% BSA (MACS buffer). A 1 mL sample was taken to perform automated cell counting as prescribed previously. The cell suspension was centrifuged at 300g 4 °C for 7 min. and resuspended in 90 µL of MACS buffer per 10^7 cells. Per 10^7 cells, 10 µL of CD8 TIL microbeads (#130-116-478, Miltenyi Biotec) were added and the cell suspension mixed before 15 min incubation at 4°C. 500 µL of MACS buffer were added per 10^7 cells. A LS column (#130-042-401, Miltenyi Biotec) was placed in the magnetic field of the MACS multistand separator (1130-042-303, Miltenyi Biotec) and washed by 3 mL of MACS buffer. A 30 µm smartStainer (#130-098-458, Miltenyi Biotec) was placed on top of the LS column and the cell suspension dropped on the smartStainer. The column was rinsed twice by 1 mL of MACSbuffer, before removing the CD8- fraction. The LS column was removed from the magnetic field, placed on a new 15 mL falcon and flushed by 3 mL of MACSbuffer using the piston associated to the column. The CD8+ fraction was put on ice, while the CD8- fraction was centrifuged at 300 g 4°C for 7 min., resuspended in 90 µL of MACS buffer per 10^7 cells and added by 10 µL of anti-F4/80 TAM microbeads (##130-110-443, Miltenyi Biotec). This mix was incubated for 15 min at 4°C, then added with 2 mL of MACS buffer and centrifuged at 300g 4°C for 7 min. The labeled cells were resuspended in 500 µL of MACS buffer per 10^7 cells and isolated on a new LS column as previously described.

10 Flow cytometry

CD8+ TILs, F4/80+ TAMs, CD8- F4/80- tumor cells and SCC-VII cells were centrifuged at 300g 4 °C for 10 min. CD8+ TILs were resuspended in 74 µL of MACS buffer and labeled by 2 µL CD45-APC-Vio770, 10 µL CD3-VioBlue, 2 µL CD8-PE-Vio770, 10 µL CD25-VioBrightFITC, 2 µL CD69 and 2 µL PD-1 (Table 4). F4/80+ TAMs were resuspended in 80 µL of MACS buffer and labeled by 2 µL CD45-VioBlue, 2 µL F4/80-APC, 2 µL CD11b-VioBirghtFITC 10 µL Ly6G-PE-Vio770, 2 µL Ly6C-PE and 2 µL MHC-II-APC-Vio770 (Table 4). CD8- F4/80- tumor cells and SCC-VII cells were resuspended in 97 µL of MACS buffer and labeled by 3 µL of PD-L1 (Table 4). After 15 min. of incubation at 4 °C in the dark, cells were washed by 2 mL of MACS buffer and centrifuged 10 min. 300 g at 4 °C. All cells were resuspended in 500 µL of MACS buffer before being analyzed by FACS Verse (BD Bioscience) using FACS suits software.

Target protein	Supplier	Fluorochorme	Reference number
CD45 (TILs)	Miltenyi Biotec	APC-Vio770	130-110-662
CD45 (TAMs)	Miltenyi Biotec	VioBlue	130-110-664
CD3	Miltenyi Biotec	VioBlue	130-114-519
CD8	Miltenyi Biotec	PE-Vio770	130-110-680
CD25	Miltenyi Biotec	VioBright-FITC	130-108-999
CD69	Miltenyi Biotec	APC	130-115-461
PD-1	Miltenyi Biotec	PE	130-111-800
F4/80	Miltenyi Biotec	APC	130-116-547
CD11b	Miltenyi Biotec	VioBright-FITC	130-113-243
Ly6G	Miltenyi Biotec	PE-Vio770	130-107-915
Ly6C	Miltenyi Biotec	PE	130-111-778
MHC-II	Miltenyi Biotec	APC-Vio770	130-112-233
CD80	Miltenyi Biotec	APC-Vio770	130-116-463
m_PD-L1	BioLegend	PE	329705
h_PD-L1	Cell Signalling	/	86744
Rabbit mcAb	Thermo Fisher Scientific	Alexa 488	A-11008

Table 3. Antibodies used for flow cytometry analyses

11 Tissue preparation for histologic analyses and immunolabeling

After their resection, tumors, spleens and lymph nodes chosen for histologic analysis were rinsed three times in a 0.9% NaCl solution before being placed in an embedding cassette and emerged for 24 h into formaldehyde 10%. After fixation, the samples were dehydrated by four consecutive baths of methanol 100% at 35°C and transformed into an organic phase by two 45 min and two 60 min incubations in toluene 100% at 35°C. Samples were then immerged four times 60 min into paraffin at 60°C before being cooled down to room temperature to form solid paraffin blocks containing the samples, ready for microtomisation (RM2145, Leica) into 6 µm thick slices and transferred onto microscope slides (#631-0108, VWR).

12 Hemalun-Erythrosin-Safran staining

Once transferred tonto microscope slides, they were dried to 42°C during 90 min, before being deparaffinized by two baths of 3 min toluene. Rehydration occurred by immersion two times 3 min in absolute methanol and one time 3 min methanol 70 %. The sides were bleached during 10 min in tapped water, before 7 min nuclear staining with hemalun. Then slides were rinsed during 1 min with tapped water and dedifferentiated during 2 min in HCL-ethanol and rinsed again for 10 min in tapped water. A 6 min bath in erythrosine allowed cytoplasmic staining, followed by 1 min rinsing in tapped water. Slides were dedifferentiated for 1 min in ethylene alcohol 70% and dehydrated during three bathes of 30 seconds each in absolute isopropylic alcohol. 7 min safran staining of connective tissues was then performed, followed

by three times 30 seconds rinsing in absolute isopropylic alcohol. At this point, microscopic slides were immerged in toluene before adding DPX and a coverslip in top of the tissue. Samples were pressed and dried during 24 h before microscopic analysis.

13 Immunohistofluorescence

Samples on microscopic slides were deparaffinized and bleached by consecutive baths of two times 3 min toluene, two times 3 min methanol 100%, one time 3 min methanol 70% and one time 10 min tapped water. Epitope retrieval was achieved by a 20 min incubation in 0.21% citric acid pH 6 at 95°C. Samples were then rinsed by PBS and incubated into two times 3 min glycine 0.1 M followed by another PBS rinsing before blocking through a 1 h incubation in a blocking buffer (PBS - BSA 0.2%). The samples were incubated with the primary antibody (Table 5) at 4°C overnight. The microscope slides were then washed three times 3 min with the blocking buffer before a 1 h incubation with the corresponding secondary antibody. Next, the microscope slides were washed three times with the blocking buffer before 15 min nuclear staining by Hoechst (1/100) (33258, Sigma Aldrich) and three times 3 min rinsing with PBS. Cover slides were then mounted using DPX (#1.005790500, Merk). 24 hours later, the samples were analyzed using a fluorescence microscope (BX63, Olympus).

Protein	Primary antibody	Secondary antibody
CD3	Anti-CD3 (Rabbit, Abcam, #ab56290, 1/50)	Anti-rabbit-Alexa 568 nm (Goat, Thermo Fisher Scientific, #A-11011, 1/1000)
F4/80	Anti-F4/80 (RM0029-11H3) (Rat, Abcam, #ab56297, 1/50)	Biotinylated anti-rat IgG (Goat, Vector Laboratories #BA-9400, 1/50)

Table 4. Antibodies used for immunohistochemistry and immunohistofluorescence

RESULTS

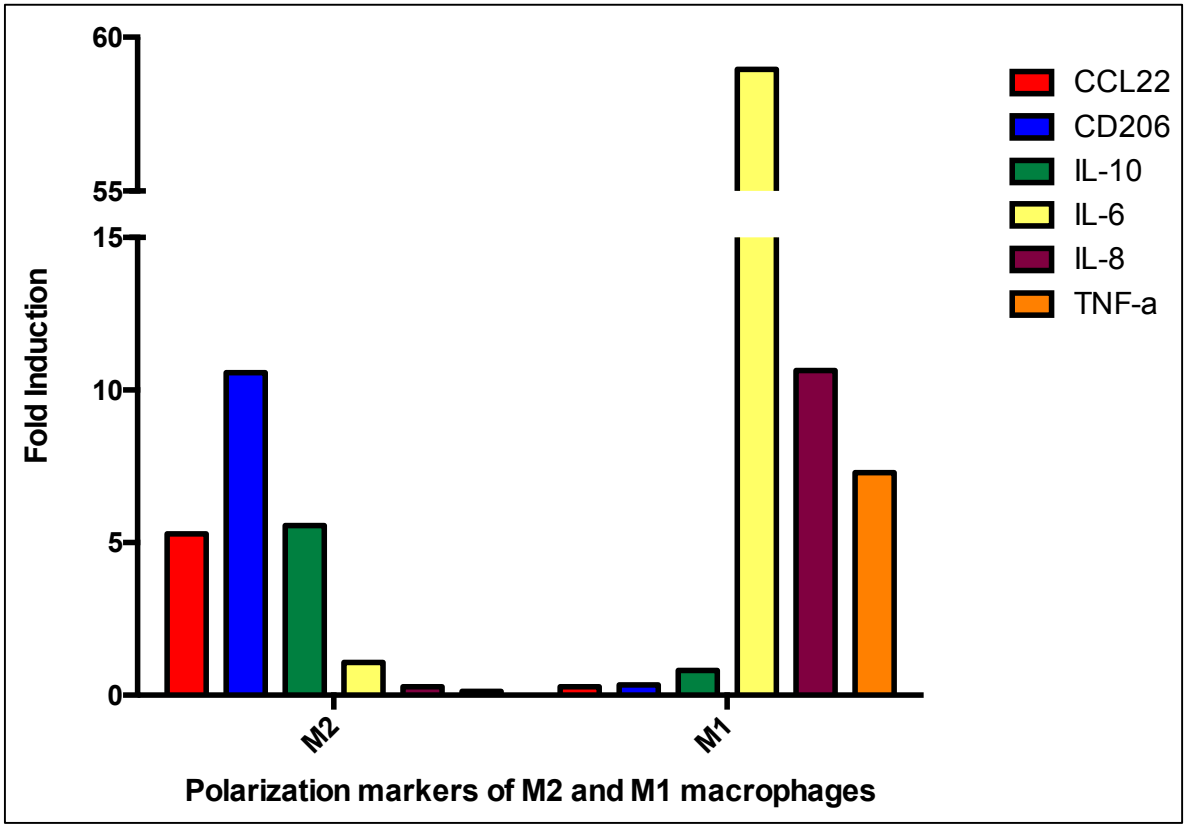

Figure 25. mRNA expression of macrophage polarization markers in M2 and M1 macrophages normalized to unpolarized M0 macrophages. THP-1 cells were differentiated into MO macrophages, which were then polarized into either M1 or M2 macrophages. After total mRNA extraction, the relative mRNA expression of specific polarization markers normalized by RPS9 expression was determined by RT-qPCR.

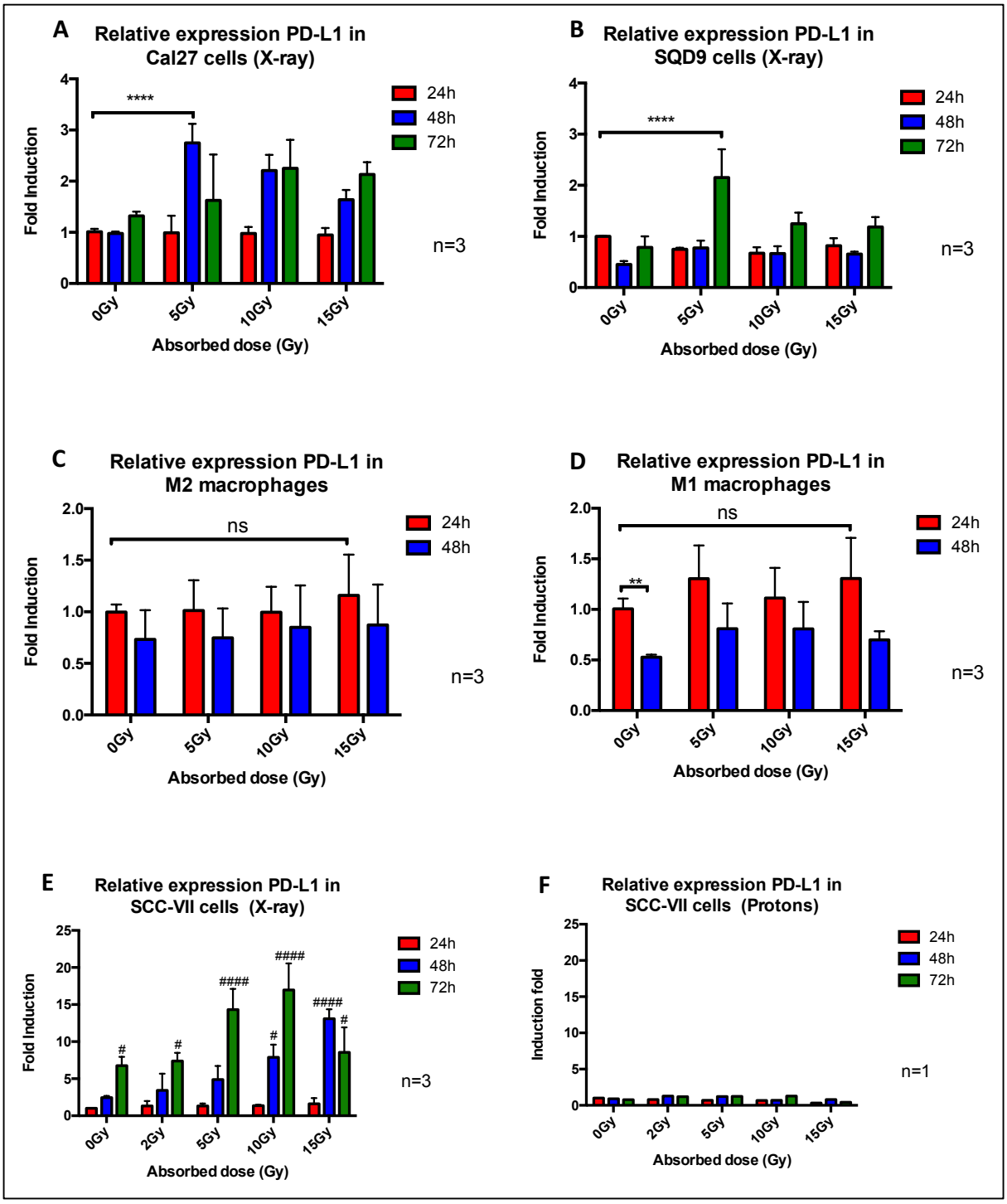

Figure 26. mRNA expression of PDL-1 in Cal27 (A) and SQD9 (B) cells as well as M2 (C) and M1 (D) macrophages and SCC-VII cells (E) after X-ray irradiation or proton irradiation of SCC-VII cells (F) normalized to non-irradiated control cells at 24 h. Cells were irradiated at 0 Gy, 5 Gy, 10 Gy and 15 Gy and cancer cells additionally at 2Gy. Total mRNA extraction was performed 24, 48 and 72 h after irradiation for Cal27, SQD9 and SCC-VII cells and 24 and 48 h after irradiation for M2 and M1 macrophages. The relative mRNA expression of PD-L1, normalized to the expression of 23 kDa for Cal27, SQD9 and SCC-VII cells and RPS9 for M2 and M1 macrophages, was determined by RT-qPCR. Statistical analyses consist of a two-way ANOVA test. #, ##, ###, ####: significantly different from control condition respectively with $p<0.05$, $p<0.01$, $p<0.001$ and $p<0.0001$; Results are presented as mean ± SD.

1 *In vitro* assessment of PD-L1 expression after irradiation

1.1 Macrophage polarization

THP-1 monocytes were differentiated into M0 macrophages by incubating them in the presence of phorbol-12-myristat-13-acetate (PMA) during 24 h followed by a 24 h incubation in PMA-free medium. M0 macrophages were then polarized either during 48 h in the presence of IL-13 and IL-4 into anti-inflammatory M2 macrophages or during 24 h in the presence of LPS and IFN-γ into pro-inflammatory M1 macrophages. The expression of specific polarization markers was assessed by RT-qPCR to determine if the polarization was successful. The results indicated an increased expression of CCL22, CD206 and IL-10 mRNA for M2 macrophages and an increased expression of IL-6, IL-8 and TNF-α mRNA for M1 macrophages (Figure 25), confirming the successful macrophage polarization.

1.2 PD-L1 induction by X-ray irradiation

In order to investigate the effects of X-ray irradiation on PD-L1 expression, Cal27 and SQD9 cells were irradiated at different doses (0 Gy, 5 Gy, 10 Gy, 15 Gy) and the expression of PD-L1 was assessed by RT-qPCR and flow cytometry at different timings post-irradiation (pi. 24, 48, 72 h). At mRNA level, the most significant increase for SQD9 cells was obtained 72 h after 5 Gy irradiation. For Cal27 cells, the highest significant increase was observed 48 h pi. after irradiating cells at a 5 Gy dose (Figure 26A and B).

The mRNA expression of PD-L1 was also analyzed in THP-1-derived M2, M1 and M0 macrophages. Considering that 72 h pi. the macrophage polarization was not maintained (data not shown), the expression of PD-L1 was only assessed 24 h and 48 h after irradiation. While the results indicate a slight decrease in PD-L1 expression at 48 h compared to 24 h, no significant increase was observed neither for M2 macrophages nor M1 macrophages, at all doses (Figure 26C and D).

Since future *in vivo* experiments first need to be performed in mice before being tested on human, the mRNA expression of PD-L1 was additionally assessed in SCC-VII cells. These cells were also used to compare the impact of proton vs photon irradiation on PD-L1 expression as well as the previously described PD-L1 induction pathway by DDR. PD-L1 expression was assessed at 24, 48, 72 h after 0 Gy, 2 Gy, 5 Gy, 10 Gy, 15 Gy irradiation. While for SCC-VII cells, significant dose- and time-dependent increases could be observed after X-ray irradiation (Figure 26E), there was no PD-L1 induction following proton irradiation (Figure 26F).

In preparation of the *in vivo* part of this project, the optimal conditions to administrate an anti-PD-1 antibody to the mice needed to be determined. Since it is necessary, in order to obtain an efficient response to the anti-PD-1 antibody, to focus on PD-L1 abundance on the cell

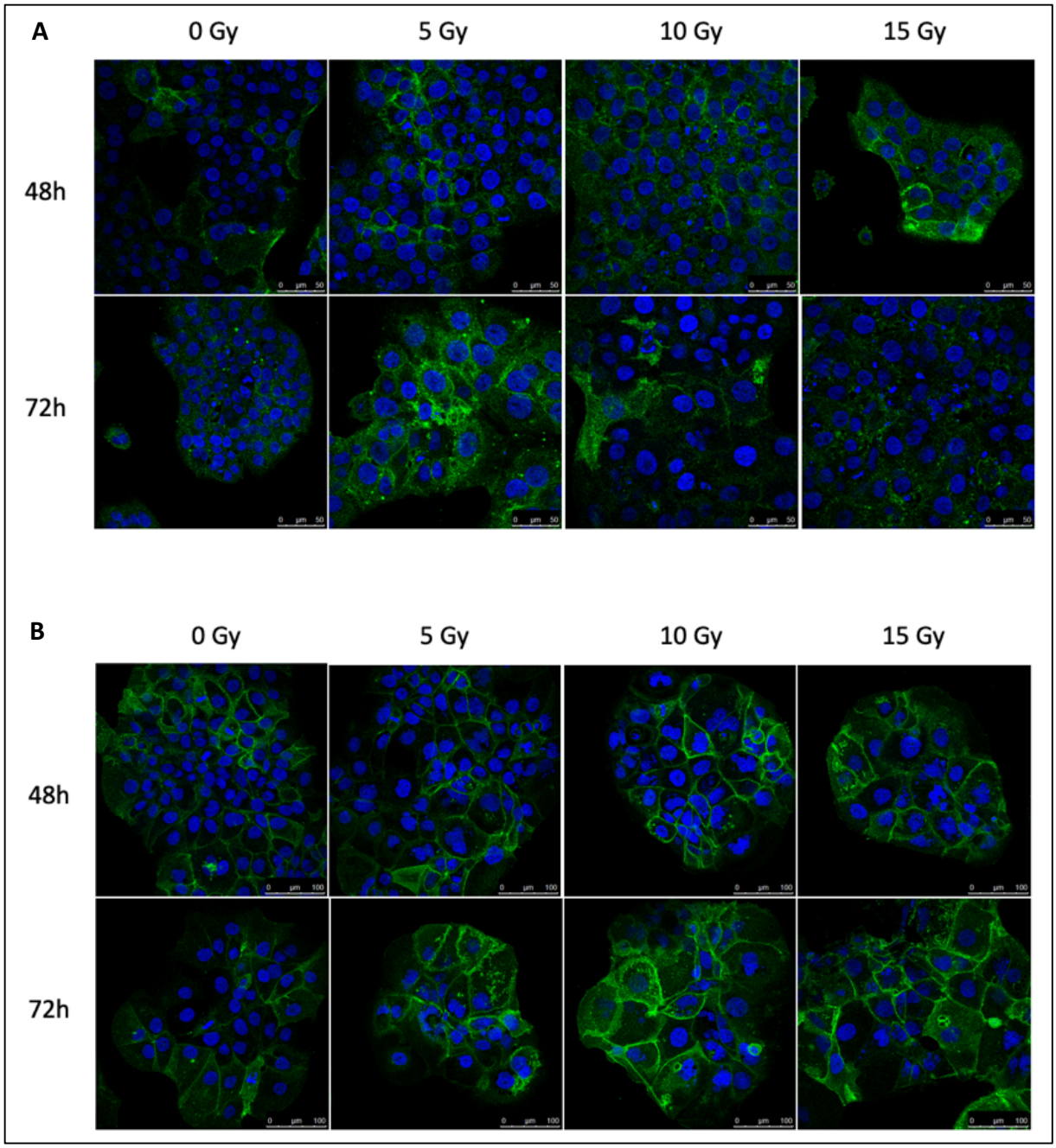

Figure 27. Analysis of PD-L1 protein expression and subcellular localization in Cal27 (A) and SQD9 (B) cells. Cells were irradiated at 0 Gy and 5 Gy and fixed after 48 h before anti-PD-L1 labeling and nuclear staining. Confocal microscopy was used to analyze PD-L1 protein expression and subcellular localization (green). Nuclei were stained with Topro (blue)

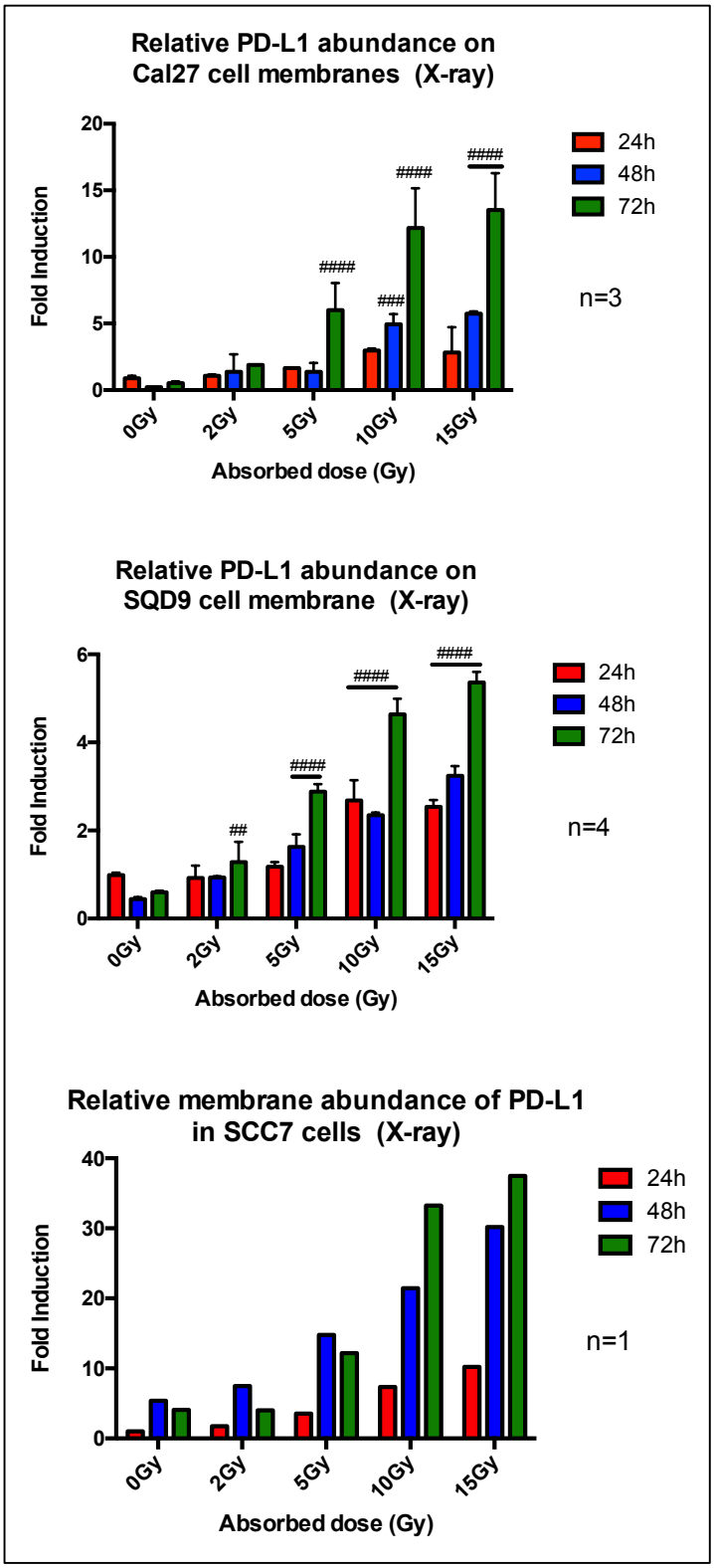

Figure 28. Relative protein expression of PD-L1 at the membrane of Cal27 (A), SQD9 (B) and SCC-VII (C) cells after X-ray irradiation normalized to non-irradiated control at 24 h. All cells were irradiated at 0 Gy, 2Gy, 5 Gy, 10 Gy and 15 Gy. PD-L1 expression was analyzed by flow cytometry 24, 48 and 72 h after irradiation. Results are expressed as relative to the non-irradiated control cells at 24h pi. Statistical analyses consist of a two-way ANOVA test. #, ##, ###, ####: significantly different from control cells (0 Gy 24 h) respectively with $p<0.05$, $p<0.01$, $p<0.001$ and $p<0.0001$; Results are presented as mean ± SD.

membranes only, confocal microscopy after immunofluorescence labeling of PD-L1 was performed to visualize and localize the PD-L1 protein following X-ray irradiation (Figure 27A and B). On one hand, the results confirmed the increase in PD-L1 expression after X-ray irradiation and on the other hand, they confirmed that the increase was not restricted to the endoplasmic reticulum but that it was clearly observed at the cell plasma membrane.

Hence flow cytometry was performed to assess the induction fold of PD-L1 on cell membranes of Cal27, SQD9 and SCC-VII cells. While proton irradiations still remain to be performed, a significant dose- and time-dependent increase in the relative PD-L1 abundance on the cell surface was observed in all three HNSCC cell lines (Figure 28A, B and C), from 24 h to 72 h. These results suggest that this dose- and time-dependent effect, needs to be considered, in order to chose the appropriate timing when using an anti-PD-1 immune-checkpoint blockage *in vivo*.

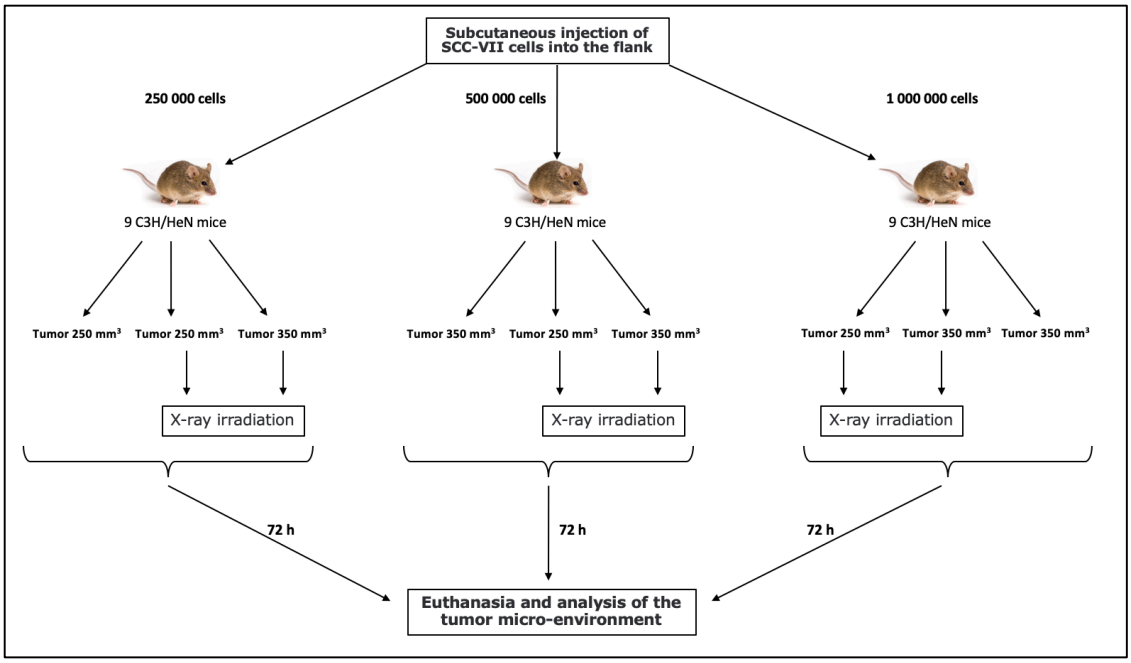

Figure 29. Experimental strategy of in vivo pilot project. Twenty-seven mice were divided into 3 groups of 9 mice that were injected with either 250 000 cells, 500 000 cells or 1 000 000 cells. Each of these 3 groups was subdivided into 3 subgroups of 3 mice, one control group that was not to be treated, 1 subgroup that was to be irradiated once tumors grew up to 250 mm^3 and 1 subgroup that was to be irradiated once tumors grew up to 350 mm^3. 72h after achieving the tumor size of 250 or 350 mm^3, mice were sacrificed.

2 Set up of a syngenic *in vivo* mouse model of HNSCC

2.1 Context

A syngeneic mouse model of HNSCC using C3H/HeN mice injected subcutaneously with SCC-VII cells was chosen for the study of the impact of macrophage repolarization on anti-PD-1 ICB efficiency, when using the combined treatment of X-ray irradiation and an anti-PD-1 antibody. First, a pilot project was set up to determine three parameters necessary for the main project: the optimal number of cancer cells to be injected to result in the formation of tumors within an acceptable delay (less than 8 weeks); the immune infiltration and the homogeneity of the immune cell's spread throughout the subcutaneous tumors, to allow arbitrary cutting of the tumors into three pieces for down-stream analysis; the minimal required tumor volume at the time of the treatment (250 or 350 mm^3, 72 h before the sacrifice) to perform TIL and TAM isolation for flow cytometry analysis, tumor RNA extraction and histologic analysis. To this aim, 27 mice were divided into three experimental groups according to the number of injected SCC-VII cells (250 000, 500 000 or 1 000 000). Each group was subdivided into three subgroups, one unirradiated subgroup, one irradiated subgroup with 250mm^3 tumors and one irradiated subgroup with 350mm^3 tumors. Each subgroup contained three mice

Figure 29). Of these three mice, one was intended to histologic analysis only, one to isolation, RNA extraction and histologic analysis and one backup in case a mouse does not develop a tumor. Additional information and practical information can be found in the ethics protocol as authorized by the local ethics committee (Appendix 1).

2.2 Tumor development

In the group that was injected with 1 000 000 cells, 89% of the mice developed tumors after less than 8 weeks. In the groups injected with 500 000 and 250 000 cells, only 44% and 56% of the mice respectively developed tumors within the defined timeframe.

Even though some tumors were spherical, most tumors were either oval or multispherical. Hence, tumor volumes needed to be calculated differently. For spherical, oval and multipherical tumors, the volume was calculated as descripted in formulas 1, 2 and 3 respectively:

Formula 1: $V = \frac{3}{4} \times \pi \times radius^3$

Formula 2: $V = \frac{\pi}{6} \times \left((length \times width)^{\frac{3}{2}} \right)$

Formula 3: $V = \sum_{i=1}^{n} V_i$

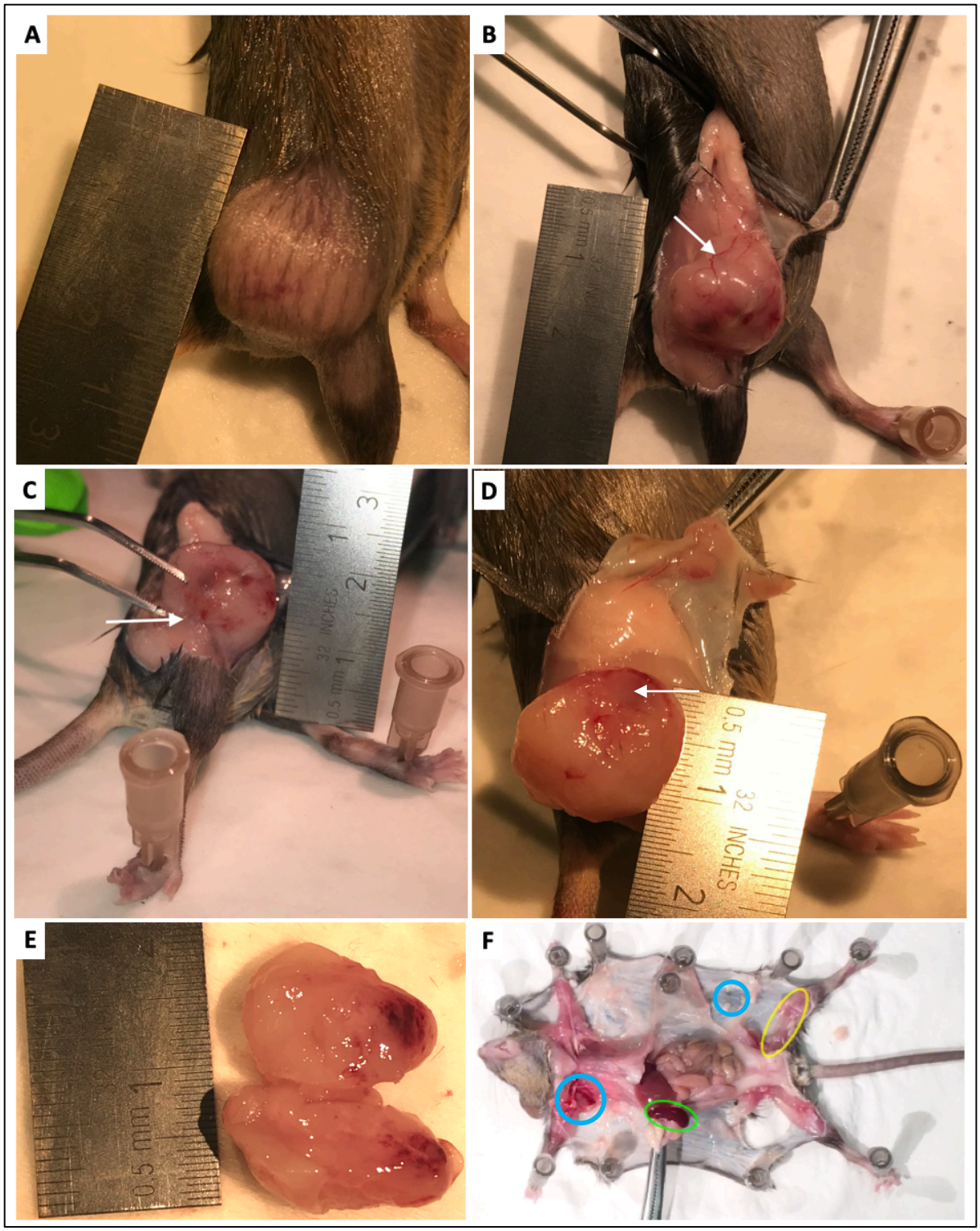

Figure 30. Macroscopic tumor analysis. Tumors are measured before resection (A). Macroscopic analysis show blood vessels at the surface of the tumor (B), tumor invading nearby muscles forming tight adhesions (C), visible hemorrhagic areas at the surface (D) and hemorrhagic zones inside the tumor (E). Spleen (green border), distant lymph node extraction (blue border) and femur extraction (yellow border) site can be seen in picture (F).

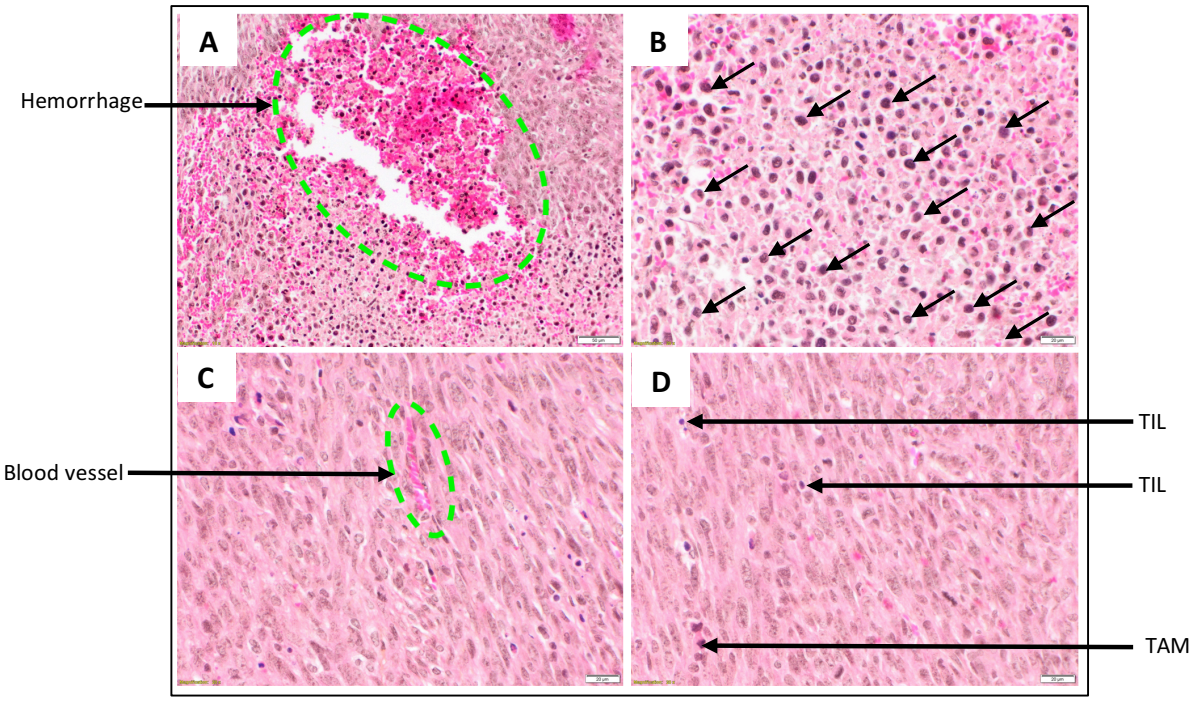

Figure 31. Vascularization and immune infiltration throughout tumors of untreated mice. HES stained tumors tissue. A: intra-tumoral hemorrhage and consequent erythrocyte and immune infiltration. B: magnification of perihemorrhagic erythrocyte and immune-infiltration (arrows). C: intra-tumoral blood vessel and erythrocytes. D: intra-tumoral immune-infiltration. Magnification: 10x (A) and 20x (B, C and D)

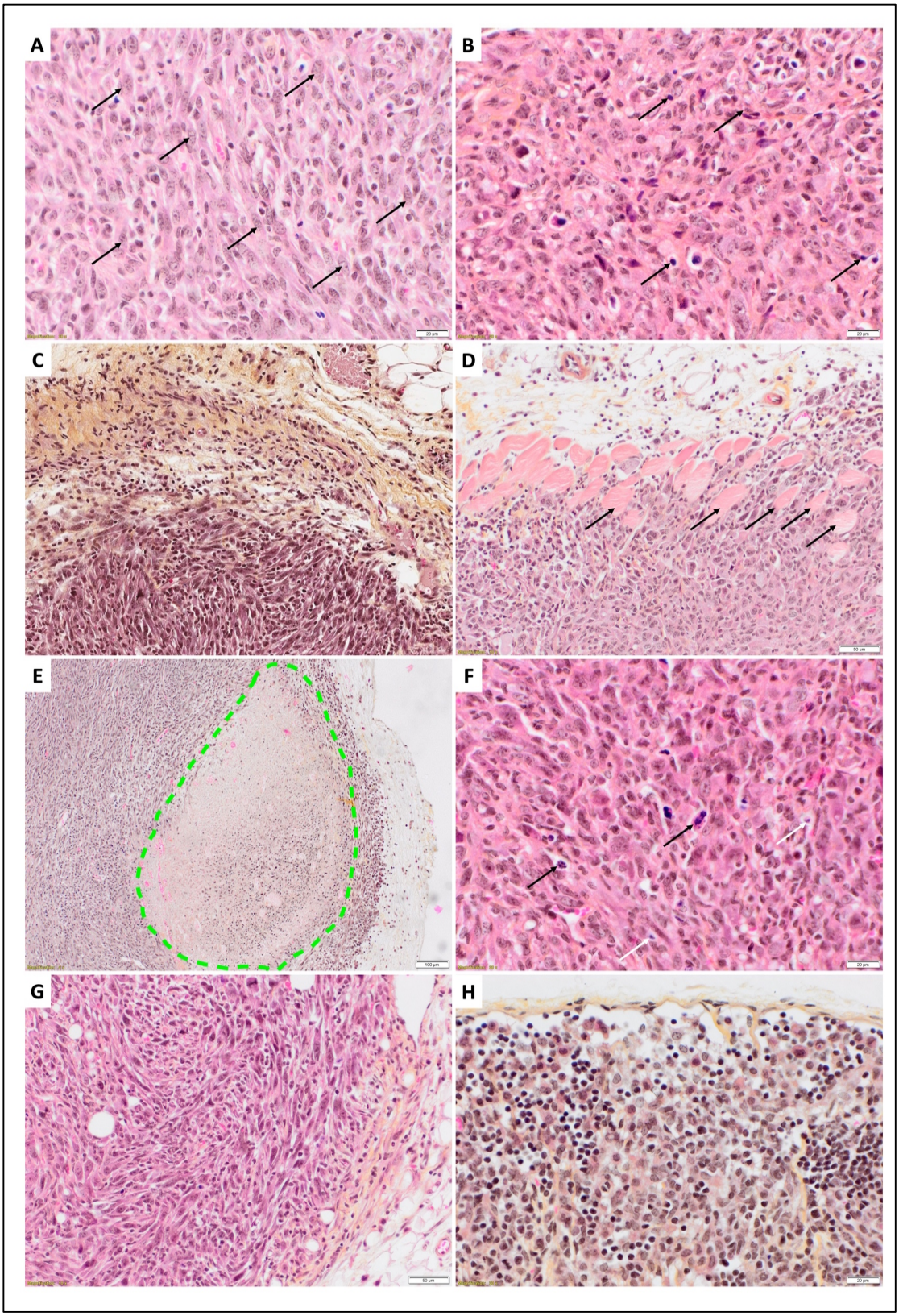

Figure 32. Topologic analysis of HES stained tumor sections (A-G) and tumor distant lymph nodes (H) of untreated mice. Cancer cells (black arrow) can be identified by anisocytosis, anisocaryosis, the presence of multiple nucleoli, increased nucleus to cytoplasm ratio, polyploïdi and projecting nucleoli (A and B). Tumor periphery contain very high numbers of immune cells infiltrating as well the tumor as the surrounding adipose tissue (C). Invasion of abdominal muscles (black arrows) by cancer cells (D). Necrotic area at the tumor periphery (green border) (E). Cancer cells undergoing apoptotic mitosis (black arrows) and apoptosis (white arrows). Cancer cells at tumor periphery presenting an altered, mesenchymal-like morphology (G). Important cancer cell infiltration at proximity to the connective capsule of a tumor distant lymph node (H). Magnification: 4x (E), 10 (C, D and G) 20x (A, B, F and H)

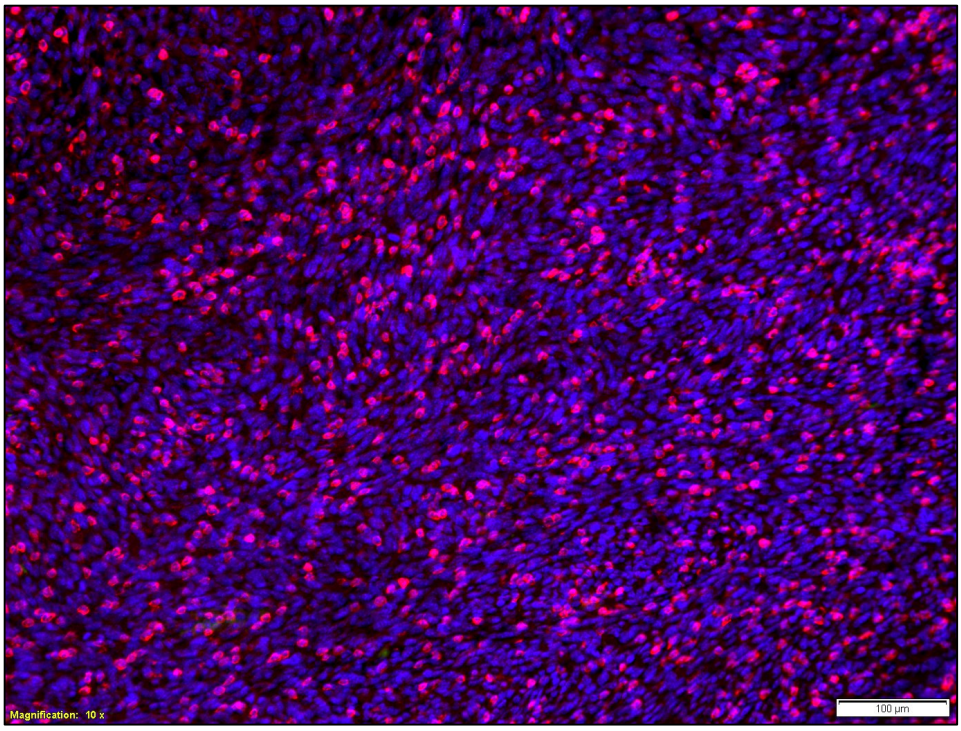

Figure 33. Cytotoxic T cell infiltration of the tumor. CD3+ immunolabeling of cytotoxic tumor infiltrating T cells (red) showing a high degree of T cell infiltration and overall homogeneous spread throughout the tumor. Nuclei were stained by Hoechst (blue). Magnification: 5x

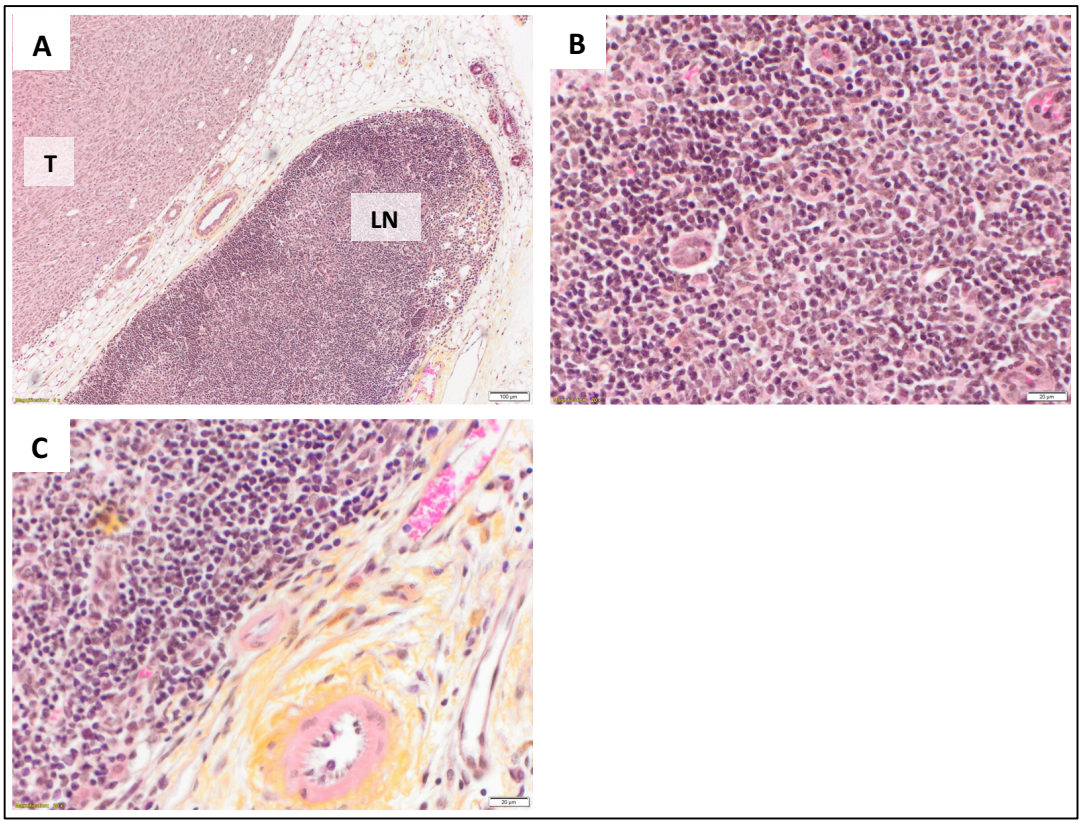

Figure 34. Abdominal lymph node adjacent to the tumor. HES stained section of the tumor and associated lymph node of an untreated mouse. The tumor (T) and lymph node (LN) are surrounded by fat tissue rich in blood vessels (A). The inside of the adjacent lymph node rich in immune cells showing cancer cell invasion (B). Tumor periphery at proximity to blood vessels of the fat tissue show an important number of immune cell infiltration (C). Magnification: 5x (A) and 20x (B and C).

In order to divide the resected tumors into three parts, one for histologic analyses, one for TIL and TAM isolation and the third one for tumor RNA extraction, 250 mm^3 at the time of the treatment (72 h before the sacrifice, untreated mice included) was insufficient, since the number of isolated TILs and TAMs was too low to perform flow cytometry analysis. Enough cells could be isolated from 350 mm^3 (72 h before the sacrifice, untreated mice included) big tumors (data not shown). Tumor samples for RNA isolation were stored at -72°C after snap freezing in liquid nitrogen and still need to be processed.

2.3 Histologic features

As mentioned previously, from one mice of each subgroup, the entire tumor was used for histologic analyses. Tumor were measured and macroscopic analysis performed (Figure 30 A). The presence of blood vessels was confirmed of all tumor but the density was variable (Figure 30 B). Most tumors had, by the time of the resection, formed tight adhesions with nearby muscle tissue (Figure 30 C), making it difficult to resect tumors tissue only. In some cases, at the surface of a tumor and the inside, hemorrhagic areas were found, that could later be seen in histology too (Figure 30 D and E). In addition to the tumor, femurs, distant lymph nodes (LNs) and the spleen were resected for downstream histologic analysis (Figure 30 F). After tumor resection, HES staining was performed to visualize the overall morphology of the different tissues that were taken, while immunofluorescence labelling of CD3+ T cells allowed the assessment of the immune infiltration and its homogeneity throughout the tumor. Immunohistochemistry staining of F4/80+ macrophages is beeing performed as well but the technique needs to be improved. HES stained histologic analyses for tumors showed, rich vascularization and possible hemorrhages as well as high immune cell infiltration inside the tumor (Figure 31 A, B, C and D). Cancer cells can be easily identified by the presence of irregularly shaped cell membranes and nuclei, anisocytosis, anisocaryosis, an increased nucleus to cytoplasm ratio, high rate of mitosis, polyploïdi or projecting nucleoli (Figure 32 A and B). In the periphery of tumors as well as the surrounding fat tissue, a strongly enriched immune infiltration was observed (Figure 32 C). In the same area of the tumors, for those who formed tight adhesions with nearby muscles, histologic analysis reveal muscle infiltration by cancer cells indicating a high degree of invasiveness (Figure 32 D). Most tumors present to some extend necrotic areas that are visible microscopically only, as well as a large number of isolated apoptotic cancer cells as well as cancer cell in apoptotic mitosis (Figure 32 E and F). In the periphery of many tumors, independently weather mice were treated, cancer cells can be found that have a very different morphology and a mesenchymal-like phenotype (Figure 32 G). Analysis of distant lymph nodes show early stage cancer cell infiltration (Figure 32 H). Immunofluorescence labeling of CD3+ T cells showed a high degree of T lymphocyte infiltration as well as a homogeneous spread of T cells throughout the tumor (Figure 33). For some tumors that were entirely aimed for histologic analysis, during the resection, the lymph node adjacent to the tumor and that was included in the same fat tissue with the tumor was isolated together with the tumor. Microscopic slices of these samples (Figure 34 A) show cancer cell infiltration inside the LN (Figure 34 B) and enriched immune cell infiltration in the tumor

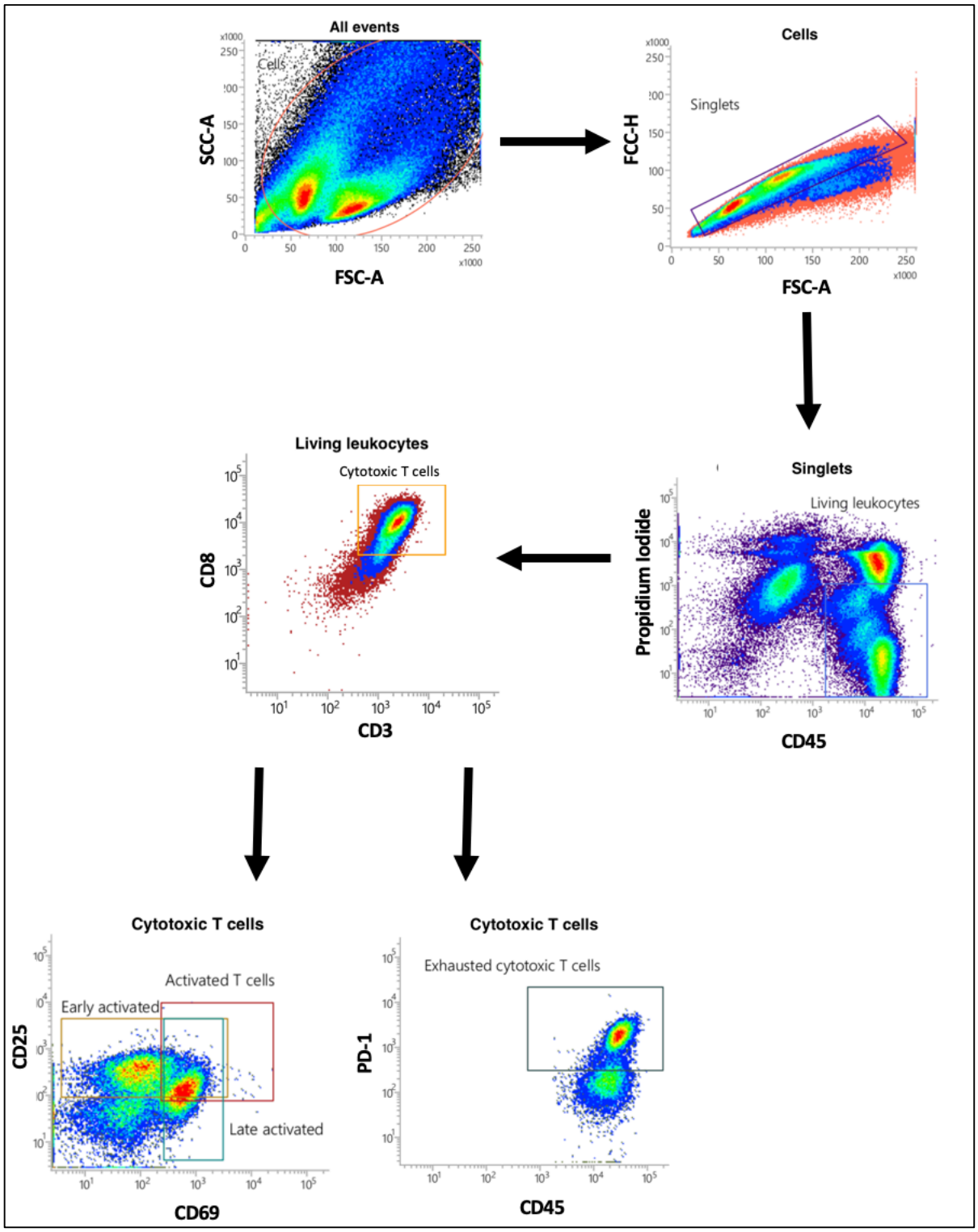

Figure 35. Schematic representation of T cell activation analysis by flow cytometry. SCC-A and FSC-A were used to gate on cells. Singlets were selected by FSC-H over FSC-A. Propidium iodide and CD45 allowed to gate on living leukocytes (PI-CD45+), from which cytotoxic T cells could be isolated (CD3+ CD8+). Early and late activation of these cytotoxic TILs was defined as by CD25+ and CD69+ respectively as well as cytotoxic TIL exhaustion as PD-1+.

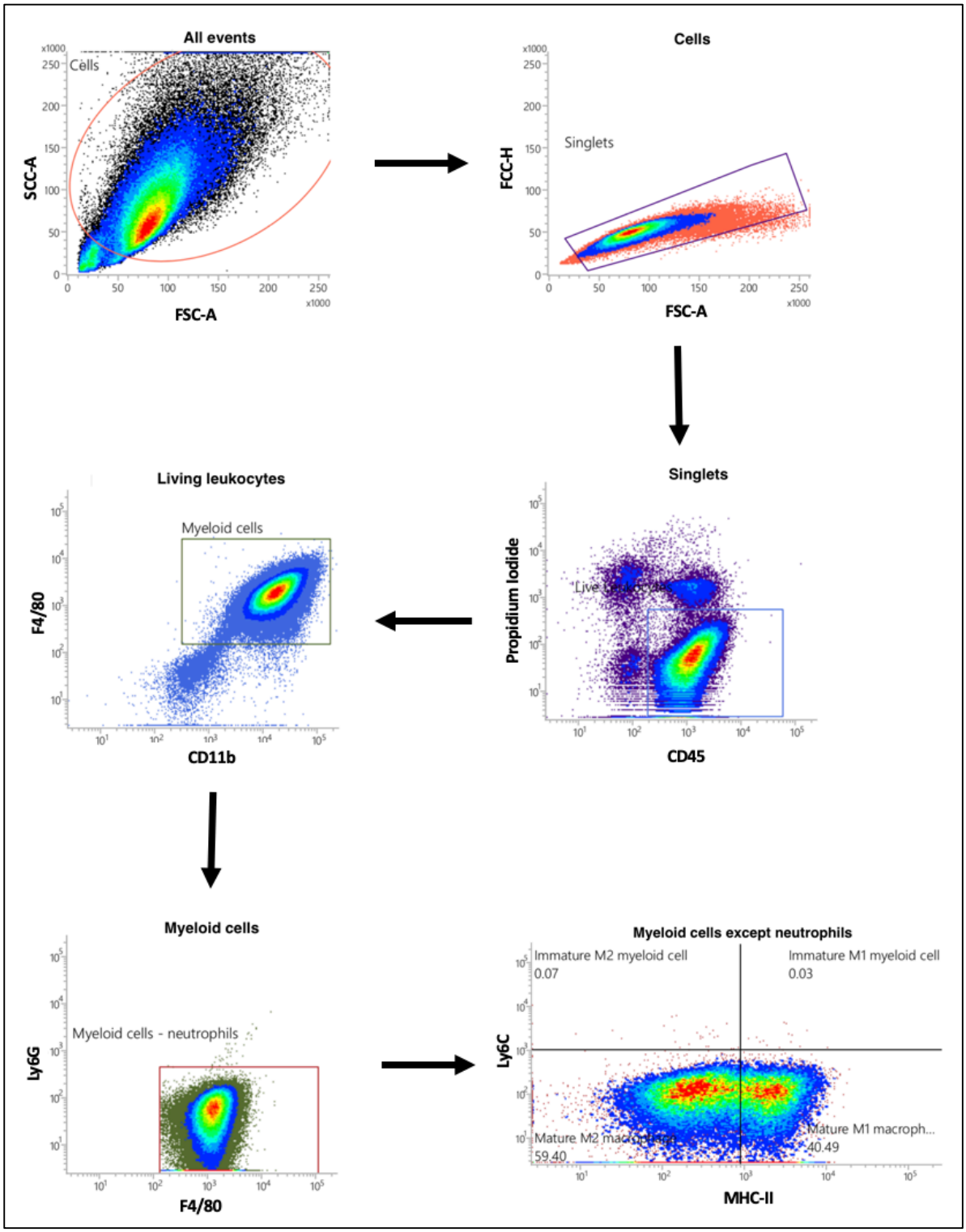

Figure 36. Schematic representation of TAM polarization analysis by flow cytometry. SCC-A and FSC-A were used to gate on cells. Singlets were selected by FSC-H over FSC-A. Propidium iodide and CD45 allowed to gate on living leukocytes (PI- CD45+), from which myeloid cells could be isolated (F4/80+ CD11b+). Contaminating neutrophils were gated out as Ly6G+. Immature myeloid cells (Ly6G^{high}) were distinguished from mature macrophages (Ly6G^{low}) and macrophage polarization determined as M1 (MHC-II^{high}) or M2 MHC-II^{low}).

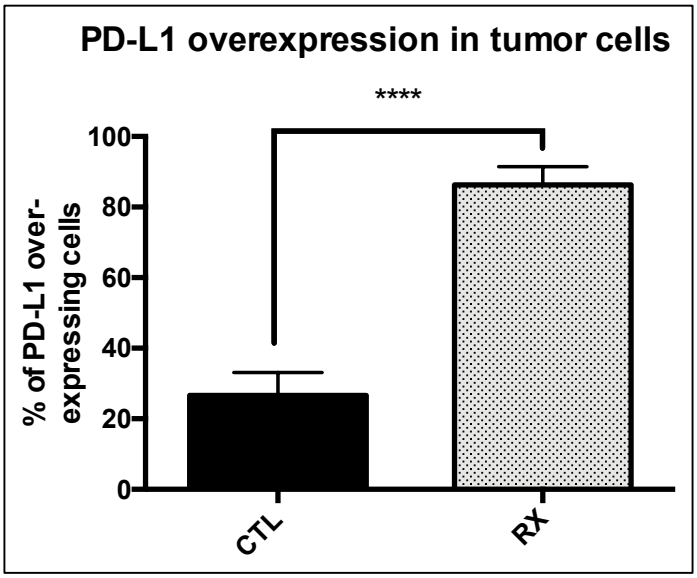

*Figure 37. Flow cytometry analysis of the percentage of PD-L1 over-expression CD8- F4/80- tumor cells 72 h after X-ray irradiation (RX) compared to untreated group (CTL). Statistical analysis consists of unpaired t-test. ****: significantly different from control with $p<0.0001$. Results are represented as mean ± SD.*

periphery at proximity to blood vessels contained in the fat tissue (Figure 34 C). The samples were used as positive control for both HES staining and CD3-immunolabelling of lymphocytes. Similarly to what was observed at proximity to tumor infiltrating blood vessels, a particularly rich infiltration of immune cells was observed at the periphery of the tumors (Figure 32 C and Figure 34 C).

2.4 Flow cytometry set up

The *in vivo* pilot project also allowed the establishment of optimal reference settings for flow cytometry analysis of TAM polarization and TIL activation after TIL and TAM isolation from the tumors. To assess the activation of tumor infiltrating cytotoxic T cells, living tumor infiltrating T cells (CD45+ CD3+ PI-) were gated in during flow cytometry. CD8+ cytotoxic TILs were analyzed for early activation (CD25), late activation (CD69) and exhaustion (PD-1) (Figure 35). In order to determine TAM polarization, living myeloid cells (CD45+ CD11b+ F4/80+ PI-) were selected during flow cytometry. Contaminating neutrophils ($Ly6G^{high}$) were gated out. In the resulting population, immature myeloid cells ($Ly6C^{high}$) were distinguished from macrophages ($Ly6C^{low}$), whose polarity was then determined by MHC-II. M1 macrophages were selected as MHC-II^{high} and M2 macrophages MHC-II^{low} (Figure 36).

We also assessed the PD-L1 expression in CD8- and F4/80- tumor cells by flow cytometry to verify if the X-ray induced-PD-L1 overexpression observed *in vitro* could be confirmed *in vivo*. The results show a significant increase in PD-L1 expression in tumor cell following X-ray treatment (Figure 37).

2.5 Conclusion

Altogether, these results confirm that injecting 1 000 000 cells and growing tumor up to 350 mm^3 before treatment allow RNA extraction, histologic analysis and sufficient TIL and TAM isolation for flow cytometry analysis in both irradiated and non-irradiated mice. During these experiments, in all mice, no signs of discomfort or pain could be observed except for one case of minor signs of pain, which totally vanished after a single injection of burprenorphin 0.05 mg/kg.

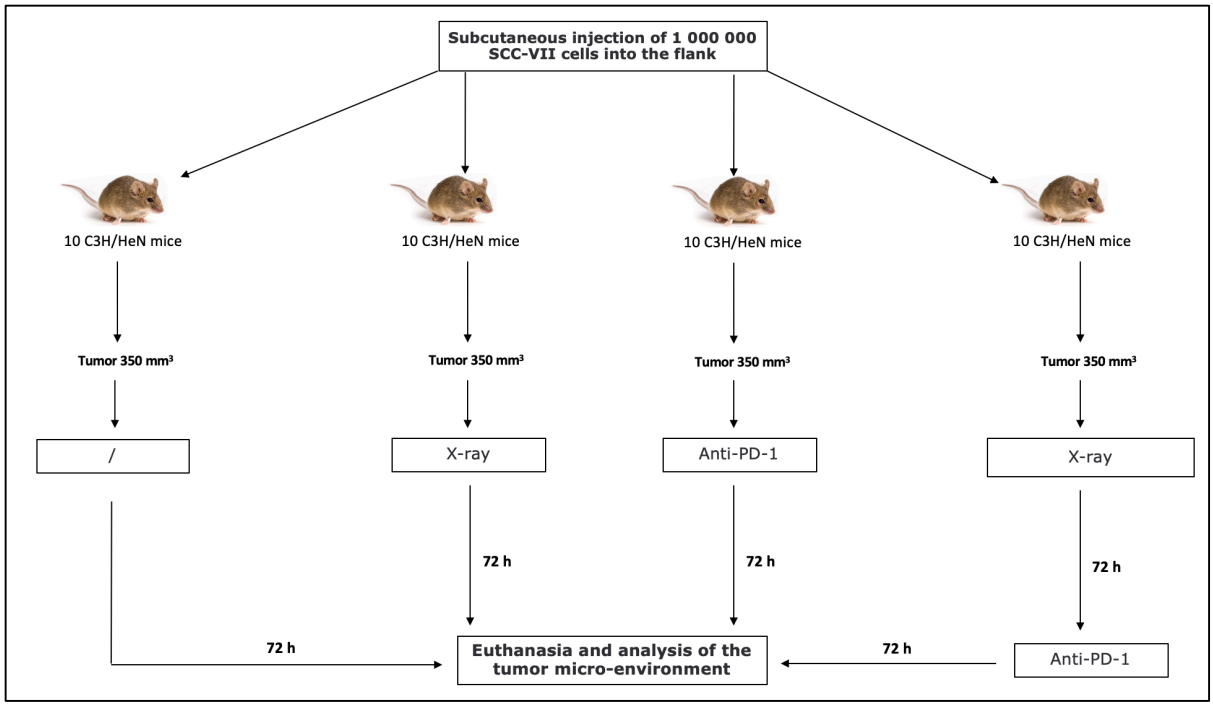

Figure 38. Workflow of the main in vivo project. Mice were divided into 4 groups of 10 mice each and they were injected with 1 000 000 SCC-VII cells subcutaneously into the right flank. Once a tumor reached the volume of 350 mm^3, the mouse was depending on the experimental group, either untreated, treated by a 10 Gy irradiation of the tumor or injected intraperitoneally with the anti-PD-1 antibody (10 mg/kg). The untreated mice, as well as the X-ray only and anti-PD-1 only mice were sacrificed 72 h later. Seventy-two hours after X-ray irradiation, mice receiving the combined treatment were injected with the anti-PD-1 antibody (10 mg/kg) and sacrificed 72 h later.

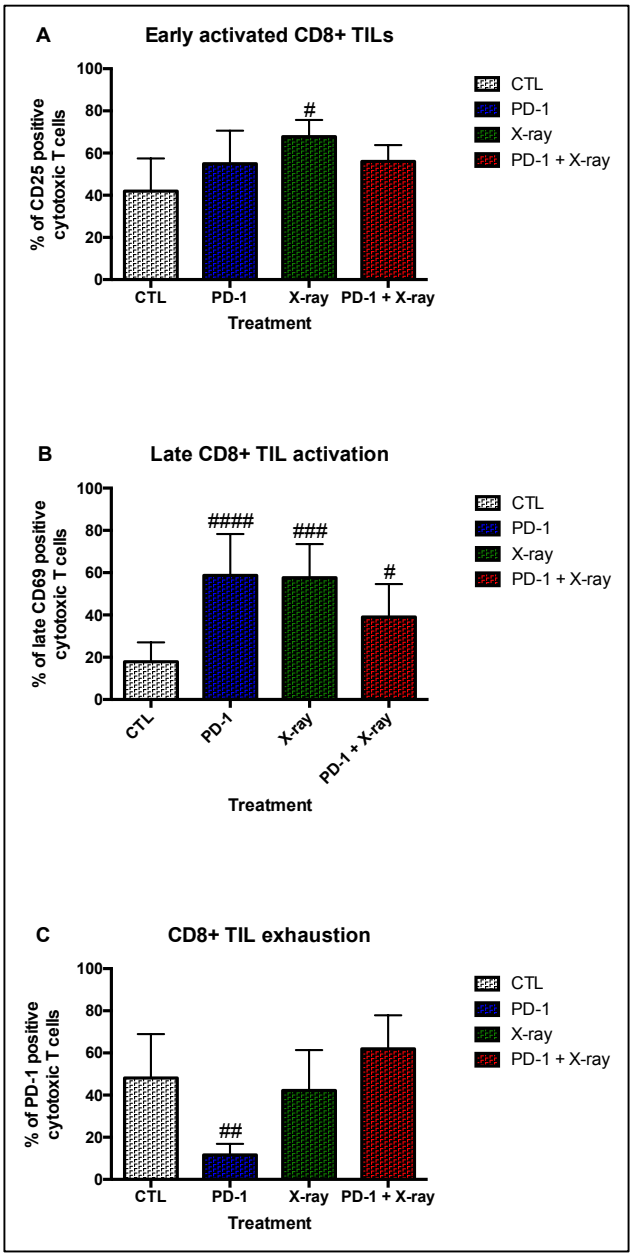

Figure 39. Evaluation of TIL activation and exhaustion by flow cytometry. Early activation was determined by CD25 (A). Late activation (B) and exhaustion (C) of CD8+ living cytotoxic T cells were defined by CD69 and PD-1 respectively. Statistical analyses were performed using one-way ANOVA. #, ##, ###, ####: significantly different from control condition (CTL) respectively with $p<0.05$, $p<0.01$, $p<0.001$ and $p<0.0001$; Results are presented as mean ± SD.

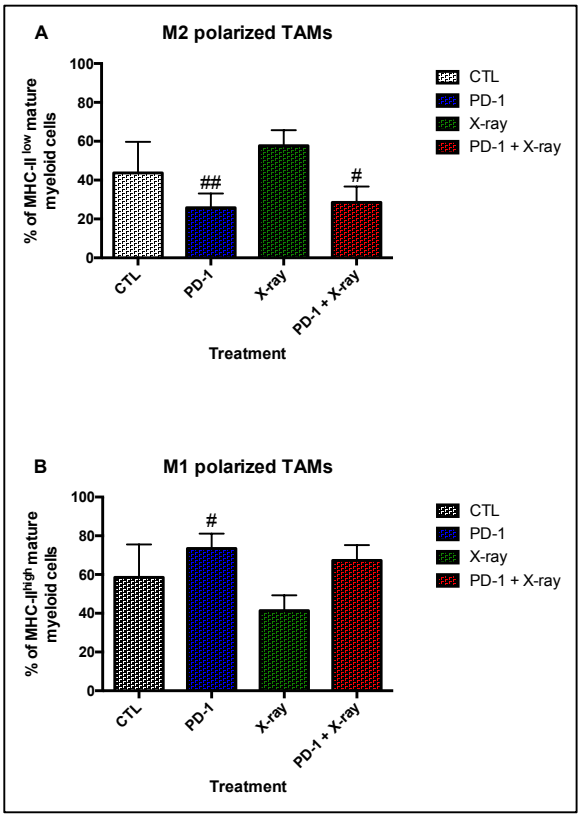

Figure 40. Evaluation of TAM polarization by flow cytometry. M2 macrophages (A) are characterized by high expression of MHC-II, while M1 macrophages (B) express low levels of MHC-II. Statistical analyses were performed using one-way ANOVA. # and ##: significantly different from control condition (CTL) respectively with $p<0.05$ and $p<0.01$. Results are presented as mean $\pm$ SD.

3 *In vivo* investigation of radiation-induced TAM repolarization to enhance anti-PD-1 ICB

3.1 Context

After establishing the syngeneic mouse model of HNSCC using C3H/HeN mice injected subcutaneously with 1 000 000 SCC-VII to grow tumors of 350 mm^3, a second project was launched in order to investigate the impact of radiation-induced macrophage repolarization on cytotoxic T cell activation and anti-PD-1 immune checkpoint blockage efficiency. For this purpose, 40 mice were split into 4 groups, one untreated, one treated by a focalized 10 Gy X-ray irradiation, one treated by an anti-PD-1 antibody and one receiving the combined treatment of X-ray irradiation and the anti-PD-1 antibody (Figure 38). For this project, treatment efficiency was defined by the level of early activation, late activation and exhaustion of living tumor infiltrating cytotoxic T cells (CD45+ CD3+ CD8+ PI-) using flow cytometry (Figure 35). For this, CD25 and CD69 were used as early and late activation markers respectively, while PD-1 was used an exhaustion marker. To assess macrophage polarization, CD11b + and F4/80+ myeloid cells were gated in from CD45+ and propidium iodide negative living leukocytes. Contaminating neutrophils were gated out as Ly6G positive and mature and immature myeloid cells were distinguished as $Ly6C^{low}$ and $Ly6C^{high}$ respectively. MHC-II then served as polarization marker for M1 ($MHC\text{-}II^{high}$) and M2 ($MHC\text{-}II^{low}$) macrophages (Figure 36). Additional information and practical information can be found in the ethics protocol as authorized by the local ethics committee (Appendix 2).

3.2 Treatment effects

3.2.1 Effects on TIL activation and exhaustion

Compared to the untreated group, early TIL activation was significantly increased in tumors of mice treated by X-rays only (Figure 39A). A significant increase in late TIL activation was observed in all treated groups (Figure 39B). The only significant decrease in TIL exhaustion was evidenced in mice treated with the anti-PD-1 antibody alone (Figure 39C). For the assessment of all three activation markers, lymphocytes isolated from peripheral blood mononuclear cells isolated from the mice blood on a Ficoll gradient after cardiac puncture was used as negative control (data not shown).

3.2.2 Effects on TAM polarization

While anti-PD-1 treatment alone decreased the proportion of M2 polarized macrophages and favored M1 macrophage polarization, X-ray-treated mice as well as mice that received the combined treatment showed an increase in the proportion of M2 macrophages and a decrease in M1 macrophages (Figure 40A and B). For the assessment of the macrophage polarization, *in vitro* polarized bone marrow-derived macrophages obtained from the bone marrow of the mice

femurs, were used as controls for M1 and M2 macrophages during flow cytometry analysis (data not shown).

DISCUSSION, PERSPECTIVES AND CONCLUSION

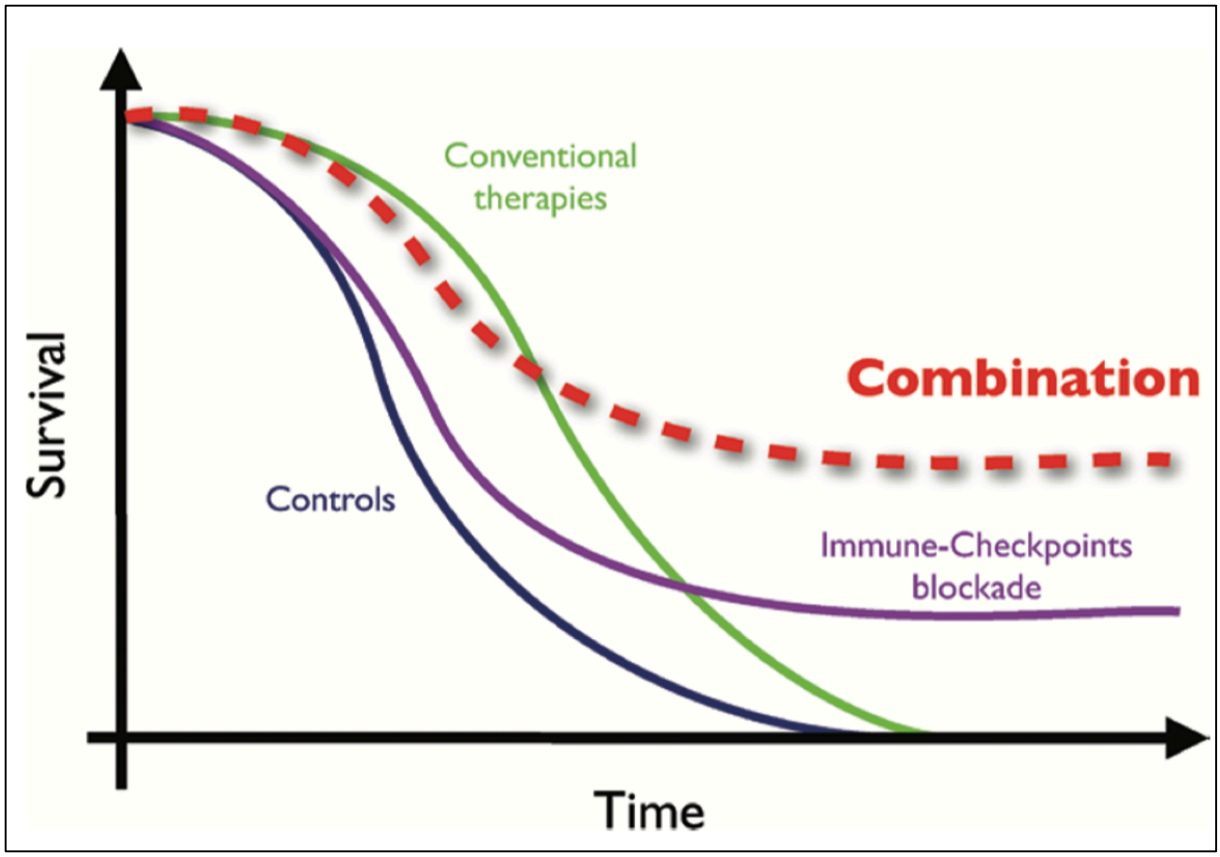

Figure 41. Schematic representation of the expected effect of a combination therapy of ICB and radiotherapy in HNSCC treatment. Conventional therapies present very high efficiency at early stages of treatment, while ICB, at early stages, seem to have very little impact on patient survival. The overall survival is however only slightly increased for conventional therapies, whereas ICB lead to long-term beneficial effects and disease-free survival for some patients. Combined therapies summon the advantages of both ICB and conventional therapy, leading to a high initial efficiency and a significantly increased overall survival and disease-free survival for a significantly increased number of patients suffering from HNSCC. (adapted from: Champiat et al., 2014)

The capacity of cancer cell to express the immune-modulator PD-L1 and to repolarize TAM towards an M2-like phenotype are two mechanisms that allow them to create an immuno-suppressive TME and to evade immune destruction. This process significantly promotes tumor growth, cancer cell resistance and poor patient outcome. Targeting these immuno-modulatory mechanisms in cancer therapy can alleviate immuno-suppression and promote efficient cancer cell eradication and improve patients' response to treatment. In this immuno-modulatory context, radiotherapy induces immunogenic cell death and macrophage repolarization towards an M1-like phenotype *in vitro*, but it also induces, via DDR, an increased expression of the immuno-suppressor PD-L1 in a dose and time-dependent manner (Krysko et al., 2012; Klug et al., 2013; Sato et al., 2017; Figures 26, 27 and 28). Radiotherapy as well as anti-PD-1 ICB present both immuno-stimulating properties, which, when used optimally in combination, could explain at a molecular level a potential synergic effect in HNSCC treatment, as it has been described in pre-clinical models and in clinics for various combinations of ICB with conventional treatments. Unlike conventional therapies, ICB is at short-term less effective, since the effective phase following ICB-induced immuno-stimulation requires some time. On the other hand, ICB is rarely affected by acquired resistance of cancer cells and is therefore capable of inducing long-term disease-free survival for a significant number of patients, compared to conventional treatments. By combining ICB to conventional therapies, such as radiotherapy, treatment can provide an important short-term efficacy as well as a highly increased rate of disease-free long-term survival for patients suffering from HNSCC (Figure 41). This effect could be further improved, by taking into account the mechanisms underlying the combined treatment, including the PD-L1 expression level after X-ray irradiation and potential radiation-induced macrophage repolarization.

During this project, several HNSCC cell lines were used to assess PD-L1 expression at the mRNA and protein levels, after X-ray irradiation. The results indicate that while at the mRNA level, PD-L1 overexpression is dose- and time-dependent, the most significant increases were not necessarily observed at the highest dose of radiation or the latest timing after irradiation. Depending on the cell line, specific conditions of PD-L1 overexpression were determined. This can be explained by the intrinsic radioresistance of each cancer cell line. Cal27 cell are radiosensitive, SQD9 cells are radio-resistant and SCC-VII cells present an intermediary radioresistance. While Cal27 and SCC-VII cells displayed a significantly increased PD-L1 expression 48 h after a 5 Gy irradiation, SQD9 cells only present an increased PD-L1 expression 72 h after irradiation, with a maximal increase after a 5 Gy irradiation. Unlike SCC-VII cells, Cal27 cells showed no increase in PD-L1 expression 72 h after irradiation. This might be due to too important DNA damage and cell function impairment. At protein level, the results clearly indicate that PD-L1 expression at the cell membrane gradually increases in a dose- and time-dependent manner. Based on these results, we suggest that when using anti-PD-1/PD-L1 ICB in combination with radiotherapy, the antibody should not be administrated simultaneously with the irradiation but it should be administrated at least 48 h after irradiation to actively block PD-L1-mediated T cell inactivation by cancer cells and induce T cell-, NK cell- and complement-mediated cytotoxicity. Further investigations should assess PD-L1 expression in cancer cells *in vivo* at later timings after irradiation to determine the period during

which, maintaining a constant level of ICB is crucial to optimally promote cancer cell eradication by the adaptive and innate immune system.

Based on the controversial information regarding whether photon and/or proton irradiation could both induce macrophage repolarization or if this can only be achieved by proton irradiation (Genard et al., 2017; Genard at al., 2018), we decided to also focus our attention on the compared immunomodulatory effect of proton vs photon irradiation. This study started by assessing PD-L1 expression following proton or photon irradiation. Due to technical limitations, currently only results of PD-L1 expression at the mRNA level in SCC-VII cell are available. The results show that only X-ray irradiation could induce PD-L1 overexpression. At this stage, we do not know, if at the protein level proton irradiation affects PD-L1 expression. This preliminary result indicates that the immuno-modulatory effects of proton vs. photon irradiation differ one from each other *in vitro*. To determine how proton irradiation acts differently on PD-L1 expression compared to X-ray irradiation, we suggest to start investigating the activation of the DDR mediated Stat1/3 – IRF-1 induction of PD-L1 following photon and proton irradiation. These experiments are already launched in progress. First results will soon be available.

Recently, Genard and colleagues showed that the impact of both types of radiation on macrophage polarization does not seem to be the same. While in vitro results regarding photon irradiation-induced macrophage repolarization from different studies are in disagreement whether radiation induces macrophage repolarization toward the M1 or M2 phenotype, it seems that *in vivo* X-ray irradiation does induces macrophage polarization towards an $iNOS^+$ M1-like phenotype (Klug et al., 2013). This shows the limitations and differences of *in vitro* TAMs models and the difficulty to accurately investigate one same biological process. For this reason, in the present study, an *in vivo* model of HNSCC was set up, to investigate more accurately X-ray irradiation-induced TAM repolarization and its impact on PD-1 ICB. This set up aimed to create a model of HNSCC, that allows the study of immune cells infiltrating the tumor. Since the immune-environment specific to each type of tissue throughout the body is known to have an impact on anti-cancer immune response within a specific organ, an orthotopic model would be optimal for our study. Although these models are much more reliable for the investigation of anti-cancer immune-reactions, we decided to exclude that option for several reasons. First, it required advanced skills for the precise injection of cancer cell into the appropriate site in the head and neck region, as well as the appropriate skills to precisely resect these tumors. Second, the formation of tumors, typically at the base of the tongue, often lead to a high number of premature deaths of mice due to cachexia (Lei et al., 2016). Third, for the intended analysis of CD8+ TILs and TAMs, a relatively important tumor volume is required (350 mm^3), which cannot be obtain in the head and neck region of mice. For this same reason, genetically engineered mice that spontaneously produce HNC were not considered. We therefore chose a synergic subcutaneous model of HNSCC. Different numbers of cells were injected to evaluate the tumor development depending on the number of injected cells. We also assessed whether 250 or 350 mm^3 of tumor volume are sufficient for the intended analysis. Histologic analysis were performed to characterize the phenotype of cancer cells, tumor vascularization, cancer cell invasiveness, formation of necrosis and immune infiltration. The results show that tumors

are highly vascularized and infiltrated by immune cells, which spread homogenously throughout the tumors. It was shown macroscopically that cancer cells are highly invasive, infiltrating nearby muscles and LNs as well as distant LNs after growing approximately 5 weeks. Cancer cells in the tumor periphery present a mesenchymal-like phenotype similar to the phenotype observed in the periphery of distant LNs cancer cells. This leads us to believe that cancer cells observed in the periphery of the tumors undergo epithelio-mesenchymal transition and invade subsequently distant LNs. No cancer cells infiltration could be observed in the spleen. From 350 mm^3 big tumors, sufficient TILs and TAMs could be isolated to perform the intended flow cytometry analysis after splitting tumor in three sections for, TILs and TAM isolation, RNA extraction and histologic analysis. At this stage, based on the histology analysis, no significant difference could be observed so far between untreated mice and mice treated by X-ray irradiation. It seems that mice treated by X-ray irradiation have an increased number of TILs, similarly to what has been described previously after low dose γ–ray irradiation (Klug et al., 2013). Immuno-fluorescence labelling and subsequent quantification of CD3+ TILs remains to be performed to confirm this observation. Based on the results, we meanwhile validated our syngenic model of subcutaneous HNSCC and initiated a second project which aimed to investigate the efficiency of a combined treatment of anti-PD-1 ICB and radiotherapy as well as the underlying mechanisms.

During this second project, mice were treated by X-ray irradiation, anti-PD-1 ICB or the combined treatment in order to investigate the potential synergic effect regarding CD8+ TILs activation and exhaustion levels but also to investigate the impact of potential radiation-induced TAM repolarization on treatment efficiency. We found that X-ray irradiation induced a significantly increased early and late CD8+ T cell activation. The hypothesis was that radiation-induced macrophage repolarization from an M2, towards an M1-like phenotype induced increased lymphocyte recruitment, lower TILs inactivation and immunosuppression, in addition to increased pro-inflammatory cytokine secretion and TIL activation after antigen presentation. In order to confirm this hypothesis, TAM polarization needed to be assessed. While flow cytometry analysis allows to specifically analyze TAMs independently of other myeloid cell such as monocytes DC or neutrophils, with the available equipment only one TAM polarization marker could be assessed. MH-CII and CD80 (data not shown), which are commonly recommended polarization markers, were both tested during the pilot project to determine which one is best suited to distinguish M1 from M2 TAMs. Only using MHC-II allowed to clearly differentiate between both polarizations (data not shown). During the main *in vivo* project using this polarization marker, no TAM repolarization from and M2 towards and M1-like could be observe. This could mean that X-ray irradiation does not induce TAM repolarization and that the increased TILs recruitment and activation is not mediated by TAM repolarization. However, the determination of TAM polarization using only one polarization marker can be an important bias. It is possible that X-ray irradiation induces TAM repolarization towards and M1-like phenotype but that this requires the assessment of several polarization markers at the protein and mRNA level. Whole tumor RNA isolations were performed assess macrophage polarization markers by RT-qPCR. It should be noted that this technique can be biased by all other cells inside the TME. It is however recognized as an acceptable method to determine macrophage polarization within an organ. The optimal method

to accurately evaluate TAM polarization is to isolate TAMs from the tumors and analyze them by mass cytometry coupled to subsequent single cell RNA sequencing. This would allow to assess the expression of numerous polarization markers at once. This way, TAMs could even be subdivided into specific populations of TAMs which might have individual functions on immuno-modulation at the TME, for instance CD8+ TILs activation and recruitment. To quantify the impact of X-ray irradiation on TAM recruitment in the TME, immune-histochemistry staining for F4/80+ cell within the tumors is required. The technique is currently in development in our lab and results can be expected soon.

During the main *in vivo* project, mice treated with an anti-PD-1 ICB showed a significantly increased CD8+ TIL activation as well as a shift in TAM polarization from an M2-like towards a M1-like phenotype. This ICB thus efficiently blocked the induction of T cell inactivation by preventing receptor to ligand interaction. Surprisingly, this anti-PD-1 ICB also induced an increase in M1-like macrophage polarization and a decrease of M2-like macrophages within the myeloid cell population. Mechanisms underlying this ICB-induced macrophage repolarization remain unclear and require further investigation.

The combined treatment of X-ray irradiation followed by anti-PD-1 ICB administration showed only very low efficiency since besides a slight increase in late CD8+ TIL activation and small decrease in MHC-II^{low} macrophages, no improvement in the anticancer immune response could be observed. However, this result would need to be confirmed by a second *in vivo* experiment. Indeed, significant technical problems with X-ray generator caused an important delay for the irradiation of mice. This delay could explain an altered immune-background within the tumor by the time the treatment was administrated and thereby influence the results. It should also be mentioned that the treatment efficiency for this project was defined as the activation and exhaustion levels of CD8+ T cells. We have no information on the efficacy of the combined treatment regarding tumor development and survival of tumor bearing mice. Independent experiments would need to be performed to determine if the combined treatment has a synergic effect regarding mice survival.

In order to determine the role of TAMs, independently of their polarization, on the efficiency of the combined treatment of anti-PD-1 ICB and X-ray irradiation, a new *in vivo* experiment should be initiated containing the four experimental groups as previously but mice would undergo macrophage depletion by clodronate-loaded liposome treatment. This way, the impact of the combined treatment on immune cell infiltration and CD8+ TIL activation and exhaustion can be evaluated independently of the impact of TAMs on the anti-cancer immune response. This would allow a better understanding of the role of TAMs in anti-cancer immunity, treatment response and cancer cell resistance. Afterwards, new *in vivo* experiments could be launched using proton or carbon ion irradiation instead of X-ray irradiation to evaluate proton vs. carbon- vs. photon-irradiation-induced immuno-modulation, based on the previously used criteria, immune infiltration, TAM polarization and T cell activation. Since the efficacy of proton and carbon-irradiation with ICBs has never been performed yet, additionally survival analysis should be performed.

In conclusion, this project allowed to elucidate *in vitro* and *in vivo* some of the radiotherapy-induced immuno-modulatory effects within the tumor microenvironment, that can be exploited in clinics for improved anti-cancer therapy, most notably immune checkpoint blockage, and contributed to reduced tumor growth, treatment resistance and promote patient survival.

Bibliography

Arasanz, H., Gato-Canas, M., et al. (2017). PD1 signal transduction pathways in T cells. Oncotarget, 8(31), 51936-51945. doi:10.18632/oncotarget.17232

Bardhan, K., Anagnostou, T., et al. (2016). The PD1:PD-L1/2 Pathway from Discovery to Clinical Implementation. Front Immunol, 7, 550. doi:10.3389/fimmu.2016.00550

Bernier, J., Hall, E. J., et al. (2004). Radiation oncology: a century of achievements. Nat Rev Cancer, 4(9), 737-47. doi:10.1038/nrc1451

Borrego-Soto, G., Ortiz-Lopez, R., et al. (2015). Ionizing radiation-induced DNA injury and damage detection in patients with breast cancer. Genet Mol Biol, 38(4), 420-32. doi:10.1590/S1415-475738420150019

Bournazos, S., Wang, T. T., et al. (2016). The Role and Function of Fcgamma Receptors on Myeloid Cells. Microbiol Spectr, 4(6). doi:10.1128/microbiolspec.MCHD-0045-2016

Brandsma, I., & Gent, D. C. (2012). Pathway choice in DNA double strand break repair: observations of a balancing act. Genome Integr, 3(1), 9. doi:10.1186/2041-9414-3-9

Champiat, S., Ileana, E., et al. (2014). Incorporating immune-checkpoint inhibitors into systemic therapy of NSCLC. J Thorac Oncol, 9(2), 144-53. doi:10.1097/JTO.0000000000000074

Chen, Y., & Ahmad, S. (2012). Empirical model estimation of relative biological effectiveness for proton beam therapy. Radiat Prot Dosimetry, 149(2), 116-23. doi:10.1093/rpd/ncr218

Dasari, S., & Tchounwou, P. B. (2014). Cisplatin in cancer therapy: molecular mechanisms of action. Eur J Pharmacol, 740, 364-78. doi:10.1016/j.ejphar.2014.07.025

Deng, L., Liang, H., et al. (2014). Irradiation and anti-PD-L1 treatment synergistically promote antitumor immunity in mice. J Clin Invest, 124(2), 687-95. doi:10.1172/JCI67313

Duarte, S., Loubat, A., et al. (2012). Isolation of head and neck squamous carcinoma cancer stem-like cells in a syngeneic mouse model and analysis of hypoxia effect. Oncol Rep, 28(3), 1057-62. doi:10.3892/or.2012.1904

Ferris, R. L., Blumenschein, G., Jr., et al. (2016). Nivolumab for Recurrent Squamous-Cell Carcinoma of the Head and Neck. N Engl J Med, 375(19), 1856-1867. doi:10.1056/NEJMoa1602252

Genard, G., Lucas, S., et al. (2017). Reprogramming of Tumor-Associated Macrophages with Anticancer Therapies: Radiotherapy versus Chemo- and Immunotherapies. Front Immunol, 8, 828. doi:10.3389/fimmu.2017.00828

Genin, M., Clement, F., et al. (2015). M1 and M2 macrophages derived from THP-1 cells differentially modulate the response of cancer cells to etoposide. BMC Cancer, 15, 577. doi:10.1186/s12885-015-1546-9

Gong, J., Chehrazi-Raffle, A., et al. (2018). Development of PD-1 and PD-L1 inhibitors as a form of cancer immunotherapy: a comprehensive review of registration trials and future considerations. J Immunother Cancer, 6(1), 8. doi:10.1186/s40425-018-0316-z

Green, C. E., Liu, T., et al. (2009). Chemoattractant signaling between tumor cells and macrophages regulates cancer cell migration, metastasis and neovascularization. PLoS One, 4(8), e6713. doi:10.1371/journal.pone.0006713

Gregoire, V., Ang, K., et al. (2014). Delineation of the neck node levels for head and neck tumors: a 2013 update. DAHANCA, EORTC, HKNPCSG, NCIC CTG, NCRI, RTOG, TROG

consensus guidelines. Radiother Oncol, 110(1), 172-81. doi:10.1016/j.radonc.2013.10.010

Gregoire, V., Lefebvre, J. L., et al. (2010). Squamous cell carcinoma of the head and neck: EHNS-ESMO-ESTRO Clinical Practice Guidelines for diagnosis, treatment and follow-up. Ann Oncol, 21 Suppl 5, v184-6. doi:10.1093/annonc/mdq185

Grosse, N., Fontana, A. O., et al. (2014). Deficiency in homologous recombination renders Mammalian cells more sensitive to proton versus photon irradiation. Int J Radiat Oncol Biol Phys, 88(1), 175-81. doi:10.1016/j.ijrobp.2013.09.041

Hanahan, D., & Coussens, L. M. (2012). Accessories to the crime: functions of cells recruited to the tumor microenvironment. Cancer Cell, 21(3), 309-22. doi:10.1016/j.ccr.2012.02.022

Hanahan, D., & Weinberg, R. A. (2000). The hallmarks of cancer. Cell, 100(1), 57-70.

Hanahan, D., & Weinberg, R. A. (2011). Hallmarks of cancer: the next generation. Cell, 144(5), 646-74. doi:10.1016/j.cell.2011.02.013

Hargadon, K. M., Johnson, C. E., et al. (2018). Immune checkpoint blockade therapy for cancer: An overview of FDA-approved immune checkpoint inhibitors. Int Immunopharmacol, 62, 29-39. doi:10.1016/j.intimp.2018.06.001

Harrington, K. J., Ferris, R. L., et al. (2017). Nivolumab versus standard, single-agent therapy of investigator's choice in recurrent or metastatic squamous cell carcinoma of the head and neck (CheckMate 141): health-related quality-of-life results from a randomised, phase 3 trial. Lancet Oncol, 18(8), 1104-1115. doi:10.1016/S1470-2045(17)30421-7

Jemal, A., Bray, F., et al. (2011). Global cancer statistics. CA Cancer J Clin, 61(2), 69-90. doi:10.3322/caac.20107

Khanna, A. (2015). DNA damage in cancer therapeutics: a boon or a curse? Cancer Res, 75(11), 2133-8. doi:10.1158/0008-5472.CAN-14-3247

Kim, L., King, T., et al. (2010). Head and neck cancer: changing epidemiology and public health implications. Oncology (Williston Park), 24(10), 915-9, 924.

Klug, F., Prakash, H., et al. (2013). Low-dose irradiation programs macrophage differentiation to an iNOS(+)/M1 phenotype that orchestrates effective T cell immunotherapy. Cancer Cell, 24(5), 589-602. doi:10.1016/j.ccr.2013.09.014

Kroemer, G., Galluzzi, L., et al. (2013). Immunogenic cell death in cancer therapy. Annu Rev Immunol, 31, 51-72. doi:10.1146/annurev-immunol-032712-100008

Krysko, D. V., Garg, A. D., et al. (2012). Immunogenic cell death and DAMPs in cancer therapy. Nat Rev Cancer, 12(12), 860-75. doi:10.1038/nrc3380

Leemans, C. R., Braakhuis, B. J., et al. (2011). The molecular biology of head and neck cancer. Nat Rev Cancer, 11(1), 9-22. doi:10.1038/nrc2982

Leemans, C. R., Snijders, P. J. F., et al. (2018). The molecular landscape of head and neck cancer. Nat Rev Cancer, 18(5), 269-282. doi:10.1038/nrc.2018.11

Lei, Z. G., Ren, X. H., et al. (2016). Immunocompromised and immunocompetent mouse models for head and neck squamous cell carcinoma. Onco Targets Ther, 9, 545-55. doi:10.2147/OTT.S95633

Lomax, M. E., Folkes, L. K., et al. (2013). Biological consequences of radiation-induced DNA damage: relevance to radiotherapy. Clin Oncol (R Coll Radiol), 25(10), 578-85. doi:10.1016/j.clon.2013.06.007

Longley, D. B., Harkin, D. P., et al. (2003). 5-fluorouracil: mechanisms of action and clinical strategies. Nat Rev Cancer, 3(5), 330-8. doi:10.1038/nrc1074

Miller, R. C., Lodge, M., et al. (2013). Controversies in clinical trials in proton radiotherapy: the present and the future. Semin Radiat Oncol, 23(2), 127-33. doi:10.1016/j.semradonc.2012.11.004

Nirschl, C. J., & Drake, C. G. (2013). Molecular pathways: coexpression of immune checkpoint molecules: signaling pathways and implications for cancer immunotherapy. Clin Cancer Res, 19(18), 4917-24. doi:10.1158/1078-0432.CCR-12-1972

Ott, P. A., Hodi, F. S., et al. (2013). CTLA-4 and PD-1/PD-L1 blockade: new immunotherapeutic modalities with durable clinical benefit in melanoma patients. Clin Cancer Res, 19(19), 5300-9. doi:10.1158/1078-0432.CCR-13-0143

Reisz, J. A., Bansal, N., et al. (2014). Effects of ionizing radiation on biological molecules--mechanisms of damage and emerging methods of detection. Antioxid Redox Signal, 21(2), 260-92. doi:10.1089/ars.2013.5489

Rostek, C., Turner, E. L., et al. (2008). Involvement of homologous recombination repair after proton-induced DNA damage. Mutagenesis, 23(2), 119-29. doi:10.1093/mutage/gem055

Sato, H., Niimi, A., et al. (2017). DNA double-strand break repair pathway regulates PD-L1 expression in cancer cells. Nat Commun, 8(1), 1751. doi:10.1038/s41467-017-01883-9

Schaue, D., Ratikan, J. A., et al. (2012). Maximizing tumor immunity with fractionated radiation. Int J Radiat Oncol Biol Phys, 83(4), 1306-10. doi:10.1016/j.ijrobp.2011.09.049

Schiller, K. C., Habl, G., et al. (2016). Protons, Photons, and the Prostate - Is There Emerging Evidence in the Ongoing Discussion on Particle Therapy for the Treatment of Prostate Cancer? Front Oncol, 6, 8. doi:10.3389/fonc.2016.00008

Schreiber, R. D., Old, L. J., et al. (2011). Cancer immunoediting: integrating immunity's roles in cancer suppression and promotion. Science, 331(6024), 1565-70. doi:10.1126/science.1203486

Siegel, R. L., Miller, K. D., et al. (2017). Cancer Statistics, 2017. CA Cancer J Clin, 67(1), 7-30. doi:10.3322/caac.21387

Tsujikawa, T., Yaguchi, T., et al. (2013). Autocrine and paracrine loops between cancer cells and macrophages promote lymph node metastasis via CCR4/CCL22 in head and neck squamous cell carcinoma. Int J Cancer, 132(12), 2755-66. doi:10.1002/ijc.27966

Ugel, S., De Sanctis, F., et al. (2015). Tumor-induced myeloid deviation: when myeloid-derived suppressor cells meet tumor-associated macrophages. J Clin Invest, 125(9), 3365-76. doi:10.1172/JCI80006

Vermorken, J. B., Mesia, R., et al. (2008). Platinum-based chemotherapy plus cetuximab in head and neck cancer. N Engl J Med, 359(11), 1116-27. doi:10.1056/NEJMoa0802656

Vermorken, J. B., & Specenier, P. (2010). Optimal treatment for recurrent/metastatic head and neck cancer. Ann Oncol, 21 Suppl 7, vii252-61. doi:10.1093/annonc/mdq453

Wang, H., Wang, X., et al. (2008). The Ku-dependent non-homologous end-joining but not other repair pathway is inhibited by high linear energy transfer ionizing radiation. DNA Repair (Amst), 7(5), 725-33. doi:10.1016/j.dnarep.2008.01.010

Wang, M., Zhang, C., et al. (2017). Mechanism of immune evasion in breast cancer. Onco Targets Ther, 10, 1561-1573. doi:10.2147/OTT.S126424

Williams, G. J., Lees-Miller, S. P., et al. (2010). Mre11-Rad50-Nbs1 conformations and the control of sensing, signaling, and effector responses at DNA double-strand breaks. DNA Repair (Amst), 9(12), 1299-306. doi:10.1016/j.dnarep.2010.10.001

Wu, C. T., Chen, W. C., et al. (2016). The role of PD-L1 in the radiation response and clinical outcome for bladder cancer. Sci Rep, 6, 19740. doi:10.1038/srep19740

Wu, C. T., Chen, W. C., et al. (2016). The role of PD-L1 in the radiation response and clinical outcome for bladder cancer. Sci Rep, 6, 19740. doi:10.1038/srep19740

Appendix

1 Appendix I

Demande d'autorisation d'essai préliminaire utilisant des animaux d'expérience

I. Présentation de l'essai préliminaire

TITRE DE L'EXPERIENCE dans laquelle l'essai préliminaire s'inscrit :

Etude de la reprogrammation des macrophages tumoraux par irradiation avec des photons afin d'amplifier l'effet d'anticorps ciblant l'immunomodulateur PD-L1 sur des tumeurs murines d'origine ORL

Laboratoire : Unité de Recherche en Biologie Cellulaire (URBC)-Narilis- Faculté des Sciences
N° d'agrément LA : LA1900053

Directeur : Thierry Arnould Tel.: +32 (0)81 72 41 25 Email: thierry.arnould@unamur.be

Personnel impliqué dans cet essai (maîtres d'expérience et bio-techniciens)

Nom	Maître d'expérience	Bio-technicien	Tel ou E-mail	Formation réglementaire
Thierry Arnould	☒ porte parole	☐	thierry.arnould@unamur.be	☒ 2007, Uliège
Carine Michiels	☒	☐	carine.michiels@unamur.be	☒ Accepté de facto, 2005
Eléonore Longton	☒	☐	eleonore.longton@unamur.be	☒ Janvier 2017, UNamur
Christoph Schifflers	☐	☒	christoph.schifflers@student.unamur.be	☒ Mai 2018, UNamur
Maude Fransolet	☐	☒	maude.fransolet@unamur.be	☒ 2011, UNamur

Nombre d'animaux :

	Nombre d'animaux	Espèce et souche
Du 15/08 au 15/10/2018	**27**	***Mus musculus* C3H/HeOuJ**

Type d'essai préliminaire :
☒ Mise au point d'une technique opératoire
☐ Mise au point d'un protocole anesthésique
☐ Mise au point d'un protocole analgésique
☐ Détermination du niveau de douleur d'une expérience
☒ Détermination du dosage d'un produit à tester
☐ Mise au point des points limites
☒ Autre : Mise au point du volume tumoral nécessaire à l'isolation des TILs et TAMs (Justification de l'essai)

Niveau de gravité de l'essai (si connu) :
☐ NR : non recovery - sans réveil : sans aucune douleur ou aucun inconfort
☐ Léger
☒ Modéré
☐ Sévère

II. Justification et description de l'essai préliminaire

Justification de l'essai, du nombre d'animaux et du temps demandé

Nous savons que parmi les nombreux acteurs qui permettent à notre système immunitaire de lutter contre les maladies, dont le cancer, les lymphocytes T jouent un rôle primordial. Toutefois, les cellules tumorales peuvent échapper au système immunitaire, notamment en exprimant à leur surface une protéine appelée PD-L1. PD-L1 va inactiver les lymphocytes T en se liant à des récepteurs dont PD-1 présents à la surface des lymphocytes T. Cette liaison entre PD-L1 et ses récepteurs constitue une cible thérapeutique intéressante pour l'immuno-oncologie. En effet, le blocage de la protéine PD-L1 peut empêcher les cellules cancéreuses d'inactiver les lymphocytes T et ainsi permettre aux lymphocytes T cytotoxiques (CD8+) de retrouver leur rôle dans la destruction des cellules cancéreuses. Récemment, il a été démontré que l'expression de l'immuno-modulateur PD-L1 dans les cellules tumorales pouvait augmenter suite à une irradiation par photons (Deng et al, 2014). *In vitro,* nos résultats préliminaires sur des lignées tumorales humaines d'origine ORL ont d'ailleurs permis de mettre en évidence une variation de l'expression de PD-L1 en fonction de la dose de rayons X et du temps post-irradiation (Christoph Schifflers, master 1 BBMC, mini-mémoire, juin 2018). L'irradiation restant un traitement standard dans de nombreux cancers, la combinaison d'un anticorps anti-PD-L1 avec des rayons X semble prometteuse, et son utilisation dans des conditions optimales favoriserait une efficacité thérapeutique maximale. Cependant, les mécanismes sous-jacents à l'efficacité de ce traitement combiné restent peu connus.

Les macrophages associés aux tumeurs (TAMs) représentent une majorité des cellules immunitaires présentes dans le micro-environnement tumoral. Ces TAMs présentent des phénotypes différents, variant entre un phénotype de type M1 (pro-inflammatoire/anti-tumoral) et un phénotype de type M2 (anti-inflammatoire/pro-tumoral). Une tumeur à un stade débutant sera principalement associée à des TAMs de type M1, c'est-à-dire de macrophages anti-tumoraux. A un stade tumoral plus avancé, le micro-environnement sera principalement constitué de TAMs de type M2 pro-tumoraux. Cependant, ces phénotypes M1 et M2 sont modulables en fonction de différents facteurs environnants. Il a notamment été démontré que l'irradiation par photons et protons pouvait permettre de repolariser les macrophages M2 pro-tumoraux vers un phénotype M1 anti-tumoral (Genard et al, 2017).

Notre hypothèse de travail est donc que l'irradiation par photons en amplifiant l'expression de PD-L1 permet d'augmenter l'effet d'une immunothérapie par un anticorps anti-PD-L1 et ce, via la désinhibition des lymphocytes cytotoxiques infiltrant la tumeur (TILs), mais également via la repolarisation des macrophages associés aux tumeurs (TAMs) vers un phénotype de type anti-tumoral.

L'étude *in vitro* nous a permis d'étudier la plasticité des macrophages humains, polarisés à partir de monocytes humains, les THP-1, après l'irradiation par photons ainsi que les mécanismes impliqués dans cette éventuelle repolarisation des macrophages (résultats repris dans la thèse de Géraldine Genard, en URBC, défendue en mai 2018). Elle nous a permis également d'étudier l'effet immunomodulateur des photons sur des cellules cancéreuses d'origine ORL ainsi que les doses et timing post-irradiation permettant une efficacité thérapeutique maximale de l'anticorps anti-PD-L1.

L'expérimentation animale nous permettra quant à elle, d'étudier dans un modèle plus complexe l'effet de l'irradiation par photons sur le phénotype des TAMs et des TILs. Ces informations sont impossibles à obtenir sur un modèle *in vitro* puisque les TAMs et les TILs sont fondamentalement différents des macrophages différenciés expérimentalement à partir de monocytes et des lymphocytes circulants qui ne sont pas antigènes spécifiques.

Afin de pouvoir investiguer la population immunitaire dans l'environnement tumoral, un modèle syngénique murin sera utilisé (Smith et al. 2006). Pour cela, une lignée cellulaire tumorale d'origine ORL, la lignée SCC-VII, développée spontanément chez la souris C3H, sera injectée en sous-cutanée afin d'induire progressivement une tumeur. Celle-ci a déjà été étudiée et décrite dans la littérature en association à une immunothérapie (Khurana et al. 2001). De plus, la lignée tumorale SCC-VII est agressive et peu immunogène. Elle représente donc un modèle idéal pour étudier la réponse tumorale spécifique des cellules T. Ce modèle nous permettra également d'analyser l'efficacité du traitement combiné sur le système immunitaire. Nous avons choisi d'utiliser la souris C3H/HeOuJ comme modèle syngénique car celle-ci est disponible chez Charles River et a déjà été étudiée *in vivo* avec la même lignée tumorale (Duarte et al. 2012).

Cette étude *in vivo* sur un modèle syngénique nous permettra d'isoler les lymphocytes T CD8+ infiltrant la tumeur (TILs) afin d'étudier l'activation par analyses en cytométrie en flux (Ahmadzadeh et al, 2009) ainsi que le phénotype des macrophages associés aux tumeurs et ce, après traitement par irradiation et/ou des anticorps anti-PD-L1. De plus, le modèle syngénique nous permettra également de faire des analyses histologiques, notamment pour étudier l'impact à court terme du traitement par irradiation et/ou des anticorps anti-PD-L1 sur les TAMs et les TILs mais aussi d'évaluer des éventuelles altérations au niveau des organes lymphoïdes drainant la tumeur.

Cette étude n'ayant jamais été réalisée, ce projet préliminaire a pour but de déterminer les conditions expérimentales optimales pour le projet principal. Pour ceci, le projet préliminaire devra déterminer 2 paramètres importants avant de commencer le projet principal :

- Le nombre de cellules murines cancéreuses d'origine ORL, les SCC-VII, à injecter par souris (250 000, 500 000 ou 1 000 000 cellules) ; le but étant de déterminer un temps de croissance tumoral suffisant que pour obtenir un infiltrat immunitaire péri-tumoral analysable. En effet, si la croissance tumorale est trop rapide, la réponse immunitaire risque d'être pauvre et la tumeur risque de contenir plus de zones de nécrose.
- Un volume tumoral suffisant que pour réaliser les analyses biologiques prévues[1], considérant que la tumeur sera scindée en 2 parties (volume tumoral total : 250 mm^3 ou 350 mm^3, déterminé après discussion avec Kathleen Schmit sur base de son projet DAEP16273AR, cfr images en annexe) ; nous souhaitons une taille tumorale suffisante pour faire nos analyses mais sans atteindre un volume trop important (> 350 mm^3) qui pourrait contenir plus de plages de nécrose et pourraient impacter sur le bien-être de la souris.

Considérant ces 2 paramètres à déterminer, nous souhaiterions utiliser 3 souris par groupe expérimental, afin de nous assurer de la faisabilité de nos expériences.
L'utilisation de 3 souris nous permettra également de comparer en histologie une tumeur analysée dans son entièreté par rapport à une tumeur scindée en deux moitiés, l'une pour comparer la répartition et la proportion des différentes populations cellulaires grâce à des coupes histologiques, et l'autre moitié pour permettre l'obtention en nombre suffisant de TILs et de TAMs pour des analyses par cytométrie en flux.

Le nombre de souris nécessaire à ce projet préliminaire est donc égale à :

Nombre de souris (3) par groupe expérimental (6), additionné de 3 souris contrôle (non irradiées) dans chaque groupe d'injection de cellules cancéreuses (3).

[1] Isolation de cellules spécifiques (TILs et TAMs) et analyses par cytométrie en flux ; Analyse histologique des tumeurs et divers tissus lymphoïdes ;

4

Paramètre 2	Paramètre 1			
Groupe	250 000 cellules	500 000 cellules	1000 000 cellules	TOTAL
250 mm3	3	3	3	9
350 mm3	3	3	3	9
Contrôle (non irradié)	3	3	3	**27**

Donc : 27 souris

De plus, cette étude préliminaire nous permettra de mettre au point les conditions d'irradiation, notamment l'utilisation d'une surface plombée, pour limiter l'irradiation au site d'injection des cellules cancéreuses (voir description de l'essai) mais également les conditions pour maintenir un confort optimal pour les souris avant, pendant et après l'irradiation.

Nous essayerons un temps de 8 semaines pour réaliser l'essai préliminaire. 27 souris femelles seront achetées à 5-6 semaines d'âge et resteront en acclimatation durant 1 à 2 semaines avant d'être injectées de 250 000, 500 000 ou 1 000 000 de cellules cancéreuses. L'irradiation aura lieu lorsque la tumeur aura atteint le volume attendu (250 mm^3 ou 350 mm^3), environ 2 à 4 semaines après l'injection. L'euthanasie aura lieu 72 h après l'irradiation et/ou l'injection de l'anticorps anti-PD-L1 afin d'étudier la réaction immunitaire.

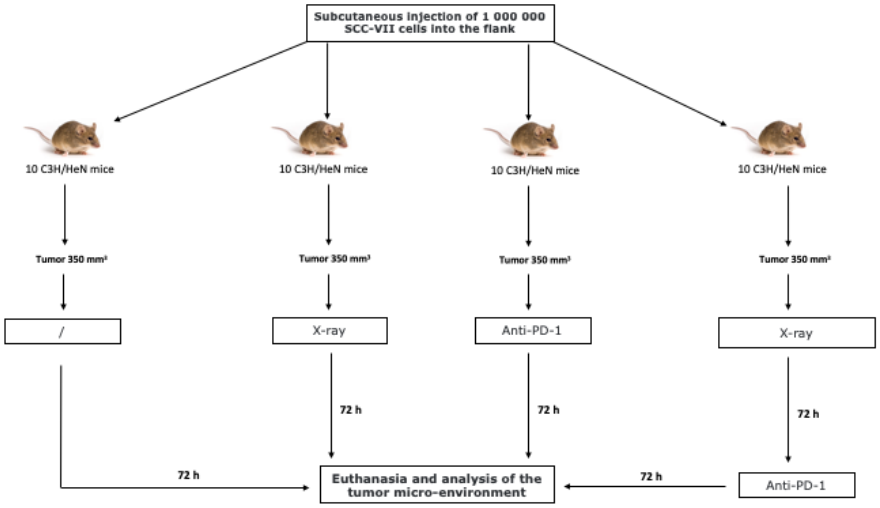

Deng, L., Liang, H., et al. (2014). Irradiation and anti-PD-L1 treatment synergistically promote antitumor immunity in mice. J Clin Invest, 124(2), 687-95. doi:10.1172/JCI67313

Genard, G., Lucas, S., et al. (2017). Reprogramming of Tumor-Associated Macrophages wi Anticancer Therapies: Radiotherapy versus Chemo- and Immunotherapies. Front Immunol, 8, 828. doi:10.3389/fimmu.2017.00828

Smith, L. P. and G. R. Thomas (2006). "Animal models for the study of squamous cell carcinoma of the upper aerodigestive tract: a historical perspective with review of their utility and limitations. Part A. Chemically-induced de novo cancer, syngeneic animal models of HNSCC, animal models of transplanted xenogeneic human tumors." Int J Cancer **118**(9): 2111-2122.

Khurana, D., et al. (2001). "Characterization of a spontaneously arising murine squamous cell carcinoma (SCC VII) as a prerequisite for head and neck cancer immunotherapy." Head Neck **23**(10): 899-906.

Duarte, S., et al. (2012). "Isolation of head and neck squamous carcinoma cancer stem-like cells in a syngeneic mouse model and analysis of hypoxia effect." Oncol Rep 28(3): 1057-1062.

Ahmadzadeh, M., Johnson, L. A., et al. (2009). Tumor antigen-specific CD8 T cells infiltrating the tumor express high levels of PD-1 and are functionally impaired. Blood, 114(8), 1537-44. doi:10.1182/blood-2008-12-195792

Description de l'essai

- Les souris (femelles) seront achetées à l'âge de 5-6 semaines et hébergées à l'animalerie centralisée de l'extension biologie de l'UNamur (L1900631).
- Après 1-2 semaines d'acclimatation, les souris seront individuellement anesthésiées à l'isoflurane (3-4% avec un débit d'oxygène de 0,8-1,5 L/min) en utilisant la table d'anesthésie disponible à l'animalerie centrale. Sous anesthésie, elles recevront alors l'injection dans 150 µl de PBS de 250 000, 500 000 ou 1 000 000 de cellules cancéreuses SCC-VII en sous-cutané au niveau du flanc droit et ce, afin d'éviter d'irradier la rate (organe lymphoïde secondaire) présente au niveau du flanc gauche. Les souris seront ensuite placées sous une lampe chauffante afin de maintenir leur température corporelle jusqu'à leur réveil. A noter que lors de l'anesthésie de la première souris, une plaque en plomb (15 cm x 10 cm x 0,5 - 1 cm) sera maintenue 1 cm au-dessus de la souris et un trou d'environ 1 cm de diamètre sera coupé dans la plaque juste au niveau de la tumeur. Cette plaque servira de moyen de radioprotection lors de l'irradiation par rayons X pour limiter l'exposition uniquement au site d'injection des cellules cancéreuses.
- Une fois réveillées, une administration d'analgésique sera réalisée par injection de buprénorphine (0,05 mg/kg, en sous-cutané - Flecknell 2018), en cas de signes de douleur. Une fois la taille tumorale atteinte selon le groupe expérimental défini, environ 2 à 4 semaines après l'injection, les souris seront irradiées. A ce moment-là, les souris, par groupe de 3, seront anesthésiées via une injection intra-péritonéale de Kétamine et de Xylazine (100 mg/kg et 10 mg/kg, en intra-péritonéal (suivant le protocole validé ANIM PO 0007 déposé sur la plate-forme SVTA) et transportées au laboratoire d'analyses par réactions nucléaires (LARN, Prof. Stéphane Lucas LA 1900053) dans une cage de transport, emballée dans un sac poubelle opaque afin de ne pas être vues par des personnes non-impliquées dans ce projet. Au LARN, elles seront irradiées individuellement par rayons X avec une dose unique de 5 ou 10 Gy, suivant les conditions préalablement déterminées *in vitro* (Christoph Schifflers, master 1 BBMC, mémoire, 2018). Pour cela, la souris sera placée dans le générateur (X-RAD 225XL/Xli X-ray generator (PXI Precision X-ray)), sur un gel préchauffé à 37°C pour éviter l'hypothermie. Un portoir, sur lequel la plaque de plomb préalablement préparée sera déposée, sera placé au-dessus de la souris, sans la toucher. Après l'irradiation, les souris seront replacées dans leur cage également munie d'un gel préchauffé et ramenées à l'animalerie centrale.
- Les souris seront euthanasiées 72 heures après l'irradiation. Pour ceci, une anesthésie générale via une injection intra-péritonéale de Kétamine et de Xylazine (100 mg/kg et 10 mg/kg, I.P.) (suivant le protocole validé ANIM PO 0007 déposé sur la plate-forme SVTA) sera réalisée à l'animalerie centrale. Une fois que les souris seront endormies, elles seront transportées au

laboratoire de physiologie générale en URPhyM (LA 1900055), où une ponction intra-cardiaque sera réalisée pour prélever un volume sanguin maximal, qui servira à l'isolation des monocytes périphériques circulants. La ponction intra-cardiaque sera suivie d'une dislocation cervicale. Post-mortem, différents tissus seront prélevés : la tumeur, ainsi que divers organes lymphoïdes (analyses histologiques) tels que la rate, l'intestin (la jonction iléo-coecale), des ganglions lymphatiques et si possible le thymus. Afin d'isoler différentes populations cellulaires à partir des tumeurs (TILs et TAMs), celles-ci doivent être dissociées et les cellules isolées au plus vite après l'euthanasie des souris et ce en utilisant un gentleMACS dissociateur. Considérant que la dissociation tumorale et l'isolation des cellules doivent être effectuées le plus rapidement possible et nécessitent un l'équipement uniquement disponible au laboratoire de physiologie générale, les euthanasies doivent avoir lieu au laboratoire de physiologie générale. L'anesthésie générale (Kétamine/Xylazine) sera cependant réalisée à l'animalerie centrale ce qui permet d'éviter le stress associé au transport que les souris subiraient autrement.

Au cours de l'expérimentation animale, le bien-être sera évalué au quotidien en réalisant un examen général de chaque animal et en regardant sa réaction à divers stimuli tels que la lumière ou le bruit. De plus, l'état de la cage sera vérifié : les niveaux d'eau et de nourriture ingérés seront analysés et il y aura un examen macroscopique des selles. Il sera impératif que la présence de la tumeur n'altère en rien les comportements physiologiques de l'animal. Un tableau de score est associé pour cette évaluation (adapté du tableau de score du projet DAEP16273AR de Kathleen Schmit) :

Animal ID: Souche + sexe: Age au moment de l'injection: Poids au moment de l'injection: Niveau de douleur:

Nom de l'expérimentateur:

		score	date	date	date	date	date	date
Paramètres étudiés	Age							
	Poids							
Examen général								
Perte de poids (par rapport au poids total de souris du même âge)	0 %	0						
	5 %	1						
	10 %	2						
	15 %	4						
	20 %	**6**						
Apparence/couleur	Normal	0						
	Abdomen bleu	1						
	Extrémités pâles	2						
Température en surface	Chaud	0						
	Indécis	1						
	Froid	2						
Reflexes/réponse au toucher	+++	0						
	++	1						
	+	2						
	-	3						

Comportement dans sa cage	Normal	0						
	Apathie	1						
	Léthargie	1						
	Rigidité	2						
Léchage	++	1						
	+	0						
	-	1						
Comportement alimentaire	Mange ++, boit ++	0						
	Mange +, boit +	1						
	Mange -, boit -	2						
	Mange --, boit --	3						
Tremblement	-	0						
	+	1						
Posture voutée	-	0						
	+	1						
Déshydratation	-	0						
	+	1						
	++	2						
Vomissement	-	0						
	+	1						
	++	2						
Excréments	Normaux	0						
	Diarrhée	1						
Respiration	Normale	0						
	Difficile	1						
Toux	Non	0						
	Oui	1						
Examen lié à l'expérience								
Infection de plaie (post-injection)	Aucune	0						
	Tissu de granulation avec rougeur	2						
	Inflammation avec exsudat	4						
	Ulcération	**6**						
Croissance de la tumeur interférant avec les fonctions vitales	Non	0						
	Oui	**6**						
	Total							

Points limites mis en place dans cet essai qui engendrera une euthanasie de l'animal :

- Volume tumoral insuffisant (inférieur au volume tumoral attendu en fonction du groupe expérimental) à 4 semaines après l'injection des cellules cancéreuses
- Perte de poids excédant 20 % du poids total par rapport au poids total de souris du même âge
- Croissance de la tumeur interférant avec les fonctions vitales
- Ulcération à l'endroit de la tumeur
- Un score ≥ 6

Devenir des animaux en fin d'essai

☒ euthanasie

☐ possibilité de réutilisation

III. Décision de la commission d'éthique

N° d'enregistrement : UN AR 18/326

Date de la réception de la demande : 19/06/18

Date de l'avis de la commission : 10/08/16

☒ Approbation par la commission d'éthique

☐ Refus

IV. Déclaration du Maître d'expérience et du Directeur du laboratoire

Cette signature suppose que le maître d'expérience et le directeur du laboratoire reconnaissent leur pleine responsabilité et leur accord avec les procédures décrites ci-dessus.
Les signataires en signant ce document :

- s'engagent à respecter toutes les modalités décrites dans ce document;
- acceptent de soumettre une adaptation au dossier pour analyse à la commission d'éthique si
- confirment que les personnes impliquées dans cette étude possèdent la formation adéquate en ce qui concerne les conditions de bien-être animal et d'expérimentation animale

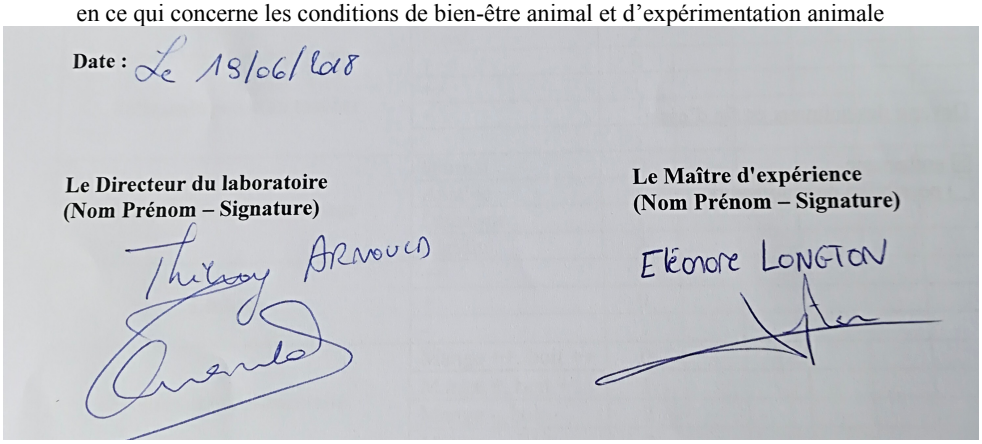

ANNEXE

Volume tumoral de 200 à 300 mm^3 Volume tumoral de 100 à 200 mm^3

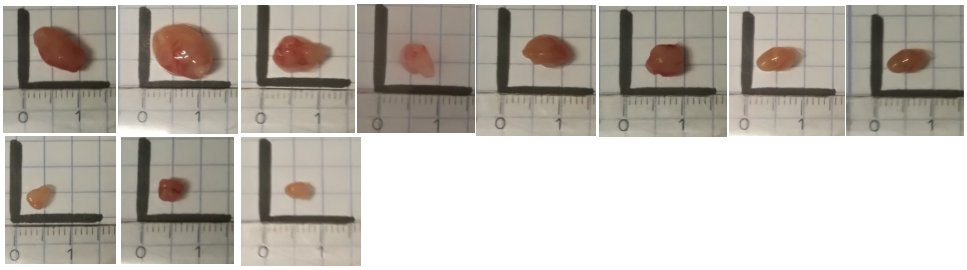

Volume tumoral de moins de 100 mm^3

2 Appendix II

+Projet destiné à l'évaluation éthique des expériences sur animaux

I. Présentation de l'expérience

TITRE DE L'EXPERIENCE :
Etude de la reprogrammation des macrophages tumoraux par irradiation avec des photons afin d'amplifier l'effet d'anticorps ciblant l'immunomodulateur PD-L1 sur des tumeurs murines d'origine ORL

Nom du Maître d'expérience : Longton Eléonore

Unité de Recherche en Biologie Cellulaire (URBC)-Narilis- Faculté des Sciences N° Agrément : LA1900053

☒ Nouveau projet
☐ Renouvellement d'un projet en fin de validité
☐ Adaptation d'un projet en cours

Durée estimée de l'expérience : 4 mois

Nombre d'animaux :

	Nombre d'animaux	**Espèce et lignée**
Du 15/08/18 au 15/12/2018	**40**	***Mus musculus* C3H/HeOuJ**

Domaine du projet :
☒ Recherche fondamentale
☐ Recherche translationnelle ou appliquée
☐ Test réglementaire
☐ Production ou service de routine
☐ Protection de l'environnement
☐ Conservation des espèces
☐ Enquête médicolégale
☐ Enseignement supérieur ou formation
☐ Maintien de colonies d'animaux génétiquement modifiés
☐ Autre : ……

Niveau de gravité du protocole :
☐ NR : non recovery - sans réveil : projet sans aucune douleur ou aucun inconfort

☐ Gravité légère
☒ Gravité modérée
☐ Gravité sévère

N° d'enregistrement : UN AR 18/326

Date de la réception de la demande : 19/06/2018

Date de l'avis de la CEEXPANI : 10/08/2018

☒ Approbation par la CEEXPANI (2 ans maximum) : du 15/08/18 au 31/12/19
☐ Refus

Date de l'évaluation rétrospective du projet : 01/03/2020

II. Commentaires de la Commission d'éthique en expérimentation animale

REMARQUES / QUESTIONS / SUGGESTIONS de la **CEEXPANI** qui a examiné la demande en date du 26/06/2018.

RÉPONDRE AUX REMARQUES DANS LE TEXTE

SUITE À L'ESSAI PILOTE : REVOIR SI NÉCESSAIRE LE NIVEAU DE SÉVÉRITÉ AU MOINS AU NIVEAU DES STATS (SEVERITÉ RÉELLE)

VOIR SI LES RÉSULTATS OBTENUS PENDANT LA PHASE PILOTE PEUVENT ÊTRE UTILISÉS DANS LES RÉSULTATS FINAUX

COMPLETER LA DAP AVEC LES RESULTATS OBTENUS LORS DE LA DAEP (EN COULEUR SVP)

CONCLUSIONS :

☒ FAVORABLE SANS CONDITION

☐ DEFAVORABLE POUR LES RAISONS SUIVANTES :

Signatures des membres de la CEEXPANI (**au moins le Président et le Vétérinaire désigné**)

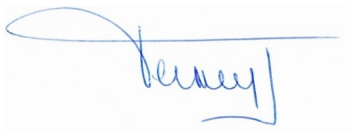

III. Avant-propos

Veuillez en quelques mots présenter la question scientifique et la démarche expérimentale utilisée ? Structurez la réponse en 3 points EN Y AJOUTANT DES REFERENCES SCIENTIFIQUES :
1. résumer les connaissances actuelles disponibles dans la littérature (= état des lieux)
2. articuler la question posée par rapport à ce contexte
3. décrire brièvement la démarche expérimentale (matériel et méthodes)

Nous savons que parmi les nombreux acteurs qui permettent à notre système immunitaire de lutter contre les maladies, dont le cancer, les lymphocytes T jouent un rôle primordial. Toutefois, les cellules tumorales peuvent échapper au système immunitaire, notamment en exprimant à leur surface une protéine appelée PD-L1. PD-L1 va inactiver les lymphocytes T en se liant à des récepteurs dont PD-1 présents à la surface des lymphocytes T. Cette liaison entre PD-L1 et ses récepteurs constitue une cible thérapeutique intéressante pour l'immuno-oncologie. En effet, le blocage de la protéine PD-L1 peut empêcher les cellules cancéreuses d'inactiver les lymphocytes T et ainsi permettre aux lymphocytes T cytotoxiques (CD8+) de retrouver leur rôle dans la destruction des cellules cancéreuses. Récemment, il a été démontré que l'expression de l'immuno-modulateur PD-L1 dans les cellules tumorales pouvait augmenter suite à une irradiation par photons (Deng et al, 2014). *In vitro,* nos résultats préliminaires sur des lignées tumorales humaines d'origine ORL ont d'ailleurs permis de mettre en évidence une variation de l'expression de PD-L1 en fonction de la dose de rayons X et du temps post-irradiation (Christoph Schifflers, master 1 BBMC, mini-mémoire, juin 2018). L'irradiation restant un traitement standard dans de nombreux cancers, la combinaison d'un anticorps anti-PD-L1 avec des rayons X semble prometteuse, et son utilisation dans des conditions optimales favoriserait une efficacité thérapeutique maximale. Cependant, les mécanismes sous-jacents à l'efficacité de ce traitement combiné restent peu connus.

Les macrophages associés aux tumeurs (TAMs) représentent une majorité des cellules immunitaires présentes dans le micro-environnement tumoral. Ces TAMs présentent des phénotypes différents, variant entre un phénotype de type M1 (pro-inflammatoire/anti-tumoral) et un phénotype de type M2 (anti-inflammatoire/pro-tumoral). Une tumeur à un stade débutant sera principalement associée à des TAMs de type M1, c'est-à-dire de macrophages anti-tumoraux. A un stade tumoral plus avancé, le micro-environnement sera principalement constitué de TAMs de type M2 pro-tumoraux. Cependant, ces phénotypes M1 et M2 sont modulables en fonction de différents facteurs environnants. Il a notamment été démontré que l'irradiation par photons et protons pouvait permettre de repolariser les macrophages M2 pro-tumoraux vers un phénotype M1 anti-tumoral (Genard et al, 2017).

Notre hypothèse de travail est donc que l'irradiation par photons en amplifiant l'expression de PD-L1 permet d'augmenter l'effet d'une immunothérapie par un anticorps anti-PD-L1 et ce, via la désinhibition des lymphocytes cytotoxiques infiltrant la tumeur (TILs), mais également via la repolarisation des macrophages associés aux tumeurs (TAMs) vers un phénotype de type anti-tumoral.

Cette étude *in vivo* sur un modèle syngénique nous permettra d'isoler les lymphocytes T CD8+ infiltrant la tumeur (TILs) afin d'étudier l'activation des lymphocytes par analyses en cytométrie en flux (Ahmadzadeh et al, 2009) ainsi que le phénotype des macrophages associés aux tumeurs et ce, après traitement par irradiation et/ou anticorps anti-PD-L1. De plus, le modèle syngénique nous permettra également de faire des analyses histologiques, notamment pour étudier l'impact à court terme du traitement par irradiation et/ou anticorps anti-PD-L1 sur les TAMs et les TILs mais aussi d'évaluer des éventuelles altérations au niveau des organes lymphoïdes. Pour cela, l'expérimentation *in vivo* préliminaire nous a permis de déterminer le nombre de cellules cancéreuses à injecter et la taille tumorale optimale pour isoler suffisamment de cellules du micro-environnement tumoral.

Deng, L., Liang, H., et al. (2014). Irradiation and anti-PD-L1 treatment synergistically promote antitumor immunity in mice. J Clin Invest, 124(2), 687-95. doi:10.1172/JCI67313

Ahmadzadeh, M., Johnson, L. A., et al. (2009). Tumor antigen-specific CD8 T cells infiltrating the tumor express high levels of PD-1 and are functionally impaired. Blood, 114(8), 1537-44. doi:10.1182/blood-2008-12-195792

Genard, G., Lucas, S., et al. (2017). Reprogramming of Tumor-Associated Macrophages with Anticancer Therapies: Radiotherapy versus Chemo- and Immunotherapies. Front Immunol, 8, 828. doi:10.3389/fimmu.2017.00828

IV. Justification du nouveau projet / du renouvellement / de l'adaptation

A. Justification de l'expérience ou de son renouvellement

Veuillez cocher les caractéristiques les plus en relation avec l'étude envisagée en ce qui concerne son caractère répétitif éventuel.

- ☒ Cette étude n'a jamais été réalisée
- ☐ Cette étude fait suite aux autres études sur le sujet (suite du projet)
- ☐ Les études antérieures furent non concluantes
- ☐ Bien que semblable à d'autres expériences, cette étude augmente le niveau de connaissance à son sujet
- ☐ Les animaux seront utilisés à des fins d'enseignement

Lors d'une demande de renouvellement, justifiez celle-ci en remplissant le document d'évaluation rétrospective de la phase précédente du projet.
Ce document doit être remis en même temps que la demande de projet.

B. Justification de l'utilisation d'animaux et absence de méthode alternative

1. Pour l'expérience envisagée, existe-t-il une méthode alternative (qui n'utilise pas d'animaux) dont la fiabilité est au moins équivalente ?

☐ Oui ☒ Non

Notre hypothèse de travail est que l'irradiation par photons en amplifiant l'expression de PD-L1 permet d'augmenter l'effet d'une immunothérapie par un anticorps anti-PD-L1 et ce, via la désinhibition des lymphocytes cytotoxiques infiltrant la tumeur (TILs), mais également via la repolarisation des macrophages associés aux tumeurs (TAMs) vers un phénotype de type anti-tumoral. L'étude *in vitro* nous permettra d'étudier la plasticité des macrophages après l'irradiation par photons ainsi que les mécanismes impliqués dans cette éventuelle repolarisation macrophagiques. Elle nous permettra également d'étudier l'effet immunomodulateur des photons sur des cellules cancéreuses d'origine ORL ainsi que les doses et timing post-irradiation permettant une efficacité thérapeutique maximale de l'anticorps anti-PD-L1.

L'expérimentation animale nous permettra quant à elle, d'étudier dans un modèle plus complexe l'effet de l'irradiation par photons sur le phénotype des TAMs et des TILs. Ces informations sont impossibles à obtenir sur un modèle *in vitro* puisque les TAMs et les TILs sont fondamentalement différents des macrophages différenciés expérimentalement à partir de monocytes et des lymphocytes circulants qui ne sont pas antigène spécifique. De plus, le microenvironnement tumoral ainsi que les cellules cancéreuses ont des effets multiples et encore peu connus sur les autres cellules au niveau de la tumeur qui ne peuvent pas être simulés *in vitro*. Cette étude *in vivo* permettra d'isoler des cellules d'intérêt au niveau de la tumeur et de son micro-environnement.

2. Justifiez le choix du modèle animal ? Donnez des références scientifiques.

Afin de pouvoir investiguer la population immunitaire dans l'environnement tumoral, un modèle syngénique murin sera utilisé (Smith et al. 2006). Pour cela, une lignée cellulaire tumorale d'origine ORL, la lignée SCC-VII, développée spontanément chez la souris C3H, sera injectée en sous-cutanée afin d'induire progressivement une tumeur. Celle-ci a déjà été étudiée et décrite dans la littérature en association à une immunothérapie (Khurana et al. 2001). De plus, la lignée tumorale SCC VII est agressive et peu immunogène. Elle représente donc un modèle idéal pour étudier la réponse tumorale spécifique des cellules T. Nous avons choisi d'utiliser la souris C3H/HeOuJ comme modèle syngénique car celle-ci est disponible chez Charles River et a déjà été étudiée in vivo avec la même lignée tumorale (Duarte et al. 2012).

*Smith, L. P. and G. R. Thomas (2006). "Animal models for the study of squamous cell carcinoma of the upper aerodigestive tract: a historical perspective with review of their utility and limitations. Part A. Chemically-induced de novo cancer, syngeneic animal models of HNSCC, animal models of transplanted xenogeneic human tumors." Int J Cancer **118**(9): 2111-2122.*

*Khurana, D., et al. (2001). "Characterization of a spontaneously arising murine squamous cell carcinoma (SCC VII) as a prerequisite for head and neck cancer immunotherapy." Head Neck **23**(10): 899-906.*

Duarte, S., et al. (2012). "Isolation of head and neck squamous carcinoma cancer stem-like cells in a syngeneic mouse model and analysis of hypoxia effect." Oncol Rep 28(3): 1057-1062.

V. Informations

A. Laboratoire et personnel

Laboratoire :
Unité de Recherche en Biologie Cellulaire (URBC)-Narilis- Faculté des Sciences

N° d'agrément :
LA1900053

Directeur de l'agrément :
Thierry Arnould Tel.: +32 (0)81 72 41 25 Email: thierry.arnould@unamur.be

Personnel impliqué dans le laboratoire d'accueil (maîtres d'expérience et bio-techniciens, à l'exclusion des ouvriers) :

Nom	Maître d'expérience	Bio-technicien	Tel ou E-mail	Formation réglementaire (date + lieu)
Thierry Arnould	☒ porte parole	☐	thierry.arnould@unamur.be	☒ 2007, ULg
Carine Michiels	☒	☐	carine.michiels@unamur.be	☒ Acceptée de facto, 2005
Eléonore Longton	☒	☐	elelongton@hotmail.com	☒ Janvier 2017, UNamur
Christoph Schifflers	☐	☒	christoph.schifflers@student.unamur.be	☒ Mai 2018, UNamur
Maude Fransolet	☐	☒	Maude.fransolet@unamur.be	☒ 2011, UNamur

Autre laboratoire où les expériences (ou parties) sont réalisées

1) Local d'expérimentation (irradiation) 19A situé au LARN (laboratoire d'analyses de réactions nucléaires), bâtiment des sciences
   LA : 1900053 (extension d'agrément de l'URBC)
   Personne de contact : Stéphane Lucas (LARN), Thierry Arnould (URBC)

   Approbation de la Commission d'éthique qui supervise ce laboratoire : ☐ Oui ☐ Non
   N° de projet : Validité : du .. /../.. au ../../..

2) Laboratoire de Physiologie générale situé en URPhyM (euthanasie des souris et analyses histologiques)
   LA 1900055
   Personne de contact : Nathalie Caron, Tél : +32 (0)81 72 43 30,
   Email: nathalie.caron@unamur.be

   Approbation de la Commission d'éthique qui supervise ce laboratoire : ☐ Oui ☐ Non
   N° de projet : Validité : du .. /../.. au ../../..

B. Animaux

	Espèce animale	Lignée	Fournisseur (+numéro d'agrément)	Sexe	Age/Poids
Exp 1	***Mus musculus***	**C3H/HeOuJ**	Charles River, L'arbresle, France	Femelle	5 à 6 semaines 15 à 20 g
Exp 2	***Mus musculus***	**C3H/HeOuJ**	Charles River, L'arbresle, France	Femelle	5 à 6 semaines 15 à 20 g
Exp 3	***Mus musculus***	**C3H/HeOuJ**	Charles River, L'arbresle, France	Femelle	5 à 6 semaines 15 à 20 g
Exp 4	***Mus musculus***	**C3H/HeOuJ**	Charles River, L'arbresle, France	Femelle	5 à 6 semaines 15 à 20 g

Des animaux génétiquement modifiés seront-ils utilisés dans cette expérience ? ☐ oui ☒ non
Des animaux présentant un phénotype douloureux seront-ils utilisés dans cette expérience ? ☐ oui ☒ non
Des animaux d'un précédent projet sont-ils utilisés ? ☐ oui ☒ non

Nombre d'animaux :

	Exp 1	Exp 2	Exp 3	Exp 4
Du 01/09/2018 au 01/01/2019	10	10	10	10

Calcul statistique :

Considérant que l'étude de l'activation des lymphocytes CD8+infiltrant la tumeur en réponse à un traitement par rayons X et/ou anticorps anti-PD-L1, n'a jamais été réalisée, il n'est pas possible sur base de la littérature, ni sur bases de résultats expérimentaux *in vitro,* de déterminer le seuil à partir duquel une différence d'activation des lymphocytes peut être considérée comme significative. Pour cette même raison, la déviation standard nécessaire au calcul du nombre de souris ne peut pas être anticipée (sous réserve des résultats obtenus grâce au projet *in vivo* préliminaire).

Cependant, nous pouvons nous baser sur une récente étude *in vivo* utilisant un traitement combiné semblable par photons et injection d'anticorps anti-PD-L1, ayant obtenu des résultats significatifs en utilisant un total de 8 souris par groupe expérimental (*Simon J. Dovedi and al. Acquired Resistance to Fractionated Radiotherapy Can Be Overcome by Concurrent PD-L1 Blockade. Cancer Research. Oct 2014*). Considérant le risque associé aux anesthésies, ainsi qu'à l'injection des cellules cancéreuses et la croissance tumorale résultante, 2 souris supplémentaires sont rajoutées à chaque groupe expérimental afin d'assurer le nombre minimal de souris nécessaires à 8 en fin de l'expérience. Nous utiliserons donc 10 souris par groupe expérimental.

Méthode d'identification des animaux :
Marquage des souris par marqueur au niveau de la queue et étiquettes annotées sur les cages.

Lieu d'hébergement des animaux (numéro de local/nom de l'animalerie) :
Animalerie centralisée de l'extension biologie L1900631

Lieu où a lieu l'expérimentation (numéro de local/ nom du laboratoire) :

- L1900631 Animalerie centralisée de l'extension biologie
- URBC
- LARN
- Physiologie générale

8

Devenir des animaux en fin d'étude
☒ euthanasie
☐ possibilité de réutilisation (dans ce cas, prouvez la non-incidence sur des études ultérieures) :

Evaluation du bien-être :
Niveau(x) de Gravité (expérience 1, 2, …) : ☐ NR ☐ léger ☒ modéré ☐ sévère

Justifiez votre choix :
L'injection sous-cutanée de cellules cancéreuses va engendrer la formation d'une masse tumorale pouvant impacter l'état de santé général et le bien-être de la souris. L'irradiation sera limité au niveau de la tumeur. Pour cela, le reste de la souris sera protégé par une plaque en plomb absorbant 99% de la radiation (0,5 à 1 cm d'épaisseur). L'anticorps sera injecté en i.p. en une seule injection.

Prévention de la douleur ? ☐ oui ☒ non
Si oui, veuillez préciser les méthodes dans le projet expérimental

Si non : pourquoi ?
Les cellules cancéreuses ne prolifèreront pas suffisamment longtemps pour engendrer des perturbation physiologiques importants. En plus, 3 jours après l'irradiation des tumeurs et/ou l'injection de l'anti-PD-L1, les souris seront euthanasiées.

Cependant, en cas de signes de douleur (modification du comportement, de la posture et de l'apparence de la souris- Miller 2011), une administration d'analgésique sera réalisée par injection de buprénorphine (0,05 mg/kg, en sous-cutané – Flecknell 2018). L'analgésie sera bien sûre adaptée en fonction de la douleur de l'animal et des données du projet préliminaire.

Type d'hébergement et nombre d'animaux par cage (en cas d'hébergement individuel justifiez) :
Les animaux seront hébergés dans des cages Tecniplast GM500 (500 cm^2). Cinq souris, uniquement du même sexe et du même groupe expérimental, pourront être hébergées dans une cage.

Quels sont les efforts pour améliorer le bien-être au quotidien ? Quel(s) type(s) d'enrichissement utilisez-vous ?
Les cages sont munies d'une litière en sciure, changée régulièrement.
Afin d'enrichir le milieu, des tubes en carton et en PVC sont placés dans la cage, ainsi que des copeaux de bois, permettant aux souris de se créer un nid. Adaptation du confort en fonction du comportement des souris.
Les cages sont munies d'un biberon d'eau qui sera remplacée tous les jours et les souris sont nourries *ad libitum* avec de la nourriture en pellets.
Les conditions de température sont maintenues constantes (22°C +- 2°C) ainsi que les conditions de luminosité (12h par jour).

Evaluation du bien-être au quotidien :
- critères d'évaluation (grille/score) ?

Le bien-être sera évalué en réalisant un examen général de l'animal et en regardant sa réaction à divers stimuli tels que la lumière ou le bruit. De plus, l'état de la cage sera vérifié. Il sera impératif que la présence de la tumeur n'altère en rien les comportements physiologiques de l'animal.

Animal ID:
Souche + sexe:
Age au moment de l'injection:
Poids au moment de l'injection:
Niveau de douleur:

Nom de l'expérimentateur:

		score	date	date	date	date	date	date
Paramètres étudiés	Age							
	Poids							
Examen général								
Perte de poids (par rapport au poids total de souris du même âge)	0 %	0						
	5 %	1						
	10 %	2						
	15 %	4						
	20 %	**6**						
Apparence/couleur	Normal	0						
	Abdomen bleu	1						
	Extrémités pâles	2						
Température en surface	Chaud	0						
	Indécis	1						
	Froid	2						
Reflexes/réponse au toucher	+++	0						
	++	1						
	+	2						
	-	3						
Comportement dans sa cage	Normal	0						
	Apathie	1						
	Léthargie	1						
	Rigidité	2						
Léchage	++	1						
	+	0						
	-	1						
Comportement alimentaire	Mange ++, boit ++	0						
	Mange +, boit +	1						
	Mange -, boit -	2						
	Mange --, boit --	3						
Tremblement	+	0						
	-	1						
Posture voutée	-	0						
	+	1						
Déshydratation	-	0						
	+	1						
	++	2						
Vomissement	-	0						
	+	1						
	++	2						
Excréments	Normaux	0						
	Diarrhée	1						
Respiration	Normale	0						
	Difficile	1						

Toux	Non	0						
	Oui	1						
Examen lié à l'expérience								
Infection de plaie	Aucune	0						
	Tissu de granulation avec rougeur	2						
	Inflammation avec exsudat	4						
	Ulcération	**6**						
Croissance tumorale interférant avec les fonctions vitales	Non	0						
	Oui	**6**						
	Total							

L'animal est euthanasié quand un score de 6 est atteint.
La grille de scores sera adaptée suivant les observations des animaux lors du projet pilote.

- fréquence : Quotidiennement
- personne(s) en charge du suivi quotidien : Eléonore Longton, Christoph Schifflers

Des points limites ont-ils été déterminés? ☒ oui ☐ non

Si oui, veuillez les préciser ?

- Perte de poids excédant 20 % du poids total initial
- Croissance tumorale interférant avec les fonctions vitales
- Ulcération à l'endroit de la tumeur
- Un score 6 dans la grille de score
- Volume tumoral insuffisant (inférieur au volume tumoral attendu en fonction du groupe expérimental) à 4 semaines après l'injection des cellules cancéreuses

VI. Projet expérimental

A. Recherche envisagée

Le traitement des cancers tête et cou reste un énorme défi médical sans nette amélioration majeure sur la survie des patients. Les études cliniques récentes utilisant des anticorps dirigés contre les immuno-modulateurs ont démontré des résultats prometteurs mais leur succès est limité par les propriétés immunosuppressives du microenvironnement tumoral. Les macrophages associés aux tumeurs (TAMs) représentent les cellules immunitaires les plus abondantes dans la tumeur et plus de 70% d'entre eux présentent un phénotype de type M2 avec une activité immunosuppressive importante. En conséquence, reprogrammer les TAMs vers un phénotype M1, avec des propriétés anti-tumorales et immuno-stimulantes, serait un moyen efficace d'améliorer l'efficacité de ce type d'immunothérapie. La radiothérapie à l'aide de rayons X semble capable d'augmenter la destruction des cellules cancéreuses par le biais du système immunitaire. En effet, des résultats préliminaires *in vitro* montrent que l'irradiation par photons repolarise les TAMs vers un phénotype M1 anti-tumoral. Cependant, rien n'est connu concernant les effets d'un traitement par photons combiné à une immunothérapie utilisant des anticorps anti-PDL1 dans les tumeurs tête et cou. Dans ce travail, nous allons irradier des modèles *in vitro* appropriés ainsi que des modèles murins de tumeurs, afin d'initier la conversion des TAMs en macrophages de type M1. Nous étudierons également *in vivo* la possible synergie de l'irradiation avec un traitement d'immunothérapie utilisant des anticorps anti-PD-L1. *In vivo*, différents paramètres seront investigués, notamment le nombre et le phénotype des macrophages et des cellules T dans les tumeurs. Les résultats pourront guider des approches de médecine personnalisée en révélant des composants du microenvironnement tumoral qui influencent la réponse aux traitements. Les résultats préliminaires *in vivo* de l'irradiation par photons pourraient aussi nous permettre d'envisager une comparaison avec une irradiation par protons, technique d'irradiation prometteuse. En effet, des résultats préliminaires montrent que l'irradiation par protons altère le phénotype M2 de macrophages humains en culture.

B. Place de l'expérience dans le cadre de la recherche envisagée (objectifs)

- **Schéma expérimental chronologique (différentes étapes de l'expérience)**

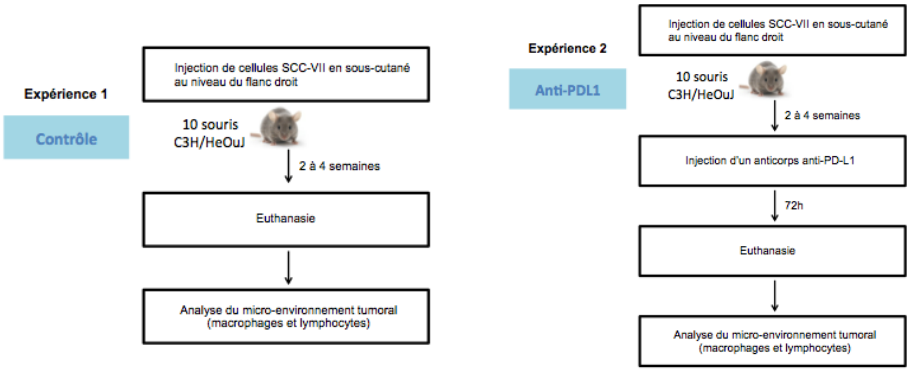

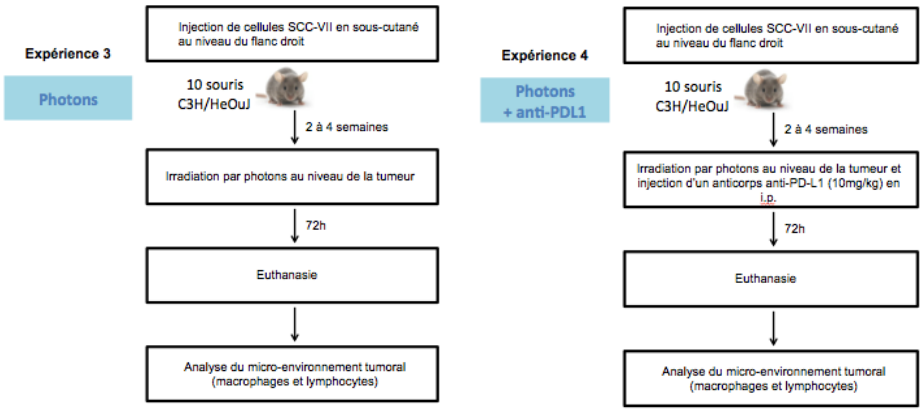

- Description précise de chaque étape de l'expérience

Injection des cellules :
Les souris C3H/HeOuJ âgées de 5 à 6 semaines seront hébergées dans l'animalerie centralisée de l'extension biologie (L1900631). Après 1 à 2 semaines d'adaptation à leur environnement, les souris seront anesthésiées par inhalation d'isoflurane en utilisant la table d'anesthésie disponible à l'animalerie centrale. Pour cela, elles seront déposées dans une chambre à induction propre reliée à l'appareil d'anesthésie. L'isoflurane sera ajusté 3-4 % et le débit d'oxygène à 0,8-1,5 L/min. Les souris seront ensuite posées une plaque chauffante, préchauffée à 37°C afin de maintenir leur température corporelle constante. La suspension de cellules tumorales SCC-VII (250 000, 500 000 ou 1 000 000 de cellules cancéreuses, sur base du projet préliminaire, suspendues dans 150 µl de PBS) sera injectée à la souris en sous-cutanée au niveau du flanc droit. En cas de signes de douleur, une administration d'analgésique sera réalisée par injection sous-cutanée de buprénorphine (0,05 mg/kg).
La taille de la tumeur sera contrôlée quotidiennement à l'aide d'un pied à coulisse.

Suivi des souris :
Les souris seront examinées quotidiennement afin de vérifier que les points limites de l'expérience ne sont pas atteints :

- Perte de poids excédant 20 % du poids total
- Tumeur interférant avec les fonctions vitales
- Ulcération à l'endroit de la tumeur
- Un score ≥ 6 dans la grille d'observation établie

Si un de ces points limites est atteint, la souris sera euthanasiée.

Irradiation par rayons X
Une fois la taille tumorale souhaitée (basée sur le projet préliminaire) atteinte, après 2 à 4 semaines, les souris (par groupes de 3 souris) seront anesthésiées par un mélange de Kétamine et Xylazine (100mg/kg et 10mg/kg, en intra-péritonéal). Elles seront ensuite mises dans une cage de transport qui sera emballée d'un sac plastique opaque et transportées au LARN. Dans le générateur, la souris sera placée sur un gel préchauffé à 37°C et placée sous un portoir couvert par une plaque en plomb (mise au point dans le projet préliminaire) de manière à ce que le trou de 1 cm de diamètre dans la plaque se trouve juste au-dessus de la tumeur, afin de limiter l'exposition aux rayons X uniquement à la tumeur.

Injection de l'anticorps anti-PDL1 :

Lorsque la masse tumorale aura atteint la taille souhaitée, ou 72 heures après l'irradiation, les souris recevront une injection intra-péritonéale d'anticorps anti-PDL1 (10 mg/kg).
Azad A, Yin Lim S, D'Costa Z, Jones K, Diana A, Sansom OJ, et al. PD-L1 blockade enhances response of pancreatic ductal adenocarcinoma to radiotherapy. EMBO molecular medicine. 2016.

Euthanasie :
Les souris seront euthanasiées 72 heures après l'irradiation. Pour ceci, une anesthésie générale via une injection intra-péritonéale de Kétamine et de Xylazine (100 mg/kg et 10 mg/kg, I.P.) (suivant le protocole validé ANIM PO 0007 déposé sur la plate-forme SVTA) sera réalisée à l'animalerie centrale. Une fois que les souris seront endormies, elles seront transportées au laboratoire de physiologie générale en URPhyM (LA 1900055), où une ponction intra-cardiaque sera réalisée pour prélever un volume sanguin maximal, qui servira à l'isolation des monocytes périphériques circulants. La ponction intra-cardiaque sera suivie d'une dislocation cervicale. Post-mortem, différents tissus seront prélevés : la tumeur, ainsi que divers organes lymphoïdes (analyses histologiques) tels que la rate, l'intestin (la jonction iléo-coecale), des ganglions lymphatiques et si possible le thymus. Afin d'isoler différentes populations cellulaires à partir des tumeurs (TILs et TAMs), celles-ci doivent être dissociées et les cellules isolées au plus vite après l'euthanasie des souris et ce en utilisant un gentleMACS dissociateur. Considérant que la dissociation tumorale et l'isolation des cellules doivent être effectuées le plus rapidement possible et nécessitent un l'équipement uniquement disponible au laboratoire de physiologie générale, les euthanasies doivent avoir lieu au laboratoire de physiologie générale. L'anesthésie générale (Kétamine/Xylazine) sera cependant réalisée à l'animalerie centrale ce qui permet d'éviter le stress associé au transport que les souris subiraient autrement.

VII. Sécurité des chercheurs et de l'environnement

(Ce domaine ne relève pas de la compétence de la commission d'éthique pour l'expérimentation animale. Il s'agit ici d'attirer l'attention sur la nécessité éventuelle de consulter le service de sécurité de l'institution).

A. Des produits dangereux sont-ils utilisés ? ☒ Oui ☐ Non
- produits physiques (radioactifs…) ☒ Oui ☐ Non

Si oui, contacter le service radioprotection (Prof. S. Lucas)

- produits chimiques (toxiques…) ☐ Oui ☒ Non Si oui, contacter le Prof. S. Laners

B. Le projet implique-t-il l'utilisation :
- d'organismes pathogènes (bactéries, virus, parasites, …) ☐ Oui ☒ Non
  Si oui, à quelle classe de risque appartiennent-ils : ☐ 1 ☐ 2 ☐ 3
- d'organismes génétiquement modifiés ☐ Oui ☒ Non

Si oui à l'une de ces deux questions, contacter S. Loret pour établir le dossier de biosécurité le cas échéant.

VIII. Déclaration du Maître d'expérience et du Directeur du laboratoire

Titre de l'expérience : Etude de la reprogrammation des macrophages tumoraux par irradiation avec des photons afin d'amplifier l'effet d'anticorps ciblant l'immunomodulateur PD-L1 sur des tumeurs murines d'origine ORL

Laboratoire : Unité de Recherche en Biologie Cellulaire (URBC)-Narilis- Faculté des Sciences

Signatures et dates :

Cette signature suppose que le maître d'expérience et le directeur du laboratoire reconnaissent leur pleine responsabilité et leur accord avec les procédures décrites ci-dessus.
Les signataires en signant ce document :
- s'engagent à respecter toutes les modalités décrites dans ce projet;
- acceptent de soumettre une adaptation au dossier pour analyse à la commission d'éthique si à un moment quelconque de cette expérience, un changement dans l'utilisation doit être apporté ;
- confirment que les personnes impliquées dans cette étude possèdent la formation adéquate en ce qui concerne les conditions de bien-être animal et d'expérimentation animale